

Medium-Span Timber Footbridges - A Comparative Analysis with Traditional Steel and Concrete Structures (Technical, Environmental, and Structural Aspects)

Auteur : D'Anna, Antonio

Promoteur(s) : Gens, Frédéric

Faculté : Faculté des Sciences appliquées

Diplôme : Master en ingénieur civil des constructions, à finalité spécialisée en "civil engineering"

Année académique : 2024-2025

URI/URL : <http://hdl.handle.net/2268.2/23368>

Avertissement à l'attention des usagers :

Tous les documents placés en accès ouvert sur le site le site MatheO sont protégés par le droit d'auteur. Conformément aux principes énoncés par la "Budapest Open Access Initiative"(BOAI, 2002), l'utilisateur du site peut lire, télécharger, copier, transmettre, imprimer, chercher ou faire un lien vers le texte intégral de ces documents, les disséquer pour les indexer, s'en servir de données pour un logiciel, ou s'en servir à toute autre fin légale (ou prévue par la réglementation relative au droit d'auteur). Toute utilisation du document à des fins commerciales est strictement interdite.

Par ailleurs, l'utilisateur s'engage à respecter les droits moraux de l'auteur, principalement le droit à l'intégrité de l'oeuvre et le droit de paternité et ce dans toute utilisation que l'utilisateur entreprend. Ainsi, à titre d'exemple, lorsqu'il reproduira un document par extrait ou dans son intégralité, l'utilisateur citera de manière complète les sources telles que mentionnées ci-dessus. Toute utilisation non explicitement autorisée ci-avant (telle que par exemple, la modification du document ou son résumé) nécessite l'autorisation préalable et expresse des auteurs ou de leurs ayants droit.



Medium-Span Timber Footbridges – A Comparative Analysis with Traditional Steel and Concrete Structures (Technical, Environmental, and Structural Aspects)

Case Study within the "Seine – Escaut Est" Project: Structural Adaptations for the 2000-Ton Navigation Standard on the Nimy-Blaton-Péronnes Canal

Student:

D'ANNA Antonio s2404632

Promoter:

Frédéric Gens (Part-time Lecturer at ULiège – Project Director at Bureau Greisch – Expert in Civil Engineering Structures)

Co-Promoter:

Stefano Silvestri (Associate Professor of Structural Design at the University of Bologna - Department of Civil, Chemical, Environmental, and Materials Engineering)

Jury Members:

José Henriques (Professor at Hasselt University)

Arnaud Pineur (Project Director at Bureau Greisch – Expert in Timber Structures)

Sébastien Seret (Administrator at Bureau Greisch – Expert in Steel Structures)

Section:

Master en Ingénieur Civil des Constructions – Finalité Spécialisée en Génie Civil

Academic Year: 2024-2025

A mio Nonno Antonio

A cui devo la persona che sono

Firmitas · Utilitas · Venustas

Vitruvius, De Architectura

ACKNOWLEDGEMENTS

I would like to express my deepest gratitude to Professor Frédéric Gens, my thesis supervisor at the University of Liège, for introducing me to the world of bridge engineering and inspiring my passion for the subject. His guidance has been fundamental in shaping the direction of this thesis.

A sincere thank you also goes to Professor Stefano Silvestri, my co-supervisor at the University of Bologna, whom I consider a mentor and a professional point of reference. Since the very beginning of my master's journey, he has accompanied me through new experiences with unwavering support and intellectual integrity.

I am also grateful to all the members of the thesis jury for their participation and for the constant availability they have shown throughout the entire process. I would like to particularly thank Professor José Henriques for agreeing to take part in this evaluation and for having provided me with theoretical foundations to understand such innovative and sustainable material as timber.

Finally, my sincere thanks go to Arnaud Pineur and Sébastien Seret, for their active involvement in the analysis and writing process, as well as for their valuable support and constructive collaboration.

TABLE OF CONTENTS

1	CASE STUDY OVERVIEW	1
1.1	THE SEINE-ESCAUT EST PROJECT IN WALLONIA.....	3
1.2	SECTOR 5 OF THE NIMY-BLATON-PÉRONNES CANAL WITHIN THE SEINE-ESCAUT EST PROJECT	4
2	HISTORICAL AND TYPOLOGICAL ANALYSIS OF TIMBER BRIDGES	5
2.1	HISTORICAL DEVELOPMENT OF TIMBER BRIDGES	5
2.2	CURRENT STATE OF THE ART IN TIMBER BRIDGES.....	8
2.3	STRUCTURAL CLASSIFICATIONS OF TIMBER BRIDGES	10
2.3.1	STRESS LAMINATED DECK (SLTD) BRIDGES.....	12
2.3.2	BEAM BRIDGES	12
2.3.3	TRUSS BRIDGES	12
2.3.4	ARCH BRIDGES	12
2.3.5	SUSPENSION AND CABLE-STAYED BRIDGES	12
2.4	MATERIALS AND CONNECTION TECHNIQUES.....	12
3	PRELIMINARY DESIGN AND FINAL PROPOSAL SELECTION	14
3.1	PRELIMINARY DESIGN PROPOSAL 1.....	14
3.1.1	ANALYSIS OF POTENTIAL CRITICAL ISSUES.....	18
3.2	PRELIMINARY DESIGN PROPOSAL 2.....	19
3.2.1	ANALYSIS OF POTENTIAL CRITICAL ISSUES.....	22
3.3	PRELIMINARY DESIGN PROPOSAL 3.....	23
3.3.1	ANALYSIS OF POTENTIAL CRITICAL ISSUES.....	26
3.4	ADDITIONAL PRELIMINARY DESIGN CONCEPTS	27
3.5	COMPARATIVE EVALUATION BETWEEN ARCH AND TRUSS BEAM SOLUTIONS – SELECTION OF THE FINAL PROPOSAL	28
3.5.1	RATIONALE FOR SELECTING THE ARCH BRIDGE	31
3.6	GENERAL ANALYSIS OF THE ARCH STRUCTURAL SYSTEM	32
3.6.1	STRUCTURAL BEHAVIOR	33
3.6.2	INSTABILITY PHENOMENA	34
3.6.3	MANAGEMENT OF HORIZONTAL THRUST	36
3.6.4	BOWSTRING BRIDGE TYPOLOGY	36
3.6.5	SLENDERNESS AND BRACING CONSIDERATIONS	38
4	INTEGRATION OF NON-STRUCTURAL ELEMENTS.....	40
5	RENDERING AND ENVIRONMENTAL INTEGRATION	42

6	STRUCTURAL ANALYSIS AND LOAD ASSESSMENT.....	45
6.1	LOAD DISTRIBUTION ALONG STRUCTURAL MEMBERS	45
6.2	LOAD EVALUATION	47
6.2.1	PERMANENT LOADS	47
6.2.2	PEDESTRIAN LOADS	49
6.2.3	SNOW LOADS.....	49
6.2.4	WIND LOADS	50
6.2.5	TEMPERATURE LOADS.....	54
6.3	LOAD COMBINATIONS	55
6.3.1	LOAD ZONING	57
6.3.2	ULTIMATE LIMIT STATE (ULS) COMBINATIONS - EN 1990 (6.4.3.2).....	59
6.3.3	SERVICEABILITY LIMIT STATE (SLS) – CHARACTERISTIC COMBINATION – EN 1990 (6.5.3).....	63
6.3.4	SERVICEABILITY LIMIT STATE (SLS) – FREQUENT COMBINATION – EN 1990 (6.5.3).....	66
7	FINITE ELEMENT MODELLING (FEM) AND STRUCTURAL RESULTS	67
7.1	LOAD APPLICATION ON STRUCTURAL ELEMENTS	70
7.2	STATIC DEFORMATION ANALYSIS.....	71
7.3	INTERNAL STRESS AND FORCE DISTRIBUTION	74
7.3.1	SECONDARY BEAMS – DECK.....	74
7.3.2	PRIMARY BEAMS – DECK	75
7.3.3	PRIMARY BEAMS – CENTRAL DECK ZONE	76
7.3.4	CENTRAL BEAMS – CENTRAL DECK ZONE.....	77
7.3.5	TRANSVERSAL BEAMS – DECK-TO-ARCH CONNECTION	78
7.3.6	ARCH BEAMS.....	79
7.3.7	VERTICAL HANGERS	80
7.3.8	SUMMARY TABLE OF STRUCTURAL RESULTS.....	80
8	VERIFICATION TO ULS AND SLS – EN 1995 – 1 -1 COMPLIANCE	81
8.1	SERVICE CLASS DEFINITION	81
8.2	DEFORMATION FACTOR k_{def}	81
8.3	DEFLECTION CONTROL	82
8.4	STRENGTH VERIFICATION – MODIFICATION FACTOR k_{mod}	84
8.5	SIZE EFFECT FACTOR k_h	85
8.6	SYSTEM FACTOR k_{sys}	85

8.7	CROSS-SECTIONAL RESISTANCE CHECKS	86
8.8	ADDITIONAL RULES FOR CURVED BEAMS – ARCH ELEMENTS	88
8.9	MEMBER VERIFICATION – BUCKLING AND LATERAL-TORSIONAL INSTABILITY	90
8.10	DESIGN CHECKS	92
8.10.1	SECONDARY BEAMS – DECK	92
8.10.2	PRIMARY BEAMS – DECK	93
8.10.3	PRIMARY BEAMS – CENTRAL DECK ZONE	94
8.10.4	CENTRAL BEAMS – CENTRAL DECK ZONE	95
8.10.5	TRANSVERSAL BEAMS – DECK-TO-ARCH CONNECTIONS	96
8.10.6	ARCH BEAMS	97
8.11	DESIGN OF VERTICAL HANGERS	101
8.11.1	CABLE STABILITY UNDER WIND AND RAIN – VORTEX EFFECTS	101
8.12	CONSIDERATIONS ON STRUCTURAL CONNECTIONS	102
8.12.1	CONNECTIONS BETWEEN HORIZONTAL ELEMENTS	102
8.12.2	VERTICAL HANGER-TO-ARCH CONNECTIONS	104
8.13	THERMAL GRADIENT EFFECTS ON THE STRUCTURE	106
9	PEDESTRIAN WALKING COMFORT ASSESSMENT	108
9.1	NUMERICAL MODEL DESCRIPTION	108
9.2	MODAL ANALYSIS	109
9.3	COMFORT CHECK ACCORDING TO SETRA GUIDELINES	110
9.4	COMFORT CHECK ACCORDING TO EUROCODE 5 - PART 2, ANNEX B	111
9.4.1	ESTIMATION FOR DISTINCT PEDESTRIAN GROUPS AND CONTINUOUS FLOW	112
9.5	TIME-DOMAIN DYNAMIC ANALYSIS	114
9.5.1	DEFINITION OF PEDESTRIAN-INDUCED LOAD	114
9.5.2	CLASSIFICATION OF LOAD MODELS	115
9.5.3	PEDESTRIAN CONFIGURATIONS	116
9.5.4	THEORETICAL CONSIDERATIONS ON THE USE OF A TUNED MASS DAMPER (TMD)	116
10	TECHNICAL AND ECONOMIC FEASIBILITY – STRUCTURAL SOLUTION COMPARISON	118
10.1	COST ESTIMATION – CONCRETE AND STEEL ALTERNATIVES	119
10.2	COMPARATIVE COST EVALUATION AND RESULTS	121

11	DURABILITY AND ENVIRONMENTAL SUSTAINABILITY – CO ₂ EMISSION ANALYSIS	123
11.1	CODE FRAMEWORK AND INPUT PARAMETERS	123
11.1.1	EMISSION FACTOR DEFINITION – STRUCTURAL MATERIALS	124
11.1.2	EMISSION FACTOR DEFINITION – TRANSPORT MODES.....	125
11.1.3	LIFE CYCLE ASSESSMENT PARAMETERS.....	126
11.2	EMISSION CALCULATIONS – RESULTS INTERPRETATION	126
11.2.1	EMISSIONS DISTRIBUTION BY PHASE	128
11.2.2	TEMPORAL EMISSION TRENDS	129
11.2.3	EMISSIONS PER SQUARE METER.....	131
11.2.4	EMISSIONS BY TRANSPORT MODE	132
11.2.5	ENERGY CLASS ESTIMATION	134
12	FINAL CONSIDERATIONS AND CONCLUSIONS	136
13	REFERENCES.....	138

LIST OF ANNEXES AND APPENDICES

This thesis is composed of a main document and several supplementary materials that provide additional detail and documentation.

The structure of the submission is as follows:

- I. MAIN THESIS DOCUMENT
 - *“Medium-Span Timber Footbridges – A Comparative Analysis with Traditional Steel and Concrete Structures (Technical, Environmental, and Structural Aspects)”*
- II. ANNEX 1
 - *“State of Art” - A review of reference works and comparable projects related to the structural use of timber in pedestrian bridge design, with focus on form, typology and contemporary design strategies.*
- III. ANNEX 2
 - *“Mechanical Properties of Timber” - Detailed mechanical characterization of the timber adopted for the structural design, including material classes, strength parameters and normative references.*
- IV. ANNEX 3
 - *“Structural Renderings” - Selection of 3D views illustrating the structural configuration and integration of the bridge within its environment.*
- V. APPENDICES
 - *Drawing No. 1: “Frontal and Top Views – Sections A-A’ and B-B’ – Structural Reference and Dimensions”*
 - *Competition Board: “XILEMA – A structural Harmony Between Form and Meaning”*

All documents are referenced within the main thesis and are intended to complement and support the core analysis and design process.

TABLE OF FIGURES

Figure 1: Pre-Design Proposal 1 - Cable Stayed Bridge - Steel and Concrete – Bureau Greisch	1
Figure 2: Pre-Design Proposal 2 - Arch Bridge - Steel and Concrete - Bureau Greisch	1
Figure 3: Pre-Design Proposal 3 - Frame Bridge - Steel and Concrete - Bureau Greisch.....	1
Figure 4: Le Projet du Réseau Seine-Escaut - (Le Projet Seine - Escaut, 2022)	3
Figure 5: Cesar's Bridge across the Rhine - (Rome versus the Germans, Part II, 2019)	5
Figure 6: Ponte degli Alpini, Bassano del Grappa, Italy - (Ponte degli alpini, 2019)	6
Figure 7: Model of the Main Structural Members of the Timber Bridge over the Rhine River in Schaffhausen, Switzerland - (Model of the main structural members of the timber bridge over the Rhine River in Schaffhausen, Switzerland., 2017)	6
Figure 8: Walkham Viaduct - (Brunel's Timber Viaducts, 2007).....	7
Figure 9: Table of Maximum Spans - Analyzed Bridges	9
Figure 10: Structural Typologies – Timber Bridges – Pie Chart [%].....	10
Figure 11: Slotted-In Steel Plates with Dowels Connection Typology - (Crocetti, R., 2014), p.9	13
Figure 12: Pre-design Proposal 1 - Architectonic Frontal View	14
Figure 13: Pre-design Proposal 1 - Architectonic Top View	14
Figure 14: Pre-design Proposal 1 - Structural Front View	15
Figure 15: Pre-design Proposal 1 - 3D Structural Isometric View - SCIA Engineering.....	15
Figure 16: Three-Hinged-Arches Schematization	16
Figure 17: (a) Section A-A' with “Hangers - Deck - Double Arch” Connection; (b) Section B-B' with Deck-Lateral Barrier.	16
Figure 18: Deck Proposed Section with Structural Element Dimensions	17
Figure 19: Connection Scheme of the Primary Beam of the Deck with Vertical Tie Rods	17
Figure 20: Connection Scheme of Vertical Tie Rods with Double Three-Hinged Arch	18
Figure 21: Illustration of the Deck Section with a Support Span of 25.4 meters and Double Simple Lateral Support.....	18
Figure 22: Top View, Deck Elements between the Structural Arches - SCIA Engineering.....	19
Figure 23: Pre-design Proposal 2 - Architectonic Frontal View	19
Figure 24: Pre-design Proposal 2 - Architectonic Top View.....	20
Figure 25: Pre-design Proposal 2 - Structural Front View	20
Figure 26: Three-Hinged-Arches Schematization	20
Figure 27: (a) Section with Hangers-Deck-Arches Connection; (b) Section with Deck-Lateral Barrier and Triple Arch.....	21
Figure 28: Connection Scheme of Vertical Tie Rods with Top Three-Hinged Arch.....	21
Figure 29: Interruption of the Continuity of the Deck Beam.....	22
Figure 30: Example of Alternative Load Distribution Configuration.....	23
Figure 31: Pre-design Proposal 3 - Architectonic Frontal View	23
Figure 32: Detail of the Geometric Dimensions of the Structural Solution: Height of the Truss Beam “h” and Inclination Angle of the Diagonals (45°).....	24
Figure 33: Pre-design Proposal 3 - Structural Front View	24
Figure 34: Pre-design Proposal 3 - 3D Structural Isometric View - SCIA Engineering.....	24
Figure 35: Static Scheme of the Truss Beams.....	25

Figure 36: a) Cross-Section of the Deck and Arrangement of the Truss Beams; b) Cross-Section from the 3D Model – SCIA Engineering	25
Figure 37: Detail of the Hinged Connections of the Truss Beam	26
Figure 38: Pre-design Proposal 4 - Architectonic Frontal View	27
Figure 39: Pre-design Proposal 5 - Architectonic Frontal View	28
Figure 40: Pre-design Proposal 6 - Architectonic Frontal View	28
Figure 41: (a) Foundation of the Arch Structure with Inclined Elements; (b) Foundation of the Truss Beam with Vertical Pier	29
Figure 42: Front Elevation of the Reference Design Altimetric Section - Actual Vertical Clearance Requirements of the Obstacles to be Overcome and Approximate Levels of the Spans to be Covered	31
Figure 43: Illustrative Diagram of the Structural Components of an Arch Bridge - Reference Terminology in the Discussion - (Amir Khorraminejad, Mahmoud R. Shiravand, Mohammad Safi, 2022)	32
Figure 44: Illustrative Diagram of the Catenary and Parabolic Concept Applied to the Arch Structure - Objective of Pure Compression and Comparison with the Case of Pure Tension - (Gens F. , Design and Construction of Bridges - Chapter 03b-1 - Arch Bridges, 2024)	32
Figure 45: Schematic Illustration of the Thrust Line within the Longitudinal Section of the Arch - (Gens F. , Design and Construction of Bridges - Chapter 03b-1 - Arch Bridges, 2024)	33
Figure 46: Static Schemes of Arch Bridge Typologies with and without Hinges - (Gens F. , Design and Construction of Bridges - Chapter 03b-1 - Arch Bridges, 2024)	33
Figure 47: Static Resolution Scheme for Calculating Support Reactions - (Gens F. , Design and Construction of Bridges - Chapter 03b-1 - Arch Bridges, 2024)	34
Figure 48: Out of Plane Instability Scheme - (Gens F. , Design and Construction of Bridges - Chapter 03b-1 - Arch Bridges, 2024)	35
Figure 49: Snap-Through Instability Scheme - (Gens F. , Design and Construction of Bridges - Chapter 03b-1 - Arch Bridges, 2024)	35
Figure 50: In-Plane Asymmetric Instability Scheme and Simplification - (Gens F. , Design and Construction of Bridges - Chapter 03b-1 - Arch Bridges, 2024)	35
Figure 51: Explanatory Diagrams of the Three Described Cases with Different Stiffness Distributions in the Structure - (Gens F. , Design and Construction of Bridges - Chapter 03b-1 - Arch Bridges, 2024)	36
Figure 52: Bowstring Bridge Scheme - Compression and Tension Forces in the Structural Elements - (Gens F. , Design and Construction of Bridges - Chap 03b-2 - Bowstring Bridges, 2024)	37
Figure 53: Uniformed Distributed Load - Arch Behavior of the Bowstring Bridge - (Gens F. , Design and Construction of Bridges - Chap 03b-2 - Bowstring Bridges, 2024)	37
Figure 54: Static Scheme and Reaction Forces for the Bowstring Bridge - (Gens F. , Design and Construction of Bridges - Chap 03b-2 - Bowstring Bridges, 2024)	38
Figure 55: Bowstring Ideal Shape - Catenary - (Gens F. , Design and Construction of Bridges - Chap 03b-2 - Bowstring Bridges, 2024)	38
Figure 56: Explanatory Diagram of the Correct Positioning of Bracings - (Gens F. , Design and Construction of Bridges - Chap 03b-2 - Bowstring Bridges, 2024)	39
Figure 57: Hangers as Elastic Foundation of the Bowstring Bridge - (Gens F. , Design and Construction of Bridges - Chap 03b-2 - Bowstring Bridges, 2024)	39

Figure 58: Example of Lateral Safety Parapet – Pedestrian Bridge – (Aluminium Parapets with Perforated Panels, 2025)	40
Figure 59: Structural Level 1 - Graphical Representation of the Force Distribution	45
Figure 60: Structural Level 2 - Graphical Representation of the Force Distribution	46
Figure 61: Structural Level 3 - Graphical Representation of the Force Distribution	46
Figure 62: Structural Level 4- Graphical Representation of the Force Distribution	47
Figure 63: Exposure Zone Map - Snow Load for Belgium - National Belgian Annex	49
Figure 64: Recommended C_e Values - Selection of the Most Conservative Value	50
Figure 65: Description of the Dimensions and Directions in the Wind Calculation - EN 1991-1-5 ..	50
Figure 66: Empirical Computation of the $c_{fy,0}$ Factor in Relation to the “b/d” Ratio - EN 1991-1-5 ..	52
Figure 67: Empirical Computation of the $c_{fz,0}$ Factor in Relation to the “b/d” Ratio - EN 1991-1-5 ..	53
Figure 68: Table A2.2 - Recommended Values of ψ Factors for Footbridges	56
Figure 69: Five Deck Zones for Load Combination Analysis	57
Figure 70: Load Position - Condition 1 - Applied Loads on Deck Segments 1 & 2	57
Figure 71: Load Position - Condition 2 - Applied Loads on Deck Segment 3	57
Figure 72: Load Position - Condition 3 - Applied Loads on Deck Segments 4 & 5	58
Figure 73: Load Position - Condition 4 - Applied Loads on Deck Segments 2 & 3 & 4	58
Figure 74: Load Position – Condition 5 - Applied Loads on Deck Segments 1 & 5	58
Figure 75: Load Position - Condition 6 - Applied Loads on All Deck Segments	58
Figure 76: FEM Model: Structural Elements, Nodes and Nodal Connections	67
Figure 77: Global Structural View - Elements Grouped by Color	68
Figure 78: Global Structural View: (a) Analysis of the Cross-Sections of Structural Elements – (b) Color Scale	68
Figure 79: Properties of the Composite Cross-Section of the Structural Arch	69
Figure 80: Orientation of Structural Elements - Directional Arrows with Respect to the Local Axes of Element Orientation	69
Figure 81: Slab Areas - Definition of Slab Areas (in Blue) and Principal Layout Directions (in Bidirectional Red Arrows)	70
Figure 82: Representation of Vertical Forces Applied to the Structure – Monochromatic Polygons for the Distributed Loads on Structural Elements	71
Figure 83: Static Deformation – Permanent Loads	72
Figure 84: Static Deformation – Snow Load	72
Figure 85: Static Deformation – Wind Load	72
Figure 86: Static Deformation – Traffic Pedestrian Loads	72
Figure 87: Explanatory Representation of the Direction of Application of the Wind Lateral Force on the Structural “Right” Facade	73
Figure 88: Structural Front View: Deformation Under Permanent Loads – Asymmetrical Deflection of the Structural Arches	73
Figure 89: Axial Force F_x – Secondary Deck Beams. Maximum Compression: 11.36 kN, Maximum Tension: 4.53 kN	74
Figure 90: Shear Force F_y – Secondary Deck Beams. Maximum Shear Force: 47.15 kN	74
Figure 91: Bending Moment M_z – Secondary Deck Beams. Maximum Bending Moment: 37.72 kNm	75

Figure 92: Axial Force F_x –Primary Deck Beams. Maximum Compression: 271 kN, Maximum Tension: 413 kN	75
Figure 93: Shear Force F_y – Primary Deck Beams. Maximum Shear Force: 71 kN	75
Figure 94: Bending Moment M_z – Primary Deck Beams. Maximum Bending Moment: 162 kNm ..	75
Figure 95: Bending Moment M_y – Primary Deck Beams. Maximum Lateral Bending Moment: 4.57 kNm.....	76
Figure 96: Axial Force F_x – Primary Central Deck Beams. Maximum Compression: 274 kN, Maximum Tension: 420 kN.....	76
Figure 97: Shear Force F_y – Primary Central Deck Beams. Maximum Shear Force: 55 kN	76
Figure 98: Bending Moment M_z – Primary Central Deck Beams. Maximum Bending Moment: 339 kNm.....	76
Figure 99: Axial Force F_x – Central Deck Beams. Maximum Compression: 123 kN, Maximum Tension: 197 kN	77
Figure 100: Shear Force F_y – Central Deck Beams. Maximum Shear Force: 66 kN	77
Figure 101: Bending Moment M_z – Central Deck Beams. Maximum Bending Moment: 333 kNm ..	77
Figure 102: Axial Force F_x – Transversal Beams. Maximum Compression: 28.20 kN, Maximum Tension: 13.35 kN	78
Figure 103: Shear Force F_y – Transversal Beams. Maximum Shear Force: 161 kN	78
Figure 104: Bending Moment M_z – Transversal Beams. Maximum Bending Moment: 172 kNm ...	78
Figure 105: Axial Force F_x – Arch Beams. Maximum Compression: 2462 kN.....	79
Figure 106: Shear Force F_y – Arch Beams. Maximum Shear Force: 132 kN.....	79
Figure 107: Bending Moment M_z – Arch Beams. Maximum Bending Moment: 939 kNm.....	79
Figure 108: Bending Moment M_y – Arch Beams. Maximum Lateral Bending Moment: 287 kNm ..	79
Figure 109: Axial Force F_x – Vertical Hangers. Maximum Tension: 127 kN	80
Figure 110: Values of k_{def} for Timber and Wood-Based Material - (EN 1995 - Eurocode 5: Design of timber structures & Relative Annexes, 2004) Table 3.2	81
Figure 111: Components of Deflection - EN 1995 - 1 - 1 Figure 7.1	82
Figure 112: Value of k_{mod} - EN 1995-1-1 Table 3.1	84
Figure 113: Member on (a) Continuous and (b) Discrete Support - EN 1995-1-1 Figure 6.2.....	87
Figure 114: Curved Beam with the Fiber Direction Parallel to the Lower Edge of the Beam - Geometrical Dimensions for the Curved Elements and Definition of the Apex Zone - EN 1995-1-1 Figure 6.9	88
Figure 115: Effective Length as Ratio of the Span - EN 1995-1-1 Table 6.1	91
Figure 116: Static Scheme Description - Secondary Beams - Geometry and Applied Loads	92
Figure 117: Static Scheme Description – Primary Beams - Geometry and Applied Loads.....	93
Figure 118: Static Scheme Description – Primary Beams – Deck Central Position - Geometry and Applied Loads.....	94
Figure 119: Static Scheme Description – Central Beams – Deck Central Position - Geometry and Applied Loads.....	95
Figure 120: Static Scheme Description – Transversal Beams – Connection Deck-Arches - Geometry and Applied Loads	96
Figure 121: Static Scheme Description – Three-Hinged-Arch – Structural Arches - Geometry and Applied Loads.....	97
Figure 122: Composed Cross-Section - Arch	97

Figure 123: Arch Deformation – Permanent Loads G – Front View – $dz_{max} = 1.8$ cm	98
Figure 124: Arch Deformation – Variable Load Pedestrian Traffic Q1 – Front View – $dz_{max} = 1.34$ cm	98
Figure 125: Arch Deformation – Variable Load Wind Q2 – Front View – $dz_{max} = 1.54$ cm	98
Figure 126: Arch Deformation – Variable Load Snow Q3 – Front View – $dz_{max} = 0.4$ cm.....	98
Figure 127: Connection Design Proposal – Secondary to Primary Beams.....	103
Figure 128: Connection Design Proposal – Horizontal Beams to Structural Arches	104
Figure 129: Connection Design Proposal – Vertical Hangers to Structural Arches.....	104
Figure 130: Static Deformation - Structure under Negative Thermal Load	106
Figure 131: Static Deformation - Structure under Positive Thermal Load.....	106
Figure 132: Simplified FEM 2D - Arch Bridge - MATLAB Script.....	109
Figure 133: Amplified Deck Displacements - 6 First Natural Modes - MATLAB Script.....	110
Figure 134: Vertical Acceleration VS Natural Frequency - EC5 Part 2 - Annex B	112
Figure 135: Horizontal Acceleration VS Natural Frequency - EC5 Part 2 - Annex B.....	112
Figure 136: Relationship between the Vertical Fundamental Natural Frequency f_{vert} and the Coefficient k_{vert} - Figure B.1 EC5 Part 2 - Annex B	113
Figure 137: Relationship between the Horizontal Fundamental Natural Frequency f_{hor} and the Coefficient k_{hor} - Figure B.2 EC5 Part 2 - Annex B.....	113
Figure 138: Vertical Acceleration VS Number of Pedestrians – EC5 Part 2 - Annex B.....	114
Figure 139: Comparison Bar Chart – Cost in k€ per Unit Area in m^2 – Different Structural Solutions	121
Figure 140: Transportation Emissions VS Distance - Road VS Sea.....	125
Figure 141: Total Emissions $kgCO_2e \times 10^5$ - Comparison between Structural Solution & Difference from Highest Emission Solution	127
Figure 142: Distribution of Emissions by Phase - Timber Foot Bridge.....	128
Figure 143: Distribution of Emissions by Phase – Frame Bridge.....	128
Figure 144: Distribution of Emissions by Phase – Cable- Stayed Bridge	128
Figure 145: Distribution of Emissions by Phase – Arch Bridge	128
Figure 146: Comparative Trend of Emissions for all Solutions.....	130
Figure 147: Emissions per Usable m^2 - Comparison between Structural Solutions - Delta of Difference from the Highest.....	131
Figure 148: Total Emissions by Solution and Transport Mode.....	132
Figure 149: Pie Charts - Timber Solutions - Difference of Emissions by Phase - Road VS Sea Transport	133
Figure 150: (a) Energy Class by Structural Solution – (b) Legend - Classes from A to G	134
Rendering 1: Aerial View of the Pedestrian Bridge Over the Canal.....	42
Rendering 2: Longitudinal Perspective of the Bridge from the Riverbank	43
Rendering 3: Side View of the Bridge and Ramp Connection to the Ground	43
Rendering 4: Underside View of the Main Span Above the Water.....	44
Rendering 5: User Perspective from the Pedestrian Deck	44

TABLE OF TABLES

Table 1: State of Art - Analysis Table	8
Table 2: Typical Structural Typologies for Timber Bridges - (Crocetti, R., 2014), p.6	11
Table 3: Comparison Table – Calculation of Volumetric Footprint and Cost Estimation.....	30
Table 4: Timber Properties - (NBN EN 10480, 2013)	48
Table 5: Structural Permanent Loads - q [kg/m]	48
Table 6: Permanent Non- Structural Loads - Values in kg/m and kg/m ²	49
Table 7: Snow Weight Computation [kN/m ²]	50
Table 8: Loads Combination Factors	57
Table 9: Combination Matrix for the 6 Loads Conditions – ULS	62
Table 10: Combination Matrix for the 6 Loads Conditions – SLS Characteristic Combination	65
Table 11: Combination Matrix for the 6 Loads Conditions – SLS Frequent Combination	66
Table 12: Summary Table of Results - FEM Model - MasterSap 4U	80
Table 13: Formulas for the Computation of the w_{fin}	82
Table 14: Verification of the Geometric Dimensions - Arch 1.....	88
Table 15: Verification of the Geometric Dimensions - Arch 2.....	88
Table 16: Summary Table of Geometric Dimensions - Secondary Beams.....	92
Table 17: Vertical Deflections Control - SLS Verifications - Secondary Beams – Deck.....	92
Table 18: ULS Verifications - Secondary Beams – Deck	93
Table 19: Summary Table of Geometric Dimensions - Primary Beams	93
Table 20: Vertical Deflections Control - SLS Verifications – Primary Beams – Deck.....	93
Table 21: ULS Verifications – Primary Beams – Deck.....	94
Table 22: Summary Table of Geometric Dimensions - Primary Beams – Deck Central Position.....	94
Table 23: Vertical Deflections Control - SLS Verifications – Primary Beams – Deck Central Position	94
Table 24: ULS Verifications – Primary Beams – Deck Central Position.....	95
Table 25: Summary Table of Geometric Dimensions – Central Beams – Deck Central Position	95
Table 26: Vertical Deflections Control - SLS Verifications – Central Beams – Deck Central Position	95
Table 27: ULS Verifications – Central Beams – Deck Central Position.....	96
Table 28: Summary Table of Geometric Dimensions – Transversal Beams – Connection Deck-Arches	96
Table 29: Vertical Deflections Control - SLS Verifications – Transversal Beams – Connection Deck-Arches	96
Table 30: ULS Verifications – Transversal Beams – Connection Deck-Arches	97
Table 31: Summary Table of Geometric Dimensions – Arch Beams	97
Table 32: Vertical Deflections Control - SLS Verifications – Arch Beams	99
Table 33: Table of Coefficients and Factors – ULS Verifications – Arch Elements with Structural Apex.....	99
Table 34: ULS Verifications – Arch Beams	100
Table 35: Summary Table of Buckling Verifications Under Compression and Bending Moment Actions, in Both Principal Directions “y” and “z” – Actions also Considered in Combination.....	100
Table 36: Natural Frequencies – Modes 1–6	110
Table 37: Numerical Procedure – Calculation of the Maximum Value of Modal Acceleration	111

Table 38: SETRA Comfort Assessment - Values of the Maximum Modal Acceleration – Verification of the Criteria (max 0.7m/s^2).....	111
Table 39: Vertical and Horizontal Accelerations Formulas – EC5 Part 2 -Annex B	111
Table 40: Vertical and Horizontal Acceleration Under Pedestrian Flow – Variation of Values as a Function of n	113
Table 41: Pedestrian Load Configurations	116
Table 42: Table of Supposed Prices - €/m ³ - (Prezzario Regione Campania - Prezzario Lavori, 2025)	118
Table 43: Volumetric & Price Evaluation of the Structural Elements - Timber Foot Bridge	119
Table 44: Supposed Prices for Alternative Structural Solutions - €/m ³ - (Prezzario Regione Campania - Prezzario Lavori, 2025)	119
Table 45: Volumetric & Price Evaluation of the Structural Elements – Cable Stayed Bridge - (Prezzario Regione Campania - Prezzario Lavori, 2025)	120
Table 46: Volumetric & Price Evaluation of the Structural Elements – Single Arch & Frame Bridge - (Prezzario Regione Campania - Prezzario Lavori, 2025)	120
Table 47: Volumetric & Price Evaluation of the Structural Elements – Frame Bridge - (Prezzario Regione Campania - Prezzario Lavori, 2025).....	121
Table 48: Comparison of Structural Results in Price Evaluation - [k€] & [k€/m ²]	121
Table 49: Emissions Factors [kgCO ₂ e/kg] - (Embodied Carbon - The ICE Database - Version 4.0, 2024)	124
Table 50: Total Emissions kgCO ₂ e x10 ⁵ – Round Up.....	127
Table 51: Total Emissions per Usable m ² - Delta from the Highest	132
Table 52: Energy Classes - Definition of the Classes Range of Values [kgCO ₂ e/m ²]	134

ABSTRACT

This master's thesis aims to study the design and structural verification of a timber pedestrian bridge, conceived within the framework of the Seine-Escaut Est project in Wallonia, with specific reference to Sector 5 of the Nimy-Blaton-Péronnes Canal. The study is part of a broader comparison between alternative structural solutions using different construction materials, with the objective of proposing an alternative and contemporary design based on a sustainable material such as timber.

The structure of the thesis is divided into two main parts: The first part provides an introductory overview with an analysis of the infrastructural and territorial context; the second part adopts a technical-engineering perspective, focusing entirely on the design choices, limit state verifications, and dynamic comfort assessment of the structure.

Following a critical review of the historical evolution and typologies of timber bridges, a comparative conceptual analysis of different preliminary design solutions is conducted, leading to the selection of a glulam arch bridge as the optimal configuration. This choice is justified by its static performance, aesthetic qualities, and environmental benefits. The selected structure is then modelled and analyzed using finite element software, evaluating internal stresses, displacements, and dynamic response under pedestrian loading.

The verifications are carried out in accordance with the provisions of Eurocode 5, with particular attention to Ultimate Limit States (ULS) and Serviceability Limit States (SLS), including phenomena such as lateral-torsional instability and the effects of temperature gradients. A pedestrian comfort assessment is also conducted through modal analysis and verifications based on specific standards, including theoretical considerations regarding the study of dynamic behavior in the time domain and possible implementations for vibration mitigation (Tuned Mass Damper, TMD).

The study concludes with a comparative technical and economic analysis of alternative construction materials (timber, steel, and concrete), alongside an environmental sustainability assessment based on the calculation of the CO₂ footprint and the energy classification of the structure. The results, following a thorough analysis, confirm the validity of the adopted solution and highlight the potential of timber as an efficient and sustainable construction material, even in the context of pedestrian infrastructure.

1 CASE STUDY OVERVIEW

This study is specifically focused on the constructability and structural performance of a medium-span pedestrian bridge, constructed using timber as the primary structural material. The research is conducted within the context of the Seine-Escaut Est project, which aims to enhance the navigability of the waterway connecting the Escaut and Meuse basins. The study is particularly centered on a technical proposal for a structural solution located within Sector 5 of the Nimy-Blaton-Péronnes Canal, where a new quay wall and a crossing structure are planned to accommodate utility pipelines and potentially pedestrian traffic.

Currently, the engineering firm *Bureau Greisch* has carried out a preliminary design and structural analysis, considering steel and concrete as potential materials for the solution. This has resulted in three structural preliminary design proposals, which are presented in the following figures (*Figure 1*, *Figure 2*, *Figure 3*).

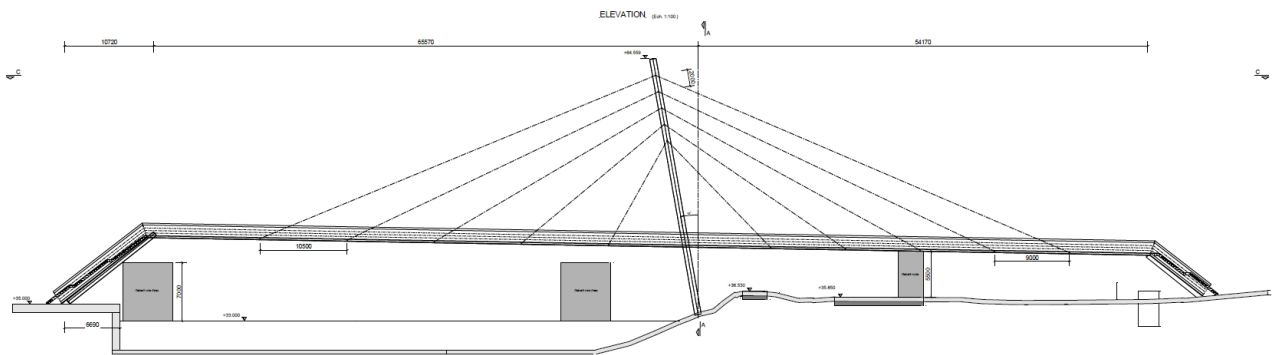


Figure 1: Pre-Design Proposal 1 - Cable Stayed Bridge - Steel and Concrete – Bureau Greisch

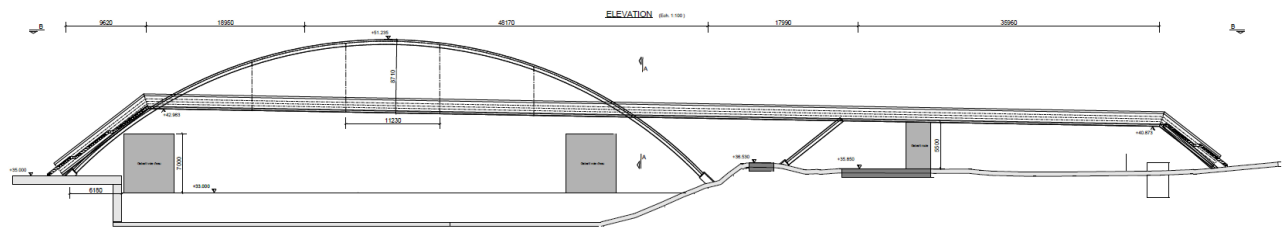


Figure 2: Pre-Design Proposal 2 - Arch Bridge - Steel and Concrete - Bureau Greisch

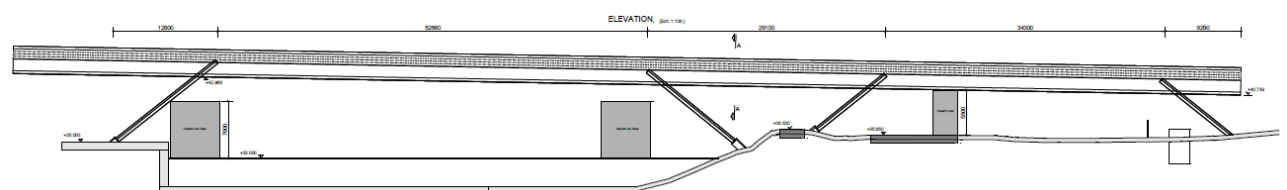


Figure 3: Pre-Design Proposal 3 - Frame Bridge - Steel and Concrete - Bureau Greisch

Although timber was initially considered a possible construction material, the lack of well-established references for similar applications led to the initial dismissal of this option.

This context directly defines the objective of the present master thesis: To conduct a structural and economic feasibility assessment of a timber-based solution and establish design guidelines that could facilitate its implementation. If a timber pre-design solution can be successfully developed, it will then be critically compared with the pre-designs in other structural materials conducted by Bureau Greisch, evaluating aspects such as weight, cost, durability, and technical feasibility.

The study further explores different structural solutions for bridges, focusing on structural performance, material limitations, and durability aspects. Based on the geometrical constraints imposed by the site, various pre-design proposals are developed. These proposals, analyzed in a dedicated chapter, are initially calculated and dimensioned to assess their feasibility in terms of real-world implementation.

Subsequently, the study shifts towards detailed structural calculations for the selected timber-based solution among those proposed in the pre-design phase. For this solution, a Finite Element Model (FEM) is developed, including analysis of results, structural computations, element sizing, and connection considerations, with specific calculations where required.

The focus then moves to a comparative analysis between the previous steel and concrete-based solutions and the timber implementation. From this, a technical and economic feasibility study is conducted, comparing material quantities, environmental sustainability, and CO₂ footprint among the different solutions.

Modal vibration analysis of the structure is also included, along with verifications of acceleration and frequency levels in accordance with specific code-based limits. Basic theoretical concepts related to vibration analysis and comfort evaluation in the time domain are presented, as well as the modeling of the force as a function of space and time. Additionally, hypotheses are introduced for the implementation of vibration mitigation elements, such as Tuned Mass Dampers (TMD).

Finally, the study concludes with considerations on the calculations and results obtained, analyzed from a purely engineering perspective, aiming to assess the most viable structural solution for implementation.

1.1 THE SEINE-ESCAUT EST PROJECT IN WALLONIA

The Seine-Escaut Est (SEE) Project is a European initiative aimed at improving inland waterway transport between Belgium and France. In the Wallonia region, in particular, the project's objective is to modernize approximately 200 kilometers of waterways to allow the transit of higher-capacity vessels, such as those classified as ECTM Va (up to 2,000 tons). This modernization process consists of a series of structural interventions, including the reinforcement and adaptation of bridges at key locations, the expansion of locks, and the rectification of river bends. The goal is to enhance the capacity and efficiency of the navigation network¹ (Figure 4).



Figure 4: Le Projet du Réseau Seine-Escaut - (Le Projet Seine - Escaut, 2022)

The engineering firm Bureau Greisch has already played a significant role in this project, having developed the bimodal platform at Pont Rouge in Comines-Warneton, which includes the construction of a quay approximately 235 meters long, designed to accommodate two Class Va vessels of 110 meters in length each simultaneously. This intervention highlights the project's overarching goal and commitment to creating multimodal transport solutions, integrating the inland waterway network with road infrastructures to optimize logistical operations².

¹ (Programme Seine-Escaut Est, 2021)

² (Pont Rouge Harbour Platform in Comines-Warneton, 2020)

From a broader perspective, the SEE project's final objective is to strengthen the position of the Wallonia region within the European transport network by improving the interconnection between the Seine and Scheldt River basins. Ultimately, this initiative aims to promote regional economic growth and provide a sustainable alternative to road transport, thereby reducing environmental impact and traffic congestion³.

1.2 SECTOR 5 OF THE NIMY-BLATON-PÉRONNES CANAL WITHIN THE SEINE-ESCAUT EST PROJECT

The Nimy-Blaton-Péronnes Canal is a Belgian navigable waterway that serves as a connection between Nimy, near Mons, and Péronnes, where it joins the Scheldt River. It was inaugurated between 1955 and 1964, with a total length of 38.9 kilometers, crossing the province of Hainaut⁴.

This canal is included within the scope of the Seine-Escaut Est project, undergoing modernization interventions that align with the general directives of the parent project, as described in the previous subchapter. These upgrades involve adapting the canal to accommodate vessels up to 2,000 tons (CEMT Va class). Originally designed for convoys of 600 tons (CEMT II class), the canal was later modified to support convoys of 1,350 tons (CEMT IV class). However, it still features a succession of narrow sections and tight bends that limit the bidirectional navigation of Class Va vessels, making navigation less efficient.

To improve navigability, widening interventions have been planned for five sections of the canal. Specifically, two crossing zones will be created to reduce the maximum length of a single-lane section to 2.4 kilometers, while three additional zones will address sharp curvature and narrow width, which currently act as bottlenecks limiting the smooth flow of traffic. In total, these interventions will involve a stretch of 2,400 meters of embankments⁵.

³ (Programme Seine-Escaut Est, 2021)

⁴ (Canal Nimy-Blaton-Péronnes, 2025)

⁵ (Widening of the Nimy-Blaton Canal, 2020)

2 HISTORICAL AND TYPOLOGICAL ANALYSIS OF TIMBER BRIDGES

Timber bridges have experienced a renaissance in recent decades due to their sustainability, aesthetic appeal, and advancements in engineered wood materials and connection techniques.

While timber was historically a predominant bridge-building material, it was largely replaced by steel and reinforced concrete during the 19th and 20th centuries.

However, growing environmental concerns, improved durability strategies, and successful modern projects have renewed interest in timber as a competitive alternative to conventional bridge construction materials.⁶

2.1 HISTORICAL DEVELOPMENT OF TIMBER BRIDGES

Wooden bridges have a long-standing history, originating in ancient civilizations where timber was regarded as a primary material in structural engineering. One of the earliest large-scale wooden bridges that can be historically dated was constructed by Julius Caesar over the Rhine River in 55BCE (*Figure 5*).

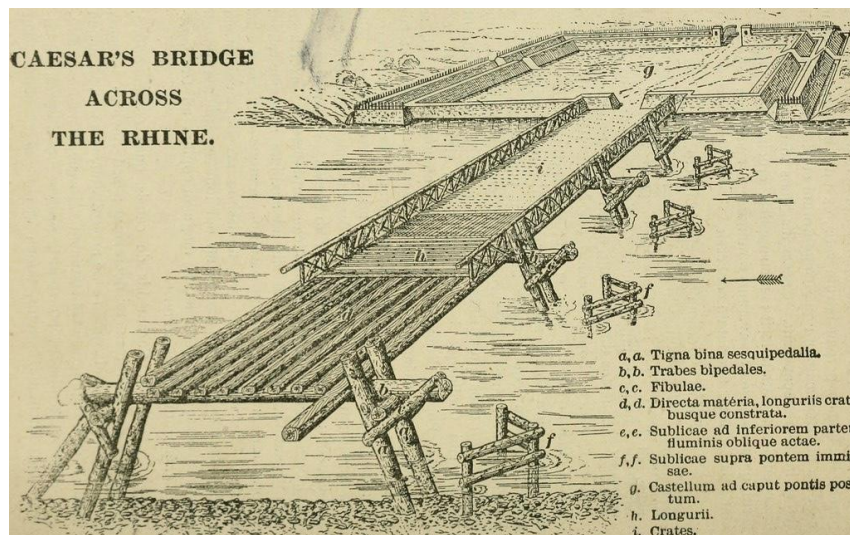


Figure 5: Cesar's Bridge across the Rhine - (*Rome versus the Germans, Part II, 2019*)

This bridge, built within a span of ten days using wooden piles and beams, exemplifies the strategic and military significance of timber bridge construction during that era⁷.

During the Renaissance period, architect Andrea Palladio made significant contributions to the evolutionary process of structural technologies for timber bridges and their design methodology. A particularly notable example is his "Ponte degli Alpini" (1567), located in Bassano del Grappa, Italy (*Figure 6*).

⁶ (Crocetti, R., 2014), p.3; (Bell, K., 2006), p.1

⁷ (Bell, K., 2006), p.2



Figure 6: Ponte degli Alpini, Bassano del Grappa, Italy - (Ponte degli alpini, 2019)

This structure represents a remarkable instance of a covered wooden bridge, specifically designed for both durability and aesthetic appeal. Palladio's approach incorporated the use of a truss structural system, enabling an efficient load distribution mechanism while simultaneously extending the lifespan of the construction.⁸

Moving to Switzerland, Johannes and Hans-Ulrich Grubenmann significantly revolutionized timber bridge engineering in the 18th century by constructing bridges with remarkably large spans, eliminating the need for intermediate supports. One of their most renowned structures, the Schaffhausen Bridge over the Rhine (*Figure 7*), built between 1755 and 1758, featured an unprecedented span of 120 meters, demonstrating a pioneering advancement in timber bridge construction techniques.⁹

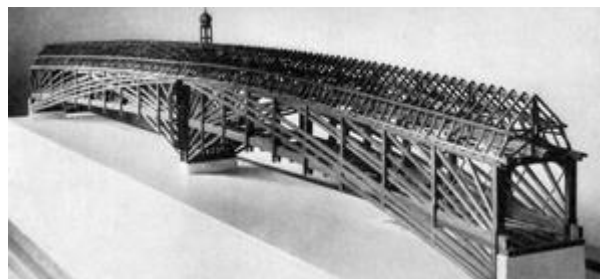


Figure 7: Model of the Main Structural Members of the Timber Bridge over the Rhine River in Schaffhausen, Switzerland - (Model of the main structural members of the timber bridge over the Rhine River in Schaffhausen, Switzerland., 2017)

Their innovative use of truss and engineering knowledge allowed them to achieve record-breaking spans that were previously thought impossible for timber structures.

⁸ (Crocetti, R., 2014), p.3

⁹ (Crocetti, R., 2014), p.4

The 19th century witnessed significant advancements in timber bridge design, with further refinements in engineering methodologies. A key figure of this period was Isambard Kingdom Brunel, who applied timber as structural material in railway bridge construction. His “Moorswater Viaduct” (*Figure 8*), built in 1859 in Great Britain, exemplified an innovative hybrid approach, combining timber and masonry to achieve a structurally efficient and cost-effective solution for a 290-meter-long span.¹⁰ This marked one of the last large-scale uses of timber before steel and reinforced concrete became dominant.



Figure 8: Walkham Viaduct - (Brunel's Timber Viaducts, 2007)

Despite the shift to modern materials in the late 19th and early 20th centuries, timber bridges persisted in some regions, particularly for short spans and pedestrian applications. In North America, the “Cascade Bridge” in the United States, constructed in 1845 by Thomson Brown, was an early example of a hybrid truss-arch design spanning 90 meters.¹¹

Although largely replaced by concrete and steel, from the 1990s onward, timber has undergone significant reassessment as a structural material for bridge construction. This renewed interest has been driven by its environmental sustainability, positioning timber as a viable and eco-friendly alternative into modern engineering practices. Countries such as Sweden, Norway, and Finland have led the way in developing modern timber bridges, leveraging advanced wood engineering techniques such as stress laminated timber decks and glulam arches to create durable, aesthetically pleasing structures.¹²

¹⁰ (Bell, K., 2006), p.3

¹¹ (Bell, K., 2006), p.4

¹² (Crocetti, R., 2014), p.6

2.2 CURRENT STATE OF THE ART IN TIMBER BRIDGES

To conduct a comprehensive study of the so-called "State of the Art" in timber bridge construction, an analysis was carried out on various examples of structural solutions that have already been adopted and built worldwide. This study followed a geographically diverse approach, identifying and examining these structures from both a structural and material perspective.

As a preliminary phase, a data collection process was conducted to gather relevant examples of this type of construction. The collected data is presented in *Annex 1*, where each selected timber bridge is analyzed in detail and graphically illustrated.

To ensure clarity and practical usability of the findings derived from the historical data analysis, a summary and explanatory table has been compiled. This table includes key information such as the bridge name, structural typology, maximum span length (in meters), and the primary construction material used. The table is presented below (*Table 1*):

BRIDGE NAME	STRUCTURAL TYPOLOGY	CONSTRUCTION MATERIAL	CONSTRUCTION METHOD	SPAN (m)
Flisa Bridge	Hybrid Arch-Truss	Glulam, Steel	Prefabricated, Assembled On-Site	70
Tynset Bridge	Timber Arch	Glulam, Concrete	Prefabricated, Assembled On-Site	70
Evenstad Bridge	Hybrid Arch-Truss	Glulam, Steel, Concrete	Prefabricated, Assembled On-Site	36
Mistissin Bridge	Timber Arch	Glulam, Concrete	Prefabricated, Assembled On-Site	43
Norsenga Bridge	Hybrid Arch-Truss	Glulam, Steel	Prefabricated, Assembled On-Site	94.5
Gangru Levert Til Favang	Pre-Stressed Glulam Beam	Glulam	Prefabricated, Assembled On-Site	23
Cubillas Foot Bridge	Timber Arch	Glulam, Steel	Prefabricated, Assembled On-Site	46
Betanzos Wood Foot Bridge	Timber Arch	Glulam, Concrete	Prefabricated, Assembled On-Site	40
Castor River Wooden Foot Bridge	Truss	Glulam	Prefabricated, Assembled On-Site	32
Anillo Verde Foot Bridge	Timber Arch	Glulam	Prefabricated, Assembled On-Site	61
Passerelle Mangin	Timber Arch	Glulam, Steel	Constructed On-Site	40
Aube Foot Bridge	Timber Arch	Glulam, Steel	Prefabricated, Assembled On-Site	50
Arroyo Guadalobón Foot Bridge	Timber Arch	Glulam, Steel	Prefabricated, Assembled On-Site	42
Arroyo Gui Foot Bridge	Hybrid Arch-Truss	Glulam, Steel	Prefabricated, Assembled On-Site	30
Guadalhorce Bridge	Timber Arch	Glulam	Prefabricated, Assembled On-Site	70
Penafiel Bridge	Timber Arch	Glulam, Steel	Prefabricated, Assembled On-Site	50
River Calore Bridge	Hybrid Cable-Stayed & Timber Arch	Glulam, Steel, Concrete	Prefabricated, Assembled On-Site	70

Table 1: State of Art - Analysis Table

Based on the collected data, two explanatory diagrams have been developed to illustrate the structural characteristics of the analyzed timber bridges.

The first aspect examined is the maximum span length of the bridges under investigation.

As shown in the next figure (*Figure 9*), the general trend indicates a predominance of relatively short spans, particularly when compared to the maximum spans achievable with steel and concrete bridges.

The longest recorded span within the analyzed dataset reaches 94.5 meters, as observed in the “Norsenga Bridge”. Beyond this, the longest spans within the series stabilize at approximately 70 meters. When compared to the maximum free spans of steel and concrete bridges, timber structures typically exhibit a span ratio of approximately 1/5 or 1/4, highlighting a significant limitation in span length relative to alternative construction materials.¹³

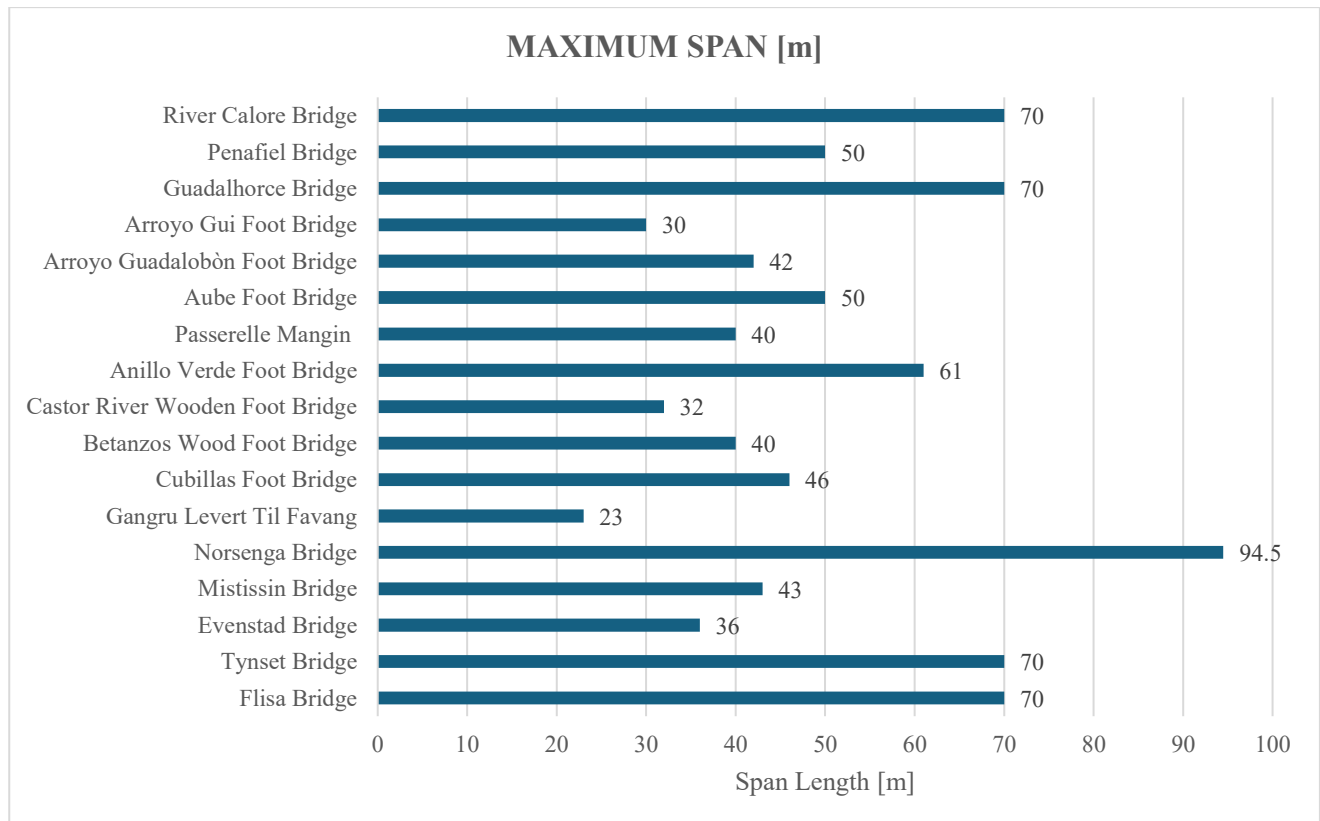


Figure 9: Table of Maximum Spans - Analyzed Bridges

Further analysis can be conducted based on the structural typologies adopted in the examined bridges. To enhance the clarity and comprehensibility of the results, this analysis is represented using a pie chart, which illustrates the relative percentage of each structural typology in relation to the total number of bridges analyzed.

¹³ A reference value is considered for the maximum construction length of an arch structural solution in steel, which reaches 518 meters, while a beam structure with a truss system extends to approximately 530 meters. These data are derived from the document (and Construction of Bridges, Frederic Gens).

This graphical representation provides an intuitive overview of the distribution of construction typologies within the dataset, facilitating a direct comparison of their prevalence. The corresponding *Figure 10* can be visualized below:

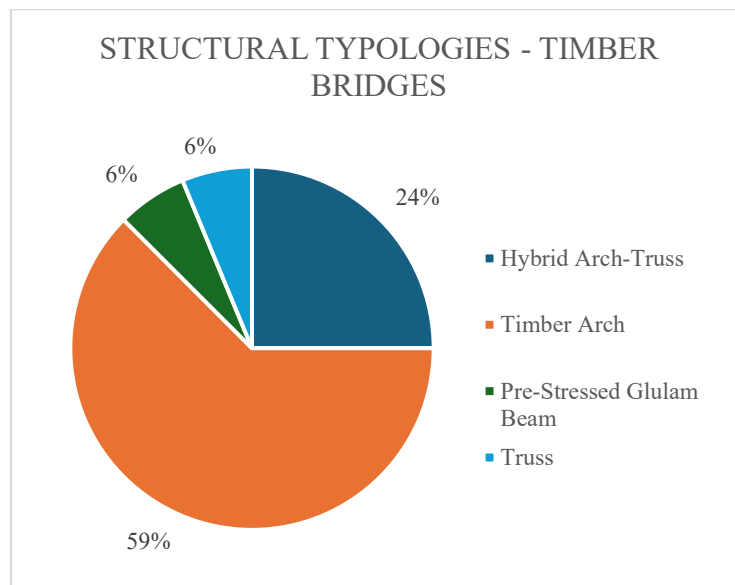


Figure 10: Structural Typologies – Timber Bridges – Pie Chart [%]

Out of a total of 17 examined bridges, 10 (59%) adopt an arch structural configuration. A noteworthy aspect is that this configuration is also found in combination with a truss system. More complex solutions are generally considered for structures requiring greater spans and distances to be covered, as well as for those subjected to higher loads compared to pedestrian bridges.

The use of an arch or truss structure emphasizes the characteristics of the construction material, which exhibits a notable compressive and tensile capacity in the direction parallel to its fibers, leading to a plastic failure mechanism (for the compression case) and a brittle failure mechanism (for the tension case).¹⁴ This also explains why, historically, timber bridges with larger spans were designed using structural systems that replicated the arch itself. By functioning primarily in compression, these systems optimize and fully exploit the mechanical properties of the material.

2.3 STRUCTURAL CLASSIFICATIONS OF TIMBER BRIDGES

Based on the findings from the analysis of the "State of the Art" and the discussions in the previous chapter, a more detailed examination is now conducted on the structural typologies applicable to timber bridges. These typologies have a direct influence on the achievable span length and the overall load-bearing performance.

¹⁴ The strength of the wood depends significantly on the type of stress (tension, compression, shear etc..) and the orientation of the load relative to the grain direction: Generally speaking, the tensile resistance parallel to the grains $f_{t,0}$, is more or less equal to 2-3 times the compression resistance parallel to the grains $f_{c,0}$ (in absence of defects) or lower of the same.

A formal classification of the main categories is presented below. It is important to note that some categories are included even though they were not covered in the data collection phase, as they pertain to spans and structural configurations that are excessively large and complex for the ultimate scope of this study.

Before proceeding with the explanation of individual structural technologies, an explanatory table summarizing the possible configurations is presented in the following table (*Table 2*).


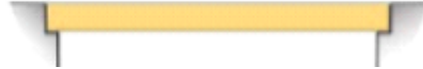


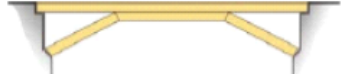


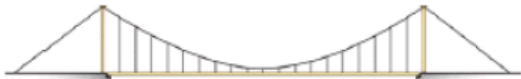

BRIDGE TYPE	STRUCTURE	TYPICAL SPAN [m]
	SLTD (*) ¹⁵	0-25
	Beams	0-30
	Truss	15-70
	King Post	10-50
	Strut Frame	20-40
	Beam on V-Supports	20-75
	Arch	30-70
	Suspension (**) ¹⁶	50-200
	Cable-Stayed	40-100

Table 2: Typical Structural Typologies for Timber Bridges - (Crocetti, R., 2014), p.6

¹⁵ (*): Stress Laminated Timber Deck

¹⁶ (**): For longer spans a heavy deck or prestressing of the main cables by means of a secondary cable system is normally required to limit displacements and vibrations. (Crocetti, R., 2014), p.6

2.3.1 STRESS LAMINATED DECK (SLTD) BRIDGES

SLTD bridges are an innovative timber bridge design, where wooden laminations are pre-stressed with high-strength steel rods to act as an orthotropic plate. This design is commonly used in Nordic countries due to its simple manufacturing and effective load distribution properties.¹⁷

2.3.2 BEAM BRIDGES

Beam bridges represent the simplest form of timber bridge construction. They are typically implemented using glue-laminated (glulam) beams positioned beneath the deck, which consist of longitudinal planks or laminated panels. This typology is particularly suitable for pedestrian use or small roadway crossings and generally features a span length not exceeding 30 meters.¹⁸

2.3.3 TRUSS BRIDGES

Truss bridges utilize a framework of timber members connected in a triangular arrangement to efficiently transfer loads. They can achieve spans of up to 70 meters and provide increased stiffness. Common truss types include king post, queen post, and Howe trusses.¹⁹

2.3.4 ARCH BRIDGES

Arch bridges emphasize the compressive strength of timber, often utilizing glulam technology to create curved or parabolic structures that follow the arch's natural shape. These bridges can achieve spans ranging from 30 to 70 meters²⁰, as observed in the well-documented “Tynset Bridge” in Norway.

2.3.5 SUSPENSION AND CABLE-STAYED BRIDGES

This structural solution is generally implemented for very long spans, with timber elements that can be integrated into suspended or cable-stayed systems. By adopting this design, spans of up to 200 meters can be achieved; however, the use of steel components is necessary to enhance structural stability and load-bearing capacity.²¹

2.4 MATERIALS AND CONNECTION TECHNIQUES

Timber bridges rely exclusively on the use of engineered materials to enhance structural performance and longevity. The primary materials used include:

- Glue-Laminated Timber (Glulam): Material that provides high strength and flexibility, allowing for the creation of curved elements and large cross-sections. It is commonly used in arch structures and beam solutions.
- Laminated Veneer Lumber (LVL): System that provides superior load resistance and dimensional stability, making it an ideal material for deck panels and structural elements responsible for supporting the primary loads.

¹⁷ (Bell, K., 2006), p.9

¹⁸ (Crocetti, R., 2014), p.6

¹⁹ (Bell, K., 2006), p.6

²⁰ (Crocetti, R., 2014), p.5

²¹ (Crocetti, R., 2014), p.6

- Cross-Laminated Timber (CLT): System composed of layers arranged perpendicularly to each other to enhance stiffness and load distribution, commonly applied in deck systems.

A detailed description of the various structural possibilities, along with an analysis of the physical and mechanical properties, is provided in *Annex 2*.

The durability and stability of timber bridges are directly linked to the effectiveness of connection systems. In this context, the following main connection systems can be classified:

- Bolted and Doweled Joints: Primarily used in connections for truss or beam systems, they require a precise installation procedure and proper protection against moisture.
- Slotted-in Steel Plates with Dowels: Ensures a high transfer capacity and is commonly used in large Nordic timber bridges (*Figure 11*).

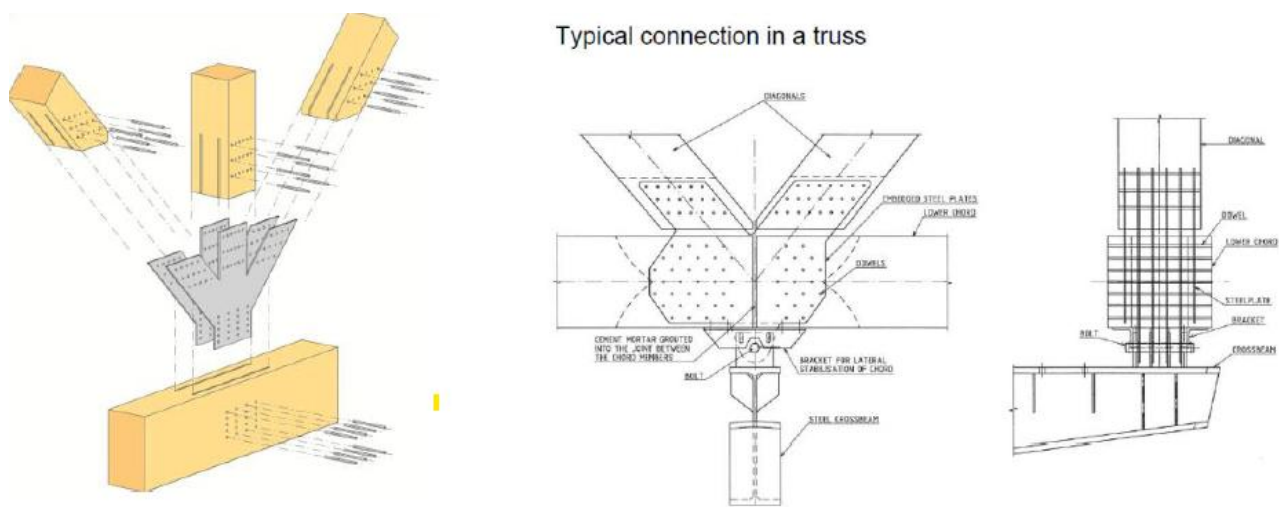


Figure 11: Slotted-In Steel Plates with Dowels Connection Typology²² - (Crocetti, R., 2014), p.9

- Bonded-in Rods and Self-Tapping Screws: They provide high joint stiffness and reduce the need for maintenance throughout the structure's lifespan.

²² Connection with slotted-in plates and dowels. Left: Exploded view of a typical connection. Centre: Elevation of a truss node (timber lower chord, timber diagonals and steel hanger). Right: Cross section of another truss node (timber lower chord, timber diagonal and cross beam of steel).

3 PRELIMINARY DESIGN AND FINAL PROPOSAL SELECTION

Based on the conducted state-of-the-art analysis, along with the collected data and considerations, a structured approach is developed to address the subject problem. The key aspect in the proper development of this study is the identification of a robust and elegant design that fully responds to the project requirements while ensuring technical and economic feasibility as well as environmental sustainability.

To this end, different structural preliminary design proposals are developed, each of which is described and graphically represented in detail to ensure a clear and structured decision-making process.

At the end of the section is presented a brief description of the selected structural scheme and technology underlying the computational analysis and pre-design process. This includes an overview of the key characteristics of the chosen structural typology, an analysis of instability and response to horizontal loads, and a focus on the primary construction methods. Justifications for the design choices are provided, along with explanatory clarifications concerning the structural components.

3.1 PRELIMINARY DESIGN PROPOSAL 1

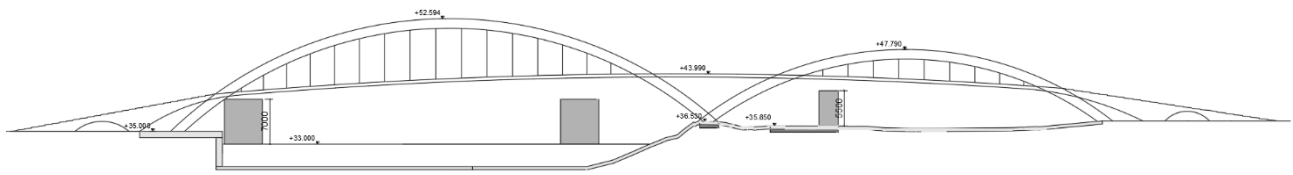


Figure 12: Pre-design Proposal 1 - Architectonic Frontal View

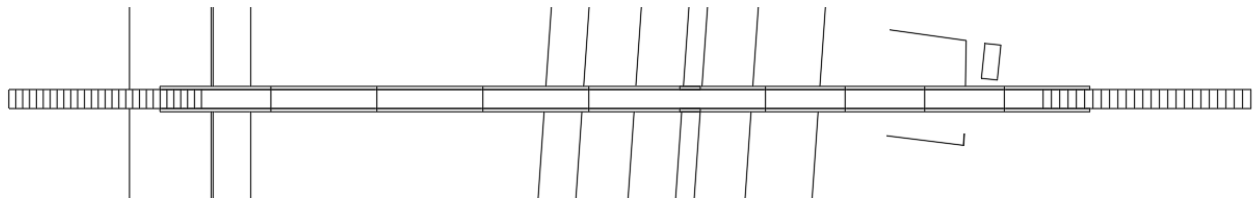


Figure 13: Pre-design Proposal 1 - Architectonic Top View

The initial pre-design proposal, developed and carried forward with brief preliminary sizing considerations of the constituent elements, is illustrated in *Figure 12* & *Figure 13*.

This solution involves the creation of two structural arches, hinged at their bases on both the right and left sides, which support the deck structure through steel tie rods. The deck itself exhibits a slight inclination in both directions, resulting in a geometry resembling that of a lowered arch.

Furthermore, the central section of the deck, which connects the two structural arches, is not supported by vertical tie rods but is entirely supported at its sides by the previously described structural arches.

Based on these considerations, which are primarily aesthetic and architectural rather than structural, the analysis shifts towards an evaluation of the system from the perspective of significant compositional schemes and the conceived load distribution.

The two consecutive arches are thus conceptualized as composed of two three-hinged arches (*Figure 14 & Figure 15*): This decision simplifies the engineering problem by creating two statically determinate elements subjected to concentrated loads distributed along the structural system. The concentrated loads originate from the vertical tie rods and are equal in magnitude and opposite to the vertical reactions generated by the decks support on the steel tie rods.

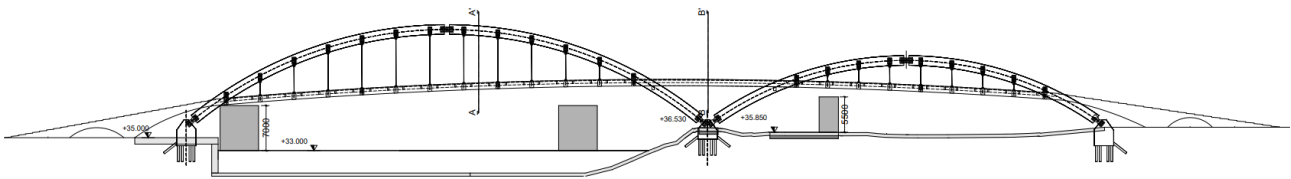


Figure 14: Pre-design Proposal 1 - Structural Front View

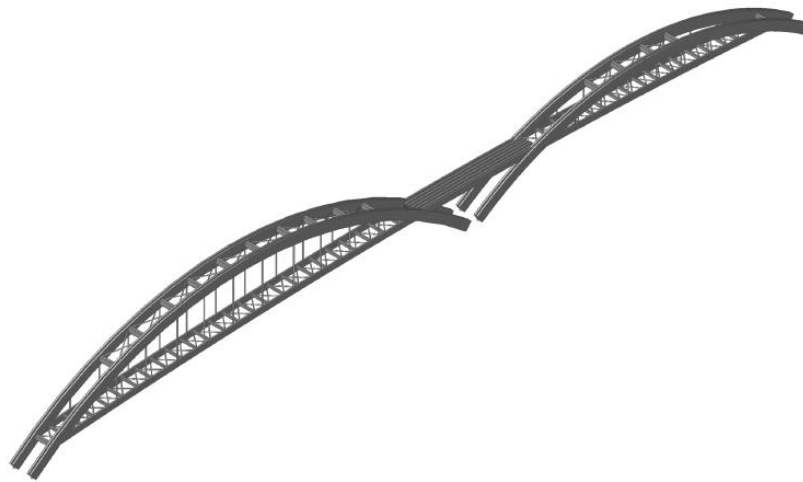


Figure 15: Pre-design Proposal 1 - 3D Structural Isometric View - SCIA Engineering

To further streamline the structural scheme, the base hinge connections are positioned at the same elevation: This results in a symmetrically defined and loaded three-hinged arch, thereby simplifying the structural analysis and resolution schemes (*Figure 16*).

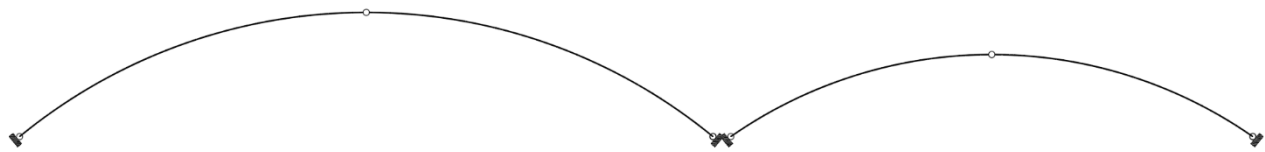


Figure 16: Three-Hinged-Arches Schematization

The deck is conceived as being composed of GL26 beam elements, all of identical dimensions (approximately 21.2 meters in length), supported by multiple simple supports (four in this case), which are constituted by the vertical tie rods themselves. In this way, the vertical reaction generated by the loads acting on the deck (which function as simple supports for the deck beams) is transmitted as a concentrated load onto the overlying structural arch.

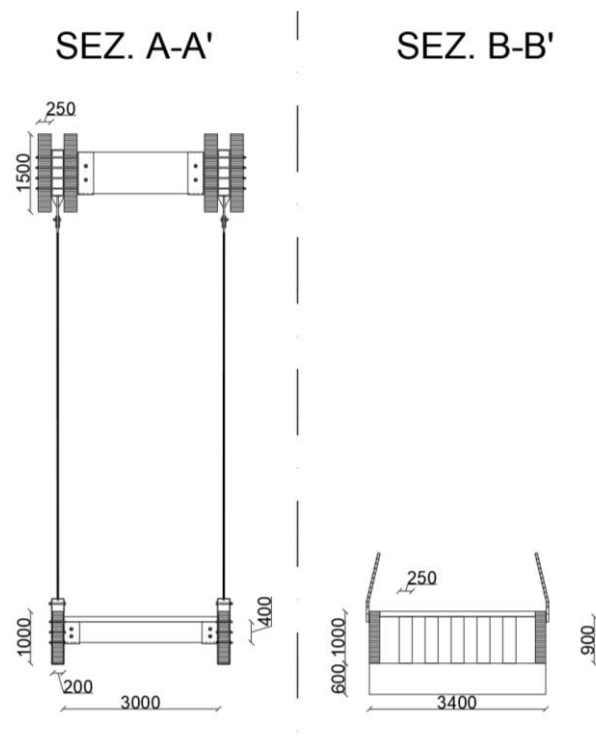


Figure 17: (a) Section A-A' with "Hangers - Deck - Double Arch" Connection; (b) Section B-B' with Deck-Lateral Barrier.

The deck section (Figure 17) features two support planes to which the steel tie rods are connected. These planes are composed of two primary beams, initially assumed to have a cross-section of 1.0x0.2 meters ($h \times b$). These primary beams support secondary beams, spaced approximately 2.6 meters apart, made of GL24 timber with a cross-section of 0.2x0.4 meters and a length of 3 meters. The secondary beams are designed as simply supported on the two lateral primary beams.

The secondary beams support the decking system, which is assumed to consist of wooden planks arranged parallel to each other. Below the secondary beams, six DN200 pipes are positioned, in accordance with the client's request. These pipes are fixed to the secondary beams by means of a steel connection system, which was not designed at this stage of the analysis. (Figure 18).

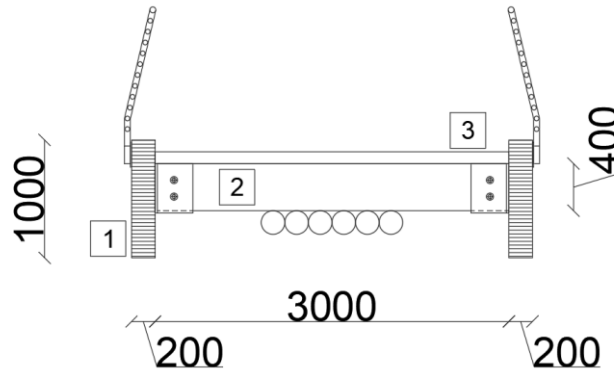


Figure 18: Deck Proposed Section with Structural Element Dimensions²³

Further attention must be given to the connections to be implemented:

- Connection between the primary beam of the deck and the vertical tie rod: This connection is conceived as a steel frame that encloses the beam at the designated connection points, bolted to it to generate a hinge-like behavior (*Figure 19*). This ensures compliance with the assumed static scheme of beam supported on multiple simple supports.

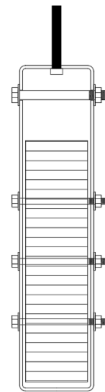


Figure 19: Connection Scheme of the Primary Beam of the Deck with Vertical Tie Rods

- Connection between the deck and the double structural arch: To ensure the proper fixation of the deck to the structural support, the two structural arches are spaced apart by a sufficient distance to allow the passage of the primary beam of the deck, which in this case is assumed to have a width of 0.2 m.
- Connection between vertical tie rods and the double structural arch: Following the considerations outlined in the previous point, the connection of the vertical tie rods to the

²³ Description of elements: 1 - Primary beam (1.0 x 0.2 m); 2 - Secondary beam (0.2 x 0.4 m); 3 - Decking system, Pipes 6 x DN200 and Lateral protection barrier.

arches is achieved through a metallic element positioned in the middle of the space between the two support planes. This connection system is bolted to both lateral arches to secure the structure and ensure the proper transmission of forces (*Figure 20*).

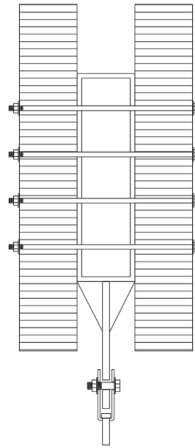


Figure 20: Connection Scheme of Vertical Tie Rods with Double Three-Hinged Arch

3.1.1 ANALYSIS OF POTENTIAL CRITICAL ISSUES

The proposed solution requires careful attention during the design phase, particularly in the deck section located between the two structural arches. This section spans considerable distance and is simply supported between the arches, transferring its self-weight and variable loads to the two lateral supports (*Figure 21*). The primary objective is to ensure that the external profile of the deck remains as linear and uniform as possible, thereby creating a structure that is not only efficient but also aesthetically pleasing and well-integrated into its surrounding context.

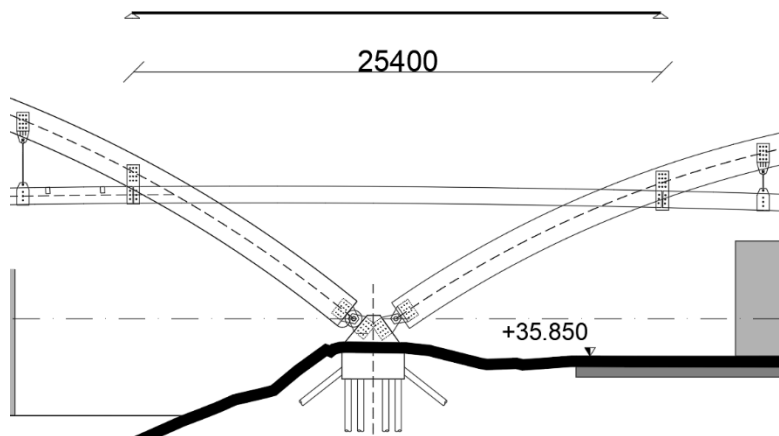


Figure 21: Illustration of the Deck Section with a Support Span of 25.4 meters and Double Simple Lateral Support.

This beam spans a significant distance of 25.4 meters and, within its static scheme, generates a considerable positive bending moment in the inflection zones compared to the moments that may develop in the respective multi-span beams located in the central areas of the arches. Consequently, it is crucial to develop a design solution that does not lead to an increase in the section of the primary beam solely in the "suspended" connection segment between the two structural arches.

To address this, the proposed solution involves designing the central deck section with multiple primary beams of identical cross-section, positioned at a reduced spacing. This configuration would result in a more uniform load distribution while ensuring that the deck's cross-section remains consistent along its entire length (*Figure 22*).

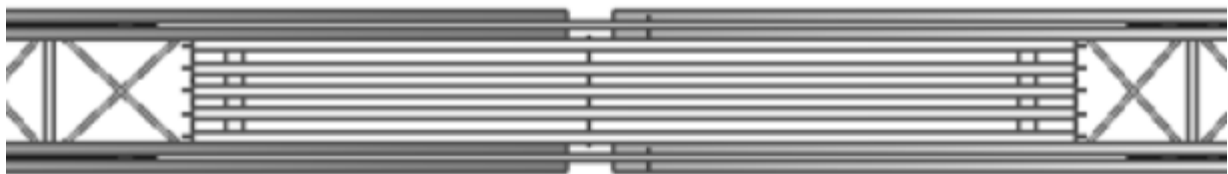


Figure 22: Top View, Deck Elements between the Structural Arches - SCIA Engineering

Further attention must be given to the lateral staircases. These can be designed as laterally supported on the arches, introducing an additional compressive force into the arch structure. While this approach contributes to making the reaction at the arch supports more vertical - reducing the horizontal component - it may also necessitate an increase in the structural arches' cross-sectional resistance due to the additional stress introduced.

An alternative solution to the issue of staircase support could be the development of a self-supporting staircase: A separate structural unit constructed independently and positioned on-site. This approach would reduce the stresses acting on the arch while also simplifying the complexity of the required connection at the arch-stair junction.

3.2 PRELIMINARY DESIGN PROPOSAL 2

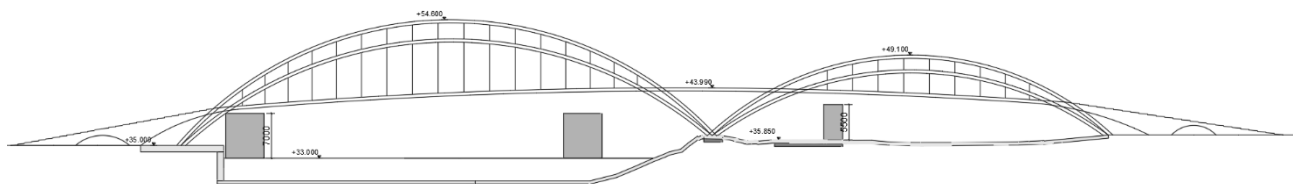


Figure 23: Pre-design Proposal 2 - Architectonic Frontal View

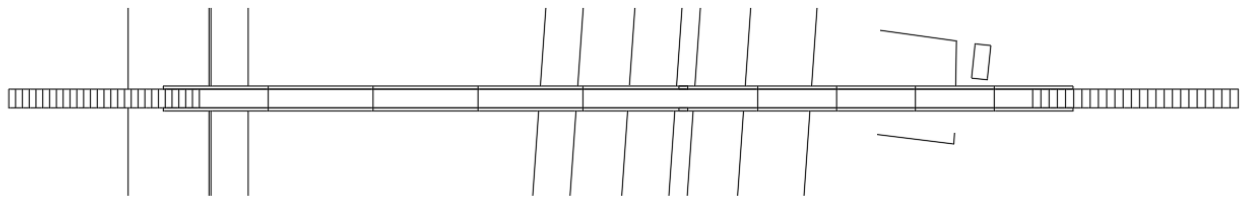


Figure 24: Pre-design Proposal 2 - Architectonic Top View

The second structural pre-design proposal follows the same guidelines as Proposal 1. As shown in *Figure 23 & Figure 24*, from the conceptual architectural representation, the concept aims to create two levels of structural arches overlapping one another, alternating in support and anchorage to the vertical tie rods.

As a general conceptual starting point, just as analyzed in detail in Proposal 1, the structural composition arches are idealized as three-hinged arches, making the structure isostatic and easy to construct (*Figure 25*). The base hinges are all positioned at the same elevation level to provide greater structural symmetry to the solution under analysis (*Figure 26*).

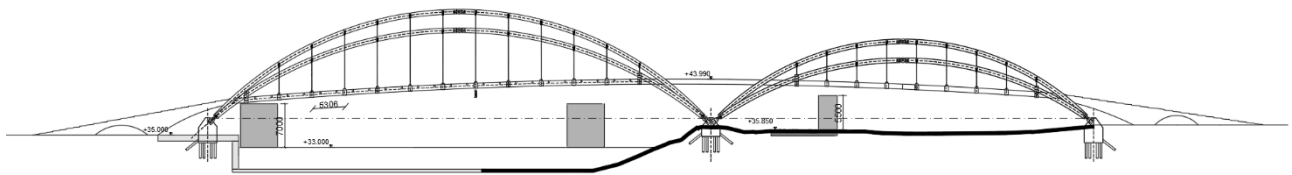


Figure 25: Pre-design Proposal 2 - Structural Front View

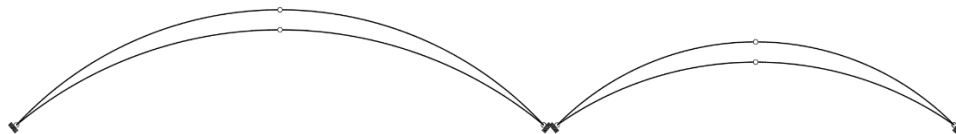


Figure 26: Three-Hinged-Arches Schematization

It is important to note that all arches converge at the same point (same base hinge): This results in greater complexity in the conception and design of the connection with the foundations, which are designed to withstand non-vertical reactions from the superstructure.

The deck design remains the same as in Proposal 1, with particular attention to the intersection point between the outermost arch and the primary beams of the deck itself.

To better understand the concept behind this arch overlap, explanatory structural sections have been developed (*Figure 27*).

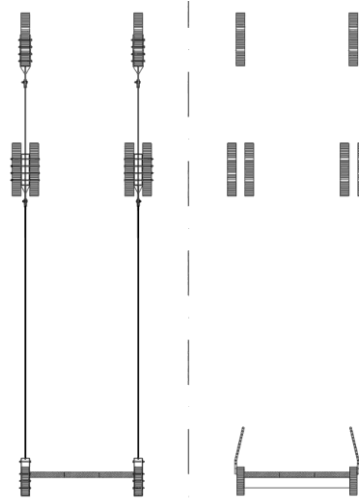


Figure 27: (a) Section with Hangers-Deck-Arches Connection; (b) Section with Deck-Lateral Barrier and Triple Arch.

The lower development plane of the first two structural arches follows the same design principles described in Proposal 1. However, it is important to note that the second upper development plane, where the third elevated arch is positioned, is symmetrically placed at the midpoint of the space left between the two lower arches.

This configuration allows the tie rods to pass between the two lower arches and connect directly and securely to the upper arch. The space between the two arches on the first lower plane must therefore be sized to accommodate both the primary deck beams and the elevated arch.

From a connection perspective, compared to what was analyzed in Proposal 1, it is essential to highlight the presence of a third type of connection in addition to those already examined. Specifically, the connection between the vertical tie rods and the elevated arch is conceptualized as a steel frame that encloses the arch itself, ensuring the correct load transmission (*Figure 28*).

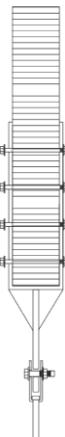


Figure 28: Connection Scheme of Vertical Tie Rods with Top Three-Hinged Arch

3.2.1 ANALYSIS OF POTENTIAL CRITICAL ISSUES

This structural solution presents several critical issues, both in terms of the conception of certain structural connections and the distribution of loads.

The first critical aspect concerns the interaction between the elevated plane structural arch and the lateral primary support beam of the deck. These two elements are located on the same vertical plane, and both pass between the two lower arches.

To enable the connection, it is necessary to interrupt the continuity of the deck beam (*Figure 29*), creating a specialized connection that follows the inclination of the arch. An alternative solution could involve the construction of a bearing shoulder on both sides of the arch section. In general terms, the lateral support beams of the deck would still follow a continuous beam scheme over multiple supports, but with additional closer support at the intersection with the arch.

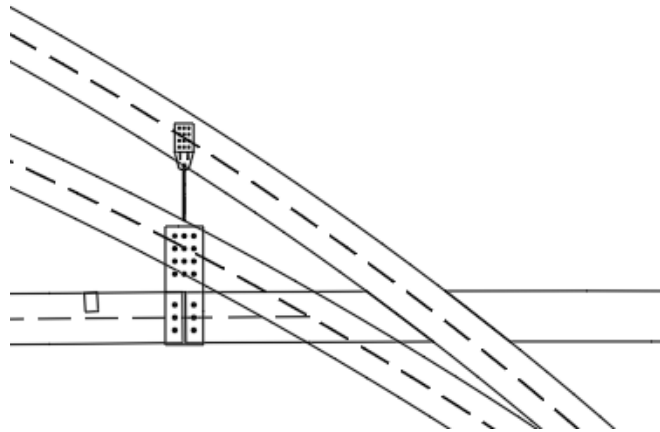


Figure 29: Interruption of the Continuity of the Deck Beam

Although Proposal 2 is conceived to reduce concentrated loads on the structural arches - thus allowing for a smaller section and making the overall structure slimmer and more linear - the load transfer mechanism represents an additional critical challenge.

The fundamental idea behind this configuration is the alternating attachment of vertical tie rods between the lower arches and the elevated arch. In this way, the two arch planes would each support half of the load from the deck, generating lower concentrated forces and significantly reduced stress compared to Proposal 1 (*Figure 30*). However, complexity arises from the need for continuous maintenance to ensure the proper functioning of this alternating, asymmetrically defined support system.

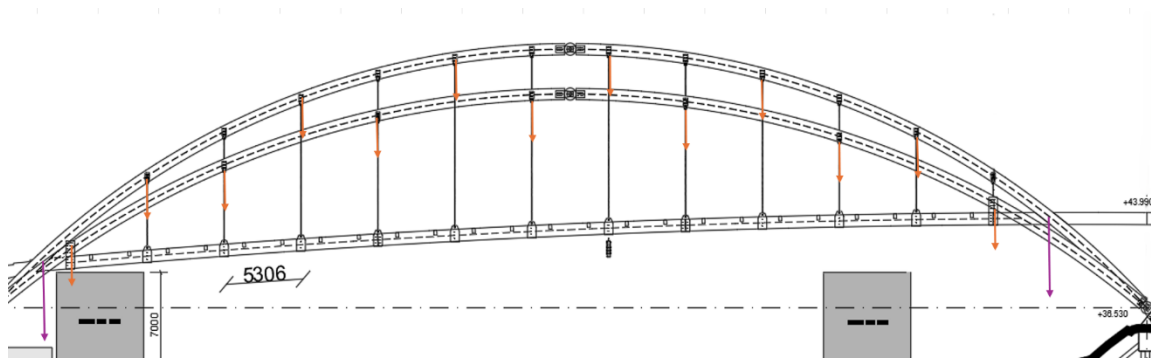


Figure 30: Example of Alternative Load Distribution Configuration

If variations in the length of the tie rods were to occur, leading to slight changes in the load distribution, the lower arches would no longer carry only half of the deck load but also the remaining portion. Considering such a scenario would require dimensioning the arches with a section comparable to that of Proposal 1, ultimately nullifying the benefits of introducing the elevated arch in terms of structural simplification and material savings.

3.3 PRELIMINARY DESIGN PROPOSAL 3

With the aim of providing a structural alternative to the arch-based technology already analyzed, the possibility of implementing a solution using truss beam technology is explored. This solution is examined with the objective of establishing a comparative framework with the other proposals, by employing a support structure characterized by a different geometry and structural concept.

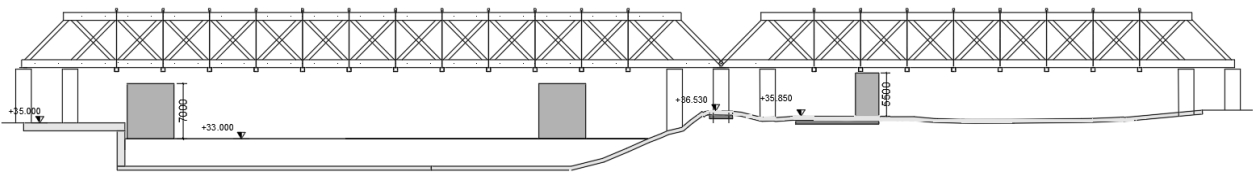


Figure 31: Pre-design Proposal 3 - Architectonic Frontal View

Figure 31 shows the proposed architectural layout for the development of the pedestrian superstructure. The entire superstructure has been divided into two distinct spans of different lengths (approximately 90 and 60 meters); the presence of two spans with significantly different lengths necessitates the definition of a height that ensures a proper height-to-span ratio for the entire structure. Specifically, taking the maximum span of 90 meters, a ratio of 1/15 is adopted, resulting in a truss beam height of 6 meters.

Furthermore, to ensure the correct distribution of axial forces within the diagonal elements, an inclination angle of 45° with respect to the horizontal axis of the lower chord is selected (Figure 32). This choice allows for the inclusion of elements that are not excessively long, thereby reducing the risk of axial instability.

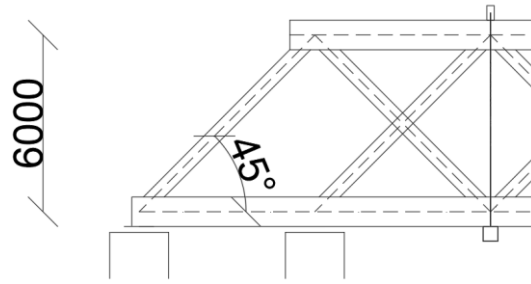


Figure 32: Detail of the Geometric Dimensions of the Structural Solution: Height of the Truss Beam “h” and Inclination Angle of the Diagonals (45°)

Based on the architectural layout illustrated in the figures, the transverse elements with respect to the longitudinal development plane of the structure are supported by vertical hangers connected to small elements aligned with the nodes of the truss. In this way, the proper transfer of loads at the node level is ensured, generating predominantly axial forces within the structural members, with negligible bending moments.

From the architectural scheme, a structural pre-design project is developed (Figure 33 & Figure 34), in which the connections and cross-sections are analyzed in detail.

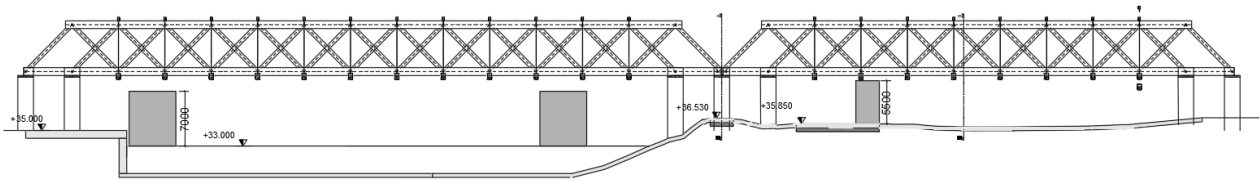


Figure 33: Pre-design Proposal 3 - Structural Front View

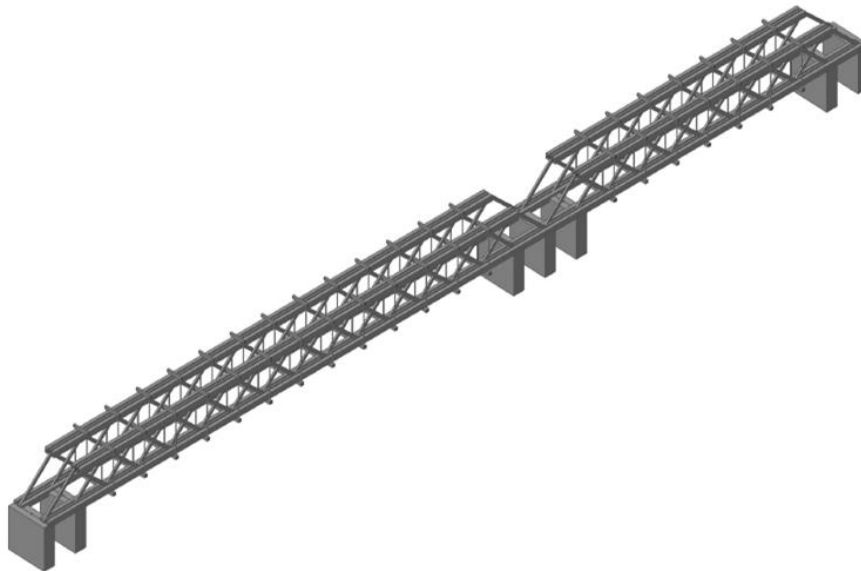


Figure 34: Pre-design Proposal 3 - 3D Structural Isometric View - SCIA Engineering

The entire solution has been conceived as a series of truss beams superimposed on one another. The simplified static scheme, shown in *Figure 35*, clearly illustrates how the overall structural composition includes four distinct truss beams geometrically stacked in sequence.

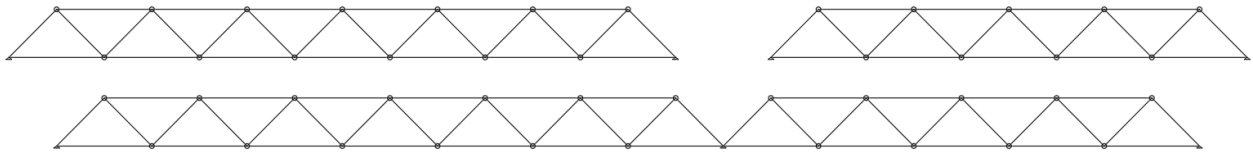


Figure 35: Static Scheme of the Truss Beams

The truss beams rest respectively on different piers, arranged in twin and adjacent pairs at an appropriate distance (corresponding to the base of a triangular element forming part of the truss). These beams are not positioned on the same plane but rather developed on two distinct planes placed side by side and connected by metallic joint elements at the location of the piers. A clearer representation of the distribution of the truss elements is provided in *Figure 36*, which presents an example of a cross-section of the deck.

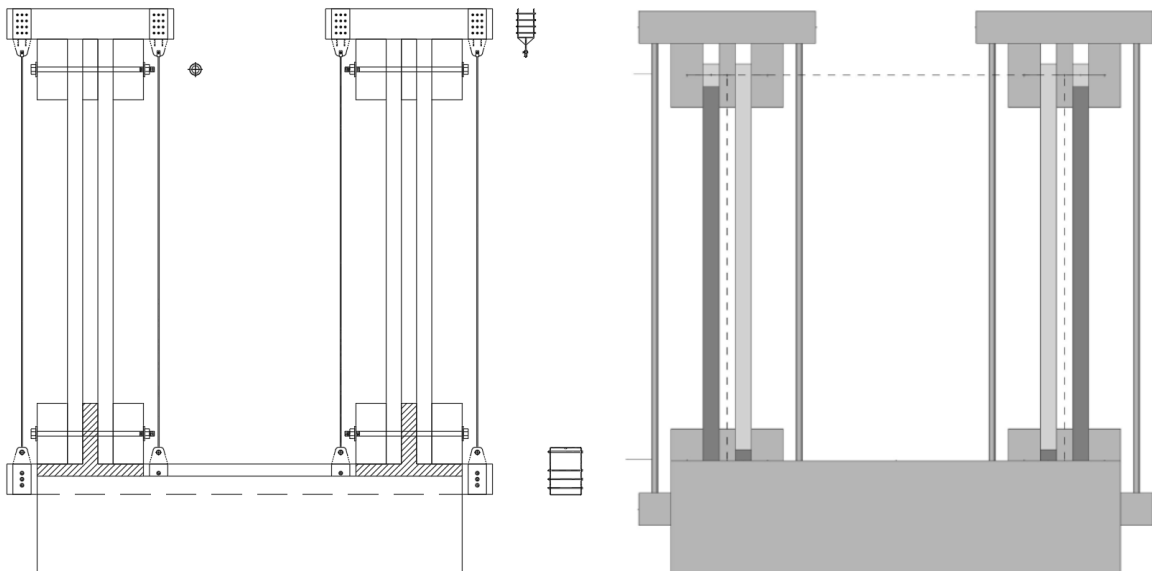


Figure 36: a) Cross-Section of the Deck and Arrangement of the Truss Beams; b) Cross-Section from the 3D Model – SCIA Engineering

The arrangement of the structural elements according to this configuration allows for the design of a double lower chord, which is consequently loaded by only one of the truss beams. This results in a clear reduction in the internal compressive and tensile stresses of the vertical members, leading to a corresponding reduction in the cross-sections of the elements themselves.

The cross-section is also conceived as a composition of simplified schemes: The base beams, oriented transversely to the lower chords, are designed as simply supported elements, thereby further reducing the static and computational complexity. These beams are connected to horizontal elements resting

on the upper ends of the trusses through steel tie rods linked to the timber beams by means of steel connection cages (as shown in the illustration in *Figure 36*).

All connection elements are designed as hinges, with the objective of ensuring the proper functioning and load transfer typical of the Warren truss structural system (*Figure 37*). This concept is applied both to the connections between the diagonals and the upper and lower chords, as well as to the connections with the supporting piers, using specially designed steel connection plates tailored to the structural conditions under analysis.

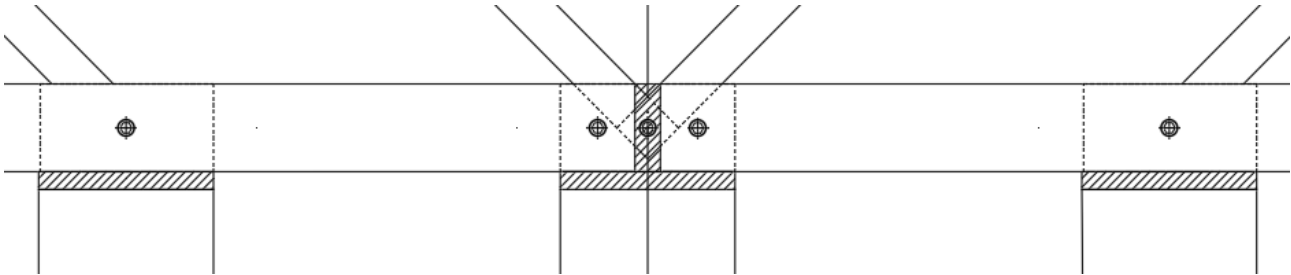


Figure 37: Detail of the Hinged Connections of the Truss Beam

3.3.1 ANALYSIS OF POTENTIAL CRITICAL ISSUES

The analyzed truss solution presents several critical issues that make its selection unrealistic. In fact, this structural solution is constrained in the definition of the element dimensions by geometric ratios between the span and the height of the truss, which directly affects the stiffness of the structure.

The geometric ratio between the span L and the height h of the truss was set at $1/15$, resulting in a truss height of 6 meters for a maximum span of 90 meters. While from a construction design perspective such dimensions contribute to increasing structural stability and stiffness, they also lead to a superstructure of considerable size and mass. This results in a “heavy” design that is not well integrated with the surrounding environment.

An additional critical issue is represented by the high number of connections required within the structure: The presence of 47 diagonal members results in the creation of 51-hinged connections, with elements reaching lengths of up to 11 meters that must be positioned on-site and secured. This leads to a significant construction complexity, which represents a major drawback in the selection of this structural solution.

Moreover, to maintain the superstructure with a Warren truss static scheme, each truss beam requires fixed support at both ends (either pinned or roller bearings). This requirement, combined with the complex interweaving geometry of the trusses and the misalignment of the starting points of the superstructures, necessitates the creation of seven fixed support points, idealized as reinforced concrete piers. Although relatively simple to construct, these piers obstruct panoramic views and make the structure appear bulkier and heavier to the naked eye.

The chords are also conceived as single GLT beams, which would therefore reach a length of 90 meters. Although this does not pose a problem from a construction standpoint, it does raise significant issues in terms of transport logistics, leading to a dramatic increase in costs and a more complex construction process.

This issue could be addressed by introducing connection elements between two shorter beams (even half the original length), which would serve as structural joints for both the chords and the truss beam itself, without altering the load distribution or the axial force reactions.

Finally, the distribution of the nodal loads at the ends of the structure, according to this hypothetical structural solution, remains uncertain: Without a more detailed and in-depth analysis, it is not possible to determine the actual load distribution in accordance with truss theory. In fact, a configuration change at the extremities may be necessary to ensure the effective structural contribution of all elements.

3.4 ADDITIONAL PRELIMINARY DESIGN CONCEPTS

The structural analysis aimed at conceiving multiple pre-design solutions did not stop at those presented in the previous subsections; in fact, additional proposals were also examined and are briefly discussed below, providing a clear explanation as to why they were excluded from the final computational process.

The underlying approach followed for these additional proposals still pursued the concept of a double-arch geometry, which was, however, developed based on different geometric considerations, including the possibility of combining multiple technical solutions within the same structural configuration.

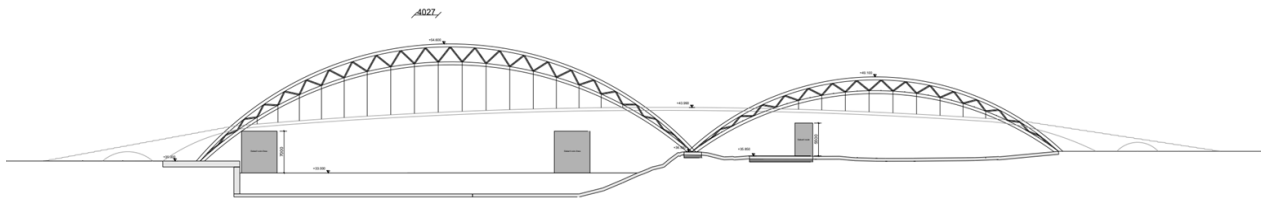


Figure 38: Pre-design Proposal 4 - Architectonic Frontal View

The pre-design proposal shown in *Figure 38*, with architectural representation, was conceived as the combination of a structural arch bridge typology with a double support plane, integrated with truss beam technology. The objective was to decompose the structural stresses into simple compressive and tensile forces, divided into shorter elements in length, thereby achieving a slenderer profile capable of spanning a large distance, as required by the case under analysis.

The main issue with this solution lies in the high number of structural connections, which significantly increases the construction complexity of the structure, ultimately leading to the decision to discard the proposal as it was deemed too complex for the intended scope of the present study.

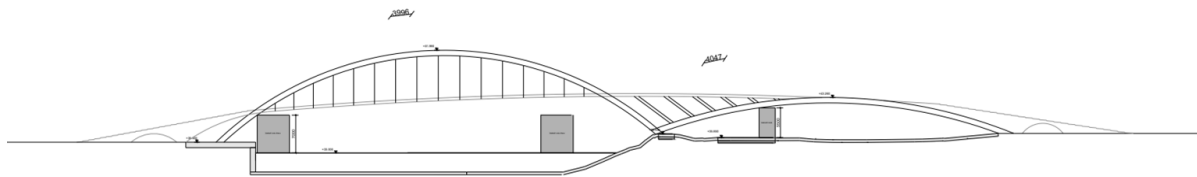


Figure 39: Pre-design Proposal 5 - Architectonic Frontal View

An additional hypothesized solution is represented in *Figure 39*, in which the use of a double arch is proposed, with the second arch having a lower profile. This solution is driven solely by aesthetic considerations rather than structural ones. In fact, the use of a lowered arch makes the structural system more complex in terms of load analysis and the study of the stability of the arch itself.

An arch with such a span-to-rise ratio generates support reactions at the external restraints of the structure with very high horizontal components. This condition necessitates a more in-depth structural analysis in the design of the foundations, an aspect that, however, falls outside the scope of the present study.

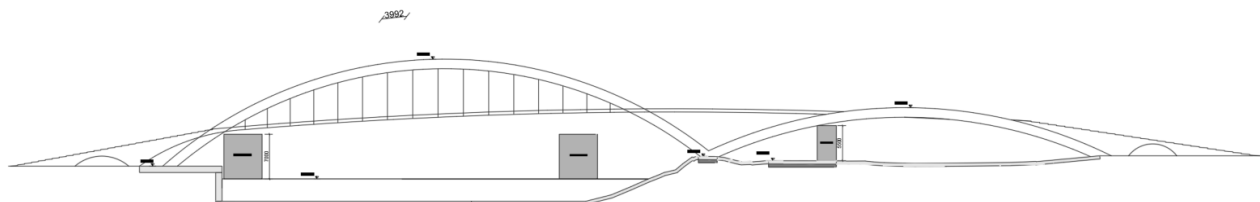


Figure 40: Pre-design Proposal 6 - Architectonic Frontal View

The same concept was considered for the pre-design solution shown in *Figure 40*, with the only difference being that no inclined support elements are placed on the lower arch. This alternative solution requires an additional analysis of the internal forces generated within the deck, which would remain unsupported over a significant span.

Obviously, the issue not only results in high horizontal reaction forces at the foundation level but also - and more critically - affects the cross-section of the central portion of the deck. To maintain a consistent structural composition throughout the entire structure, this central portion would need to be designed with significantly larger cross-sections than those required for the remaining segments of the deck.

3.5 COMPARATIVE EVALUATION BETWEEN ARCH AND TRUSS BEAM SOLUTIONS – SELECTION OF THE FINAL PROPOSAL

In order to make the decision-making process regarding the final solution as clear and precise as possible, a direct comparison is carried out between the two pre-design solutions referred to as “Pre-design Solution 1” and “Pre-design Solution 3”, corresponding respectively to a double arch in sequence (*Figure 14*) and a truss beam structural solution (*Figure 33*).

This comparison is not conducted from the perspective of structural behavior under loads, as this aspect is not deemed strictly relevant at this stage. In fact, the two structures are compared at the level of conceptual design, since it is precisely at this stage that the main differences emerge from an engineering standpoint in terms of structural conception.

The first point of comparison lies in the substantial differences in structural typology, which are reflected in the distribution of loads as well as in the direction and magnitude of the support reactions:

- The arch solution, idealized as a three-hinged arch and thus statically determined, exhibits internal axial compressive forces developing along the two structural branches of the arch. These forces result in support reactions at the external hinge supports that are not purely vertical.
- The truss solution, on the other hand, features a high number of structural elements (chords, diagonals, etc.) subjected to concentrated loads at the nodes, to generate internal axial compressive and tensile forces within the structure. The support reactions at the external supports, which are also simply supported in this case, are predominantly vertical.

Although the two structures are conceptually equivalent in terms of the nature of internal forces, there is a substantial difference in the support reactions: The presence of a horizontal component in the reaction forces of the arch solution necessitates the design of a foundation capable of withstanding significant horizontal actions, with elements aligned along the tangent direction of the arch itself. In contrast, for the truss solution, the support reactions are predominantly vertical and result in the design of vertical piers with adequate cross-sections to support the applied loads (*Figure 41*).

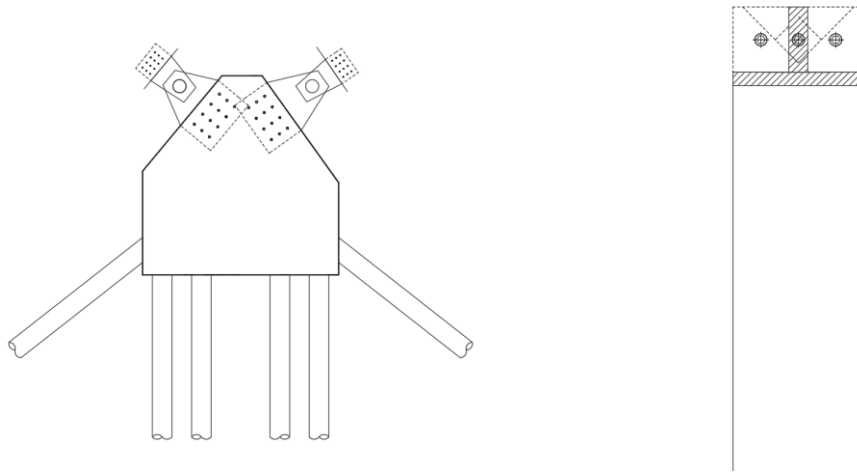


Figure 41: (a) Foundation of the Arch Structure with Inclined Elements; (b) Foundation of the Truss Beam with Vertical Pier

Another point of comparison concerns the volumetric quantity of material to be used. By analyzing the two structures, it is possible to perform a volumetric estimation of the materials required for a proper comparison: Based on a base cost, and assuming the use of the same type of GLT for the entire structure, the total volumetric footprint can be multiplied by the cost per cubic meter of the material.

Consequently, greater use of material results not only in an increase in the self-weight of the structure, but also in a rise in cost, which could be significant.

To accurately assess this difference, an approximate and estimative analysis of the relevant volumes is carried out, considering the cross-sections and lengths considered during the pre-design phase. The calculated volumes, expressed in cubic meters, are compared and then multiplied by an average unit cost of 560 €/m³; this value is purely indicative, and it is important to clarify that it is used solely for comparative purposes between the two solutions, without reference to the actual selection of a collaborating manufacturing company. The results of the analysis are presented in *Table 3*.

PRE-DESIGN SOLUTIONS - VOLUME COMPUTATION						
	ELEMENT	CROSS-SECTION [m²]	LENGTH [m]	NUMBER	VOLUME [m³]	
SOL.1	Arch 1 [1.5x0.25]	0.75	86	4	258	
	Arch 2 [1.5x0.25]	0.75	63.65	4	190.95	
	Primary Beams [1.0x0.2]	0.2	134	2	53.6	
	Secondary Beams [0.2x0.4]	0.08	3	48	11.52	
	TOTAL VOLUME					514.07
	ESTIMATED PRICE [560 €/m³] [k€]					287.90
SOL.3	Diagonals [0.25x0.5]	0.125	8.46	94	99.41	
	Upper Chord [1.0x0.5]	0.5	134.53	4	269.07	
	Lower Chord [1.0x0.5]	0.5	155	4	310	
	Upper Horiz. Elements [0.25x0.5]	0.125	2.75	40	13.75	
	Lower Horiz. Elements [0.5x0.5]	0.25	8	20	40	
	TOTAL VOLUME					732.22
	ESTIMATED PRICE [560 €/m³] [k€]					410.04

Table 3: Comparison Table – Calculation of Volumetric Footprint and Cost Estimation

The analysis reveals a clear volumetric difference between the arch solution and the truss beam solution: Based purely on mathematical and indicative ratios, the volume of material required for Solution 1 is approximately 30% less than that needed for the implementation of Solution 3. Consequently, the associated cost also shows a substantial difference, which becomes significant, especially when dealing with figures approaching half a million euros.

Referring again to the data presented in the table, it is noteworthy that the number of elements with varying dimensions is considerably higher in Solution 3 compared to Solution 1. Although this is inherent to the structural concept, the data further confirms the excessive construction complexity of the truss structure, with several elements and connections that are too high for the intended design purposes.

Moreover, since the goal of this study is the selection and design of a solution that is as feasible as possible within the context under consideration, the economic aspect cannot be overlooked. The selection of Solution 1, based on a structural arch, leads to significant savings compared to the truss beam solution.

By adding these considerations to those discussed in the descriptive chapters regarding the critical aspects of each solution, as well as visual and architectural evaluations, the selected solution corresponds to that identified as Solution 1: Double structural arch (*Figure 14*).

3.5.1 RATIONALE FOR SELECTING THE ARCH BRIDGE

The most suitable solution chosen is a bridge utilizing the arch structural system to span the required distance and sustain the applied loads.

The choice of an arch system is based on considerations regarding the typical span range achievable in timber bridge construction, as analyzed in the “State of Art”, which generally allows for spans of up to 70–80 meters. The specific site conditions of the proposed case study allow for a two-span configuration, with different span lengths, both within the feasible range for an arch bridge. Specifically, the first span is designed to range between 80 and 90 meters²⁴, while the second adjacent span falls between 55 and 65 meters.

The variability in the span lengths is directly related to how the available space is divided. The total horizontal span of approximately 150 (±5) meters can be distributed between the two arches with different lengths, depending on several factors: The selected rise of the arches, the rise-to-span ratio, and the support locations chosen based on both structural efficiency and terrain morphology in the analyzed section.

Furthermore, the design of the arches considers the clearance requirements imposed by external constraints, which define the boundary conditions for an optimal structural configuration. Specifically, the presence of large vessels navigating the waterway on the left side of the section, with a maximum vertical clearance of 7 meters, and a two-lane roadway for heavy vehicles on the right side, requiring a clearance of 5.5 meters, significantly influences the feasible arch start and end points as well as the rise-to-span ratio that can be accommodated within the design constraints (*Figure 42*).

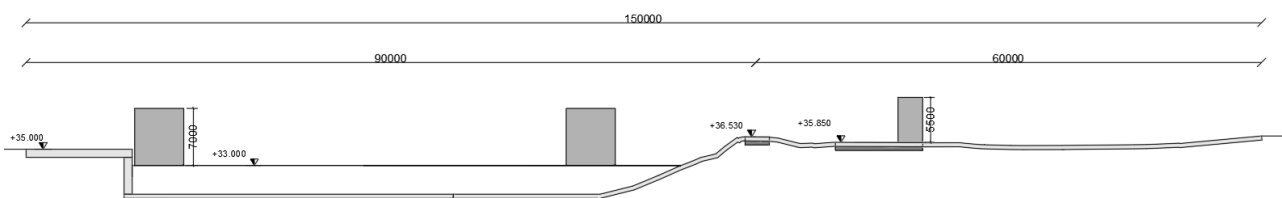


Figure 42: Front Elevation of the Reference Design Altimetric Section - Actual Vertical Clearance Requirements of the Obstacles to be Overcome and Approximate Levels of the Spans to be Covered

²⁴ Even though the maximum project span to be covered is 90 meters, which is potentially 10 meters longer than the theoretically feasible or previously constructed spans analyzed in the “State of Art”, this does not pose a significant issue. The following sections describe the static structural scheme adopted for the arches, which corresponds to a three-hinged arch system. The use of a three-hinged arch allows for the division of the total curved beam length forming the arch into two segments. Furthermore, the primary challenge does not stem from the feasibility of manufacturing beams of such lengths but rather from transportation constraints. In this specific case, these limitations can be mitigated by transporting the segments via ship, utilizing the services of the navigable canal present on site. A more detailed analysis of this aspect is provided in the subsequent chapters.

3.6 GENERAL ANALYSIS OF THE ARCH STRUCTURAL SYSTEM

The arch structural system is one of the oldest and most efficient structural solutions used in construction, particularly in the design and execution of bridges.

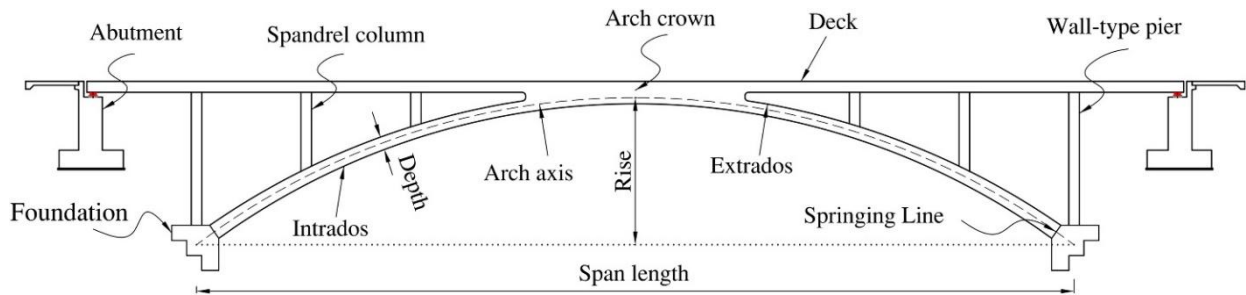


Figure 43: Illustrative Diagram of the Structural Components of an Arch Bridge - Reference Terminology in the Discussion - (Amir Khorraminejad, Mahmoud R. Shiravand, Mohammad Safi, 2022)

The primary advantage of an arch system lies in its efficient ability to transfer structural and non-structural loads through compression within the main structural elements forming the arch. This mechanism results in a purely axial action, preventing the development of bending moments within the arch itself. This distinctive characteristic makes the arch solution particularly suitable for medium to long-span structures, providing excellent resistance to both vertical and horizontal loads.

The optimal structural shape of an arch can be compared to the inverse of a catenary curve (hyperbolic cosine function), which, if subjected to tension, would function entirely under tensile forces. By inverting this form, the resulting geometry enables a load distribution mechanism that operates exclusively in compression (Figure 44). However, the stability and deformation behavior of the arch are directly dependent on the applied load distribution. Non-uniform loading conditions generate different forms of structural instability. Therefore, the thickness of the arch must be designed based on the alignment of the thrust line, ensuring that it remains within the cross-section of the arch to maintain structural stability (Figure 45).

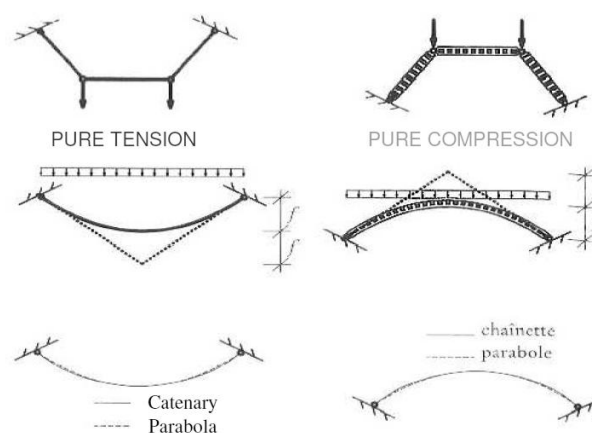


Figure 44: Illustrative Diagram of the Catenary and Parabolic Concept Applied to the Arch Structure - Objective of Pure Compression and Comparison with the Case of Pure Tension - (Gens F., Design and Construction of Bridges - Chapter 03b-1 - Arch Bridges, 2024)

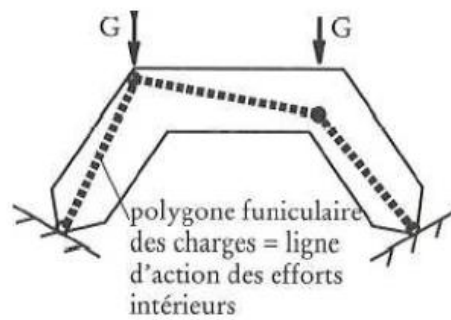


Figure 45: Schematic Illustration of the Thrust Line within the Longitudinal Section of the Arch - (Gens F. , Design and Construction of Bridges - Chapter 03b-1 - Arch Bridges, 2024)

3.6.1 STRUCTURAL BEHAVIOR

Arch structures can be classified based on the boundary support conditions and the positioning of the deck.

The most used solutions in structural construction involve the use of hinges or fixed supports. From a static perspective, these configurations influence the complexity of structural analysis and the distribution of reaction forces and moments. The introduction of hinges can lead to the three-hinged arch system²⁵, which represents an isostatic structural solution. This configuration eliminates settlement issues typical of a two-hinged arch: With the presence of a hinge in the crown of the arch, the isostatic element brings the possibility to not care about the displacement at the foundation level (Figure 46).

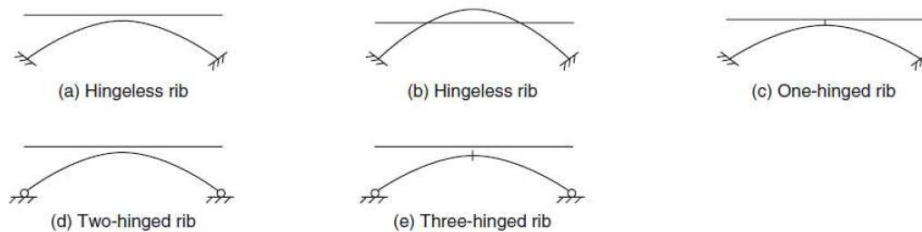


Figure 46: Static Schemes of Arch Bridge Typologies with and without Hinges - (Gens F. , Design and Construction of Bridges - Chapter 03b-1 - Arch Bridges, 2024)

Beyond these fundamental static schemes, more complex derived configurations exist, conceptually stemming from the arch structural typology.

Another key classification criterion for arch bridges is based on the positioning of the deck. Structural arch solutions can support the deck in three main configurations. The most conventional design places the deck above the arch, generating non-vertical reactions that must be properly managed through foundation design. If the deck is positioned below the arch, the structure is known as a “*bowstring*

²⁵ The three-hinged arch system is used in the pre-design and is described in the following chapters.

arch²⁶”, which produces predominantly vertical reactions. An intermediate solution consists of placing the deck at a mid-level relative to the structural arch, balancing the characteristics of the previous two configurations.

3.6.2 INSTABILITY PHENOMENA

The structural solution of an arch bridge is inherently stable due to the predominance of internal compressive forces. However, it is subject to various forms of structural instability that must be thoroughly analyzed and addressed through careful design and verification to ensure long-term durability.

The collection of geometric and structural data derived from the historical analysis of such structural systems leads to the determination of an optimal stability range based on the ratio between the arch rise and its span. This range, expressed as a fraction, can be defined as: $\frac{f}{L} = [\frac{1}{8}; \frac{1}{5}]$ ²⁷.

Once the stability range is established, the design study proceeds with the analysis and computation of the arch reactions, considering the applied loads and the external boundary conditions (supports) acting on the arch. Based on a general two-hinged arch scheme, the reaction forces can be calculated in a straightforward manner as follows (*Figure 47*):

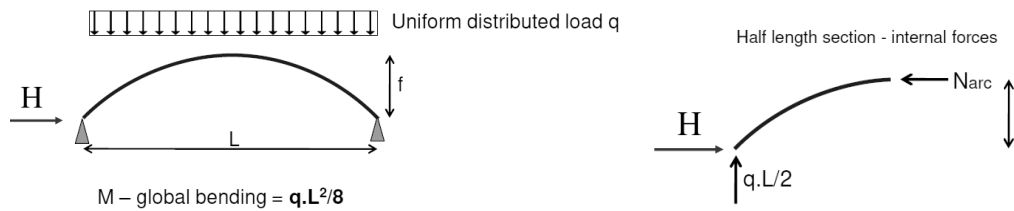


Figure 47: Static Resolution Scheme for Calculating Support Reactions - (Gens F. , Design and Construction of Bridges - Chapter 03b-1 - Arch Bridges, 2024)

$$N_{arc} = H \rightarrow M = N_{arc} * f \rightarrow H = q * \frac{L^2}{8f}$$
²⁸

Moving on to the analysis of instability modes, the main modes can be categorized into three groups:

- **Out-of-Plane Instability:** This type of instability is characterized by a loss of lateral stability, likely due to a lack of lateral bracing. This effect is commonly analyzed by modeling the arch as a straight column with a total length L_{tot} , equivalent to the distance between two potential bracing elements (*Figure 48*).

²⁶ System described in the following subsection “BOWSTRING BRIDGE TYPOLOGY”.

²⁷ (Gens F. , Design and Construction of Bridges - Chapter 03b-1 - Arch Bridges, 2024).

²⁸ The higher is “f”, the lower is “H”.

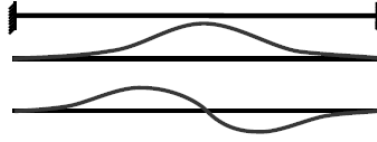


Figure 48: Out of Plane Instability Scheme - (Gens F. , Design and Construction of Bridges - Chapter 03b-1 - Arch Bridges, 2024)

- **Snap-Through Instability:** This type of instability occurs only in the case of a very shallow arch, with a rise-to-span ratio greater than $\frac{f}{L} \geq \frac{1}{11}$. The deformation associated with this failure mode is instantaneous, leading to a sudden loss of equilibrium and structural failure due to excessive deformation (Figure 49).



Figure 49: Snap-Through Instability Scheme - (Gens F. , Design and Construction of Bridges - Chapter 03b-1 - Arch Bridges, 2024)

- **In-Plane Asymmetric Instability:** This instability mode occurs due to the application of an asymmetric load, which induces localized deformation and leads to the instability of a specific portion of the structure (Figure 50). This type of instability and the necessary verifications are directly related to the calculation and the critical buckling load value.

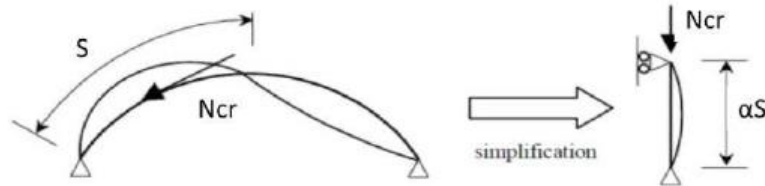


Figure 50: In-Plane Asymmetric Instability Scheme and Simplification - (Gens F. , Design and Construction of Bridges - Chapter 03b-1 - Arch Bridges, 2024)

$$N_{cr} = \frac{\pi^2 EI}{L_{fl}^2} \text{ with } L_{fl} \approx \alpha S^{29}$$

From the calculation of N_{cr} , three main reference cases are obtained:

- $N_{cr} \leq 3N_{ED} \rightarrow$ Design probably to review
- $3N_{ED} \leq N_{cr} \leq 10N_{ED} \rightarrow$ Second order effects must be considered, with non-linear calculation needed (FEM software ...). An approximation can be done, following calculation with European buckling curves to verify $\frac{N_{sd}}{N_{b,Rd}} < \sim 0.5$; also, a second

²⁹ $\alpha S = 0.7S$ (arch footage encased), $= 1.0S$ (pined arch footage).

- approximation can be followed, calculating the cross-section with N_{sd} and $M_{sd} = \frac{M_0}{1 - N_{sd}/N_{cr}}$.
- $N_{cr} \geq 10N_{ED} \rightarrow$ No instability to check (very big sections).³⁰

3.6.3 MANAGEMENT OF HORIZONTAL THRUST

A fundamental aspect to consider is the analysis of how horizontal loads are absorbed by the structure³¹. In an arch structural solution, the design approach can be outlined through three main schematic configurations (*Figure 51*):

- Arch with high stiffness: The arch resists horizontal loads by transferring them directly to the foundations.
- Deck with high stiffness: Horizontal loads are transferred to the foundations through the deck.
- Deck and arch with high stiffness: This solution results in the creation of a heavy and highly rigid structural system, providing excellent resistance to horizontal loads but leading to a poor cost-efficiency ratio in structural design.

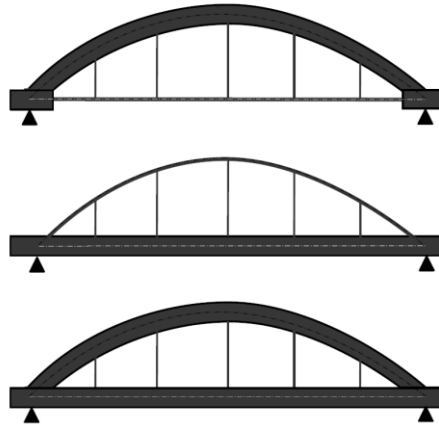


Figure 51: Explanatory Diagrams of the Three Described Cases with Different Stiffness Distributions in the Structure - (Gens F. , Design and Construction of Bridges - Chapter 03b-1 - Arch Bridges, 2024)

3.6.4 BOWSTRING BRIDGE TYPOLOGY

Further preliminary consideration must be given to the structural technology of bowstring bridges. These structures represent a solid alternative to the conventional arch bridge, with a significant variation in the direction of support reactions. This structural solution relies on the tensile resistance of the vertical elements and the deck, while the elevated arch remains in compression, like the classic arch solution previously described (*Figure 52*).

The structural geometry and the direction of vertical support reactions make this solution particularly suitable for situations where terrain morphology and soil resistance do not allow for excessive

³⁰ (Gens F. , Design and Construction of Bridges - Chapter 03b-1 - Arch Bridges, 2024)

³¹ Depending on the chosen structural solution (with higher or lower stiffness), the deformation behavior also varies, particularly with reference to deformations under non-uniformly distributed loads acting on the structure.

horizontal forces. This configuration enables the design of foundations appropriately sized to accommodate the resulting loads.

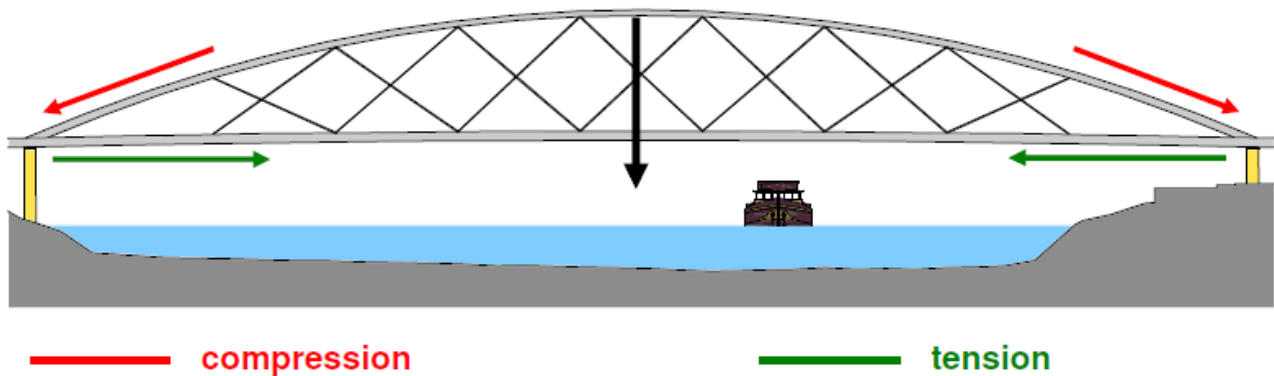


Figure 52: Bowstring Bridge Scheme - Compression and Tension Forces in the Structural Elements - (Gens F. , Design and Construction of Bridges - Chap 03b-2 - Bowstring Bridges, 2024)

From a structural perspective and in terms of load distribution, the system under analysis exhibits a dual behavioral response depending on the uniformity of the applied loads. In the case of a loading condition corresponding to a uniformly distributed load on the structure, the system behaves as an arch, effectively demonstrating arch behavior (Figure 53).

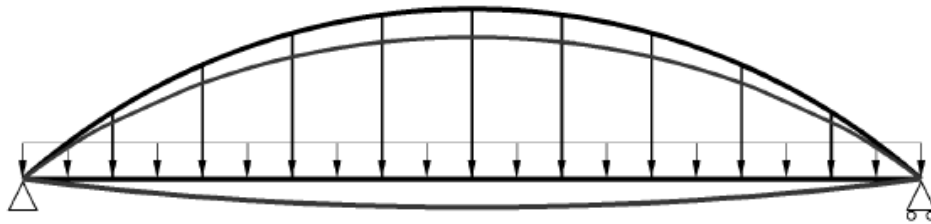


Figure 53: Uniformed Distributed Load - Arch Behavior of the Bowstring Bridge - (Gens F. , Design and Construction of Bridges - Chap 03b-2 - Bowstring Bridges, 2024)

If, on the other hand, the load distribution is not uniform across the structure, the system's behavior deviates from that of an arch, responding instead as a beam subjected to bending moments (bended beam behavior).

Another key aspect to consider is the calculation of reactions within the system. Under uniform loading conditions, the system responds with forces and reactions that are exactly equivalent to those described for the arch configuration in the previous chapter, with one fundamental difference concerning the horizontal reaction H . In the arch configuration, H represents the reaction at the hinge or fixed support, whereas in the bowstring configuration, it corresponds to the tensile force generated within the deck (Figure 54).

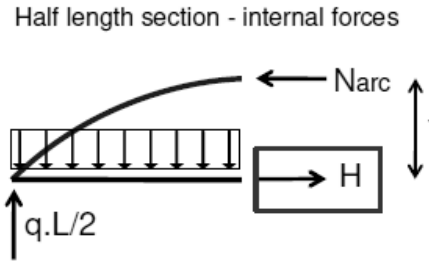


Figure 54: Static Scheme and Reaction Forces for the Bowstring Bridge - (Gens F. , Design and Construction of Bridges - Chap 03b-2 - Bowstring Bridges, 2024)

3.6.5 SLENDERNESS AND BRACING CONSIDERATIONS

Analyzing the bowstring system from the perspective of slenderness, attention must again be directed toward the ratio between the rise and the span of the bridge under consideration. The corresponding range values are $\frac{f}{L} = [\frac{1}{5}; \frac{1}{10}]$, showing a greater difference at the extremes compared to the reference range for the classic arch solution. Furthermore, for a bowstring bridge, it is possible to determine the most economically efficient rise-to-span ratio, which corresponds to $\frac{f}{L} = \frac{1}{6}$.

As with the classic arch solution, the ideal shape to maintain under uniformly distributed loading conditions is the catenary (Figure 55).

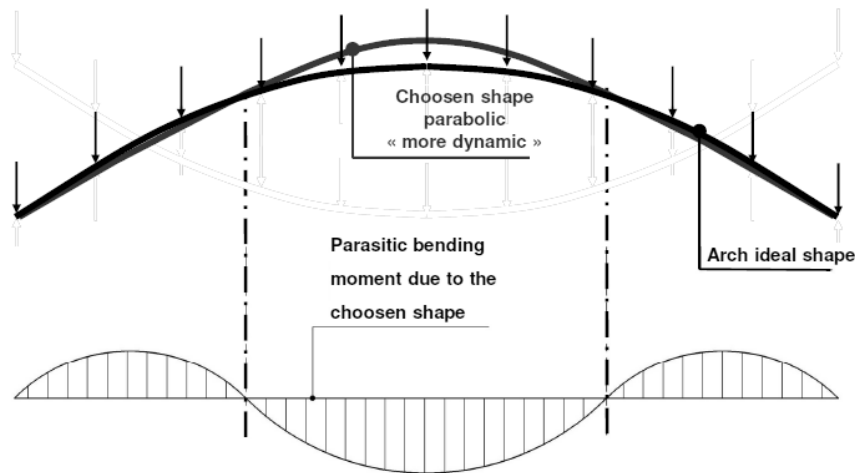


Figure 55: Bowstring Ideal Shape - Catenary - (Gens F. , Design and Construction of Bridges - Chap 03b-2 - Bowstring Bridges, 2024)

The structural composition of this solution allows for the development of various types of structural instability, particularly concerning lateral buckling and in-plane deformations. To address these issues, bracing elements are introduced to enhance stiffness and structural stability, ensuring proper load transfer and preventing excessive deformation.

Analyzing the structure in the transverse plane, the buckling modes are directly related to the following aspects:

- They are a function of the normal forces within the arch.
- They are directly influenced by the stiffness and positioning of the bracings. Placing the bracings incorrectly relative to the structural development can amplify deformation modes rather than mitigate the issue. Bracings should be positioned at the inflection point of the mode, creating a configuration that maximizes their effect, with N_{cr} dependent on the flexural stiffness (*Figure 56*).

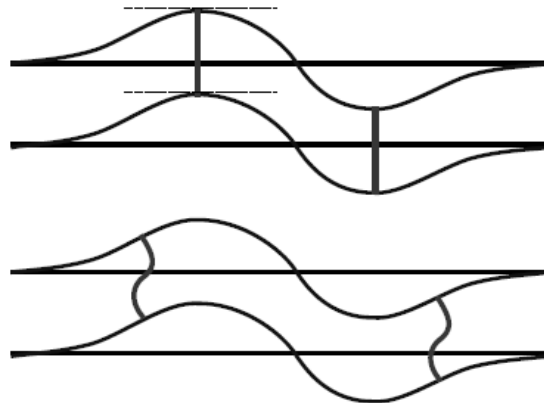


Figure 56: Explanatory Diagram of the Correct Positioning of Bracings³² - (Gens F. , Design and Construction of Bridges - Chap 03b-2 - Bowstring Bridges, 2024)

- The loads from the hangers are correlated with buckling since they act as an elastic foundation (*Figure 57*). They follow the movement of the superstructure, and the tension developed within them contributes to the overall stabilization of the system.

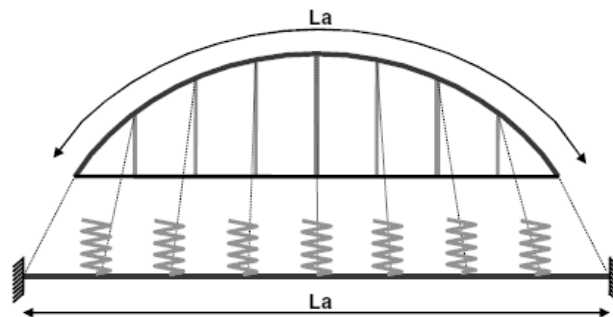


Figure 57: Hangers as Elastic Foundation of the Bowstring Bridge - (Gens F. , Design and Construction of Bridges - Chap 03b-2 - Bowstring Bridges, 2024)

³² The upper diagram in the figure represents an incorrect positioning of the bracings, as they are placed at the tangency point of the mode: This positioning has no stabilizing effect on the structure. Conversely, the lower diagram illustrates the correct placement of bracings along the structural body, at the inflection points of the mode, maximizing their stabilizing effect. It is important to note that the bracing system is effective only if it physically deforms with the structure. Otherwise, the passive addition of elements that merely follow the structural deformation does not contribute to the overall stability.

4 INTEGRATION OF NON-STRUCTURAL ELEMENTS

From the structural pre-design study and the selection of the solution to be implemented, the next step involves the selection of elements classified as non-structural. Since these elements represent loads acting on the deck of the structure, they contribute to the global calculations, and it is therefore necessary to select them based on type, shape, and technical characteristics to estimate their non-structural contributions.

In this regard, the selection focuses on the lateral safety elements (safety barriers) and on the pavement package to be installed on the bridge deck.

Starting with the lateral parapet, its selection is based on the intended function of the bridge: As it is not designed to host crowds or large gatherings of people, it can be classified within an occupancy category between Class IV (seldom used footbridges, built to link sparsely populated areas or to ensure continuity of pedestrian pathways along motorways or expressways) and Class III (footbridges for standard use, which may occasionally be crossed by large groups of people but will never be loaded across their entire bearing surface)³³. Remaining, in any case, within the classification of a footbridge subject to occasional crowd loading (in order to consider a possible higher load scenario), the lateral parapet is nonetheless identified as a Category B parapet³⁴, with a minimum horizontal load resistance of 1.0 kN/m. Accordingly, an example is selected that meets this requirement and provides a consistent design vision for the entire structure.

With reference to the company “*Aluscalae – Aluminium Structure Designers*”, an example of parapet is selected that meets these limitations: Under the name “*Parapetto Orizzonte*”, it provides a horizontal load capacity of 2 kN/m with a spacing of 120 cm between the vertical elements (*Figure 58*).

The parapet is therefore considered as an additional non-structural load with a total weight of 15 kg/m.



Figure 58: Example of Lateral Safety Parapet – Pedestrian Bridge – (Aluminium Parapets with Perforated Panels, 2025)

³³ (Gens F. , 2024), with reference to the classification provided by the SETRA Guidelines.

³⁴ With reference to the classification according to Eurocode 1, Part 1-1.

Moving on to the selection of the pavement package, the hypotheses analyzed include the possibility of maintaining the entire deck section in timber (as with the structural elements) or alternatively opting for a solution in a different material, engineered specifically for the case at hand.

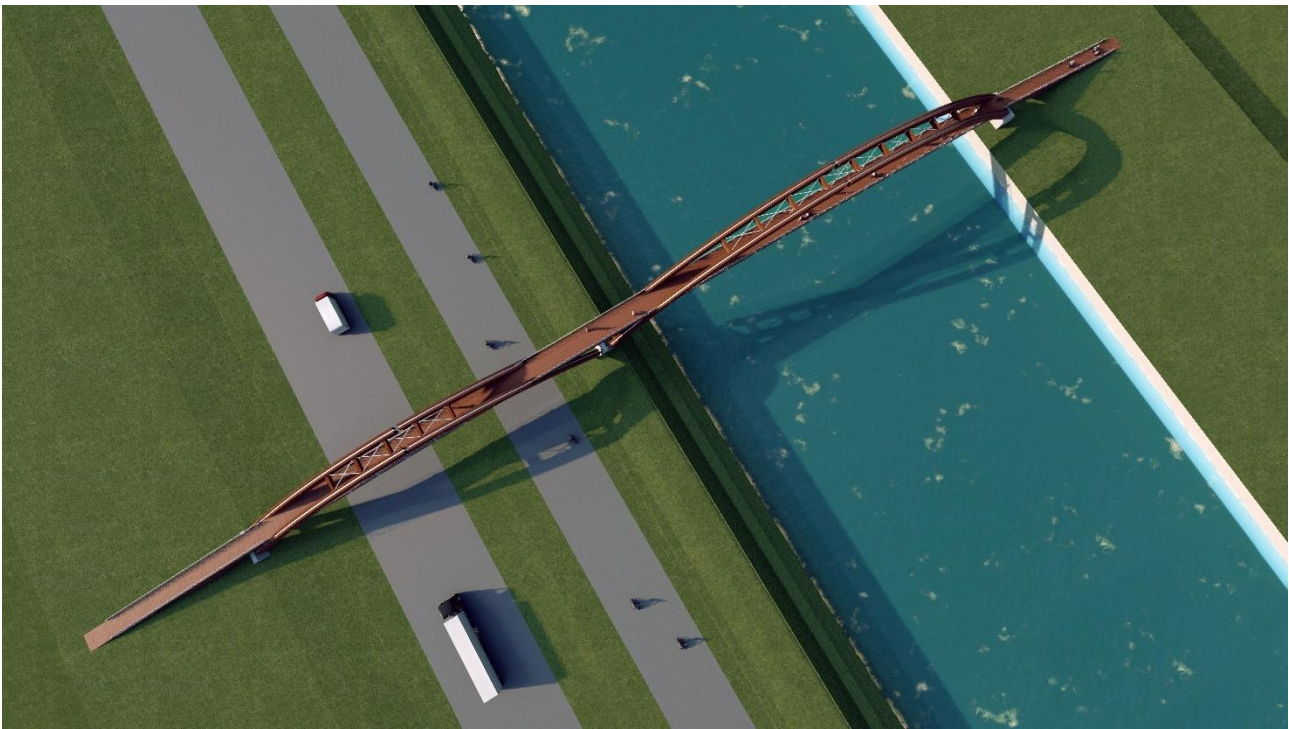
Since it is not of relevance for the development of the present analysis, a generic wooden plank flooring system is adopted, to which a maximum nominal thickness of 10 cm and a nominal weight of 50 kg/m² are assigned. Further considerations regarding this choice may follow.

5 RENDERING AND ENVIRONMENTAL INTEGRATION

Following the selection of the final structural solution, a series of architectural renderings was developed with the aim of illustrating the integration of the proposed design within its actual environmental context.

These images are intended to provide a comprehensive and realistic vision of the complete structure, highlighting its spatial relationship with the surrounding landscape. The visual simulations were generated based on the specific characteristics of the site under study, allowing for a deeper understanding of the bridge's visual impact and architectural presence in its real location.

A selection of the most representative views is presented below,³⁵ focusing on those that best support the understanding of the structural integration and overall design concept. Additional renderings, developed from multiple angles and viewpoints, are included in the *Annex 3* to the main document for further reference.



Rendering 1: Aerial View of the Pedestrian Bridge Over the Canal

³⁵ For the renderings, a dedicated label is created to avoid confusion within the list of figures and to make their position more easily accessible within the document, by placing them under a separate label.



Rendering 2: Longitudinal Perspective of the Bridge from the Riverbank



Rendering 3: Side View of the Bridge and Ramp Connection to the Ground



Rendering 4: Underside View of the Main Span Above the Water



Rendering 5: User Perspective from the Pedestrian Deck

6 STRUCTURAL ANALYSIS AND LOAD ASSESSMENT

The following chapters present a detailed analysis of the loading conditions of the pedestrian bridge in the selected structural configuration.

The analysis was carried out in accordance with the procedures and requirements established by Eurocode 0, Eurocode 1, and Eurocode 5, as well as the relevant national annexes concerning pedestrian bridge loading and structural verification. It was developed using a FEM model specifically created and loaded with the appropriate loading conditions and combinations prescribed by applicable standards.

The results obtained from this numerical model were compared with those derived from a preliminary manual analysis, which was conducted based on simplified assumptions regarding load distribution and force modelling, to verify the consistency of the FEM output with the expected structural behavior.

It should be noted that this manual verification procedure is not included within the present document, although it was effectively carried out as a means of validating the reported results.

6.1 LOAD DISTRIBUTION ALONG STRUCTURAL MEMBERS

Before proceeding with the analysis of the loads and load combinations, it is important to understand the load distribution on the structure as clearly as possible, to properly follow the calculation procedures that will be developed in the following subchapters.

To this end, simplified diagrams of load distribution are presented, dividing the structure into structural levels schematically described as follows:

- **Structural Level 1: Transverse Deck Section** – Loads are applied to the decking and directly transmitted to the secondary beams as distributed loads. These beams, idealized as simply supported on the primary lateral beams, generate point reactions on the latter (*Figure 59*), which then become distributed loads at the next structural level.

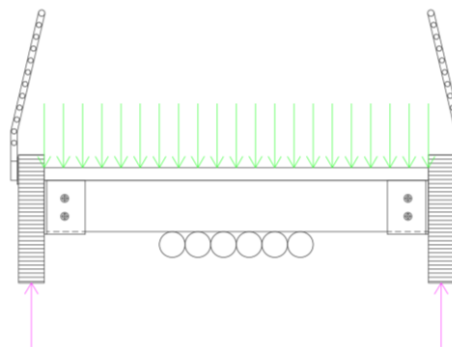


Figure 59: Structural Level 1 - Graphical Representation of the Force Distribution

- Structural Level 2: Primary Lateral Beams of the Deck** – The loads from Structural Level 1, summarized as support reactions of the secondary beams, are approximated by dividing them by the spacing between the secondary beams (approximately 2.6 meters), resulting in a distributed load along the primary beam. To this distributed load, additional loads acting directly on the primary beam are added, such as vertical snow loads acting only on the area of the primary beam, non-structural permanent loads from the lateral barrier fixed directly onto the beam, and the self-weight of the beam itself. The primary beams are then approximated as simply supported beams on multiple supports, represented by the vertical steel tension rods connected to the structural arches (*Figure 60*). In this way, the support reactions at each node become tensile forces in the vertical rods.

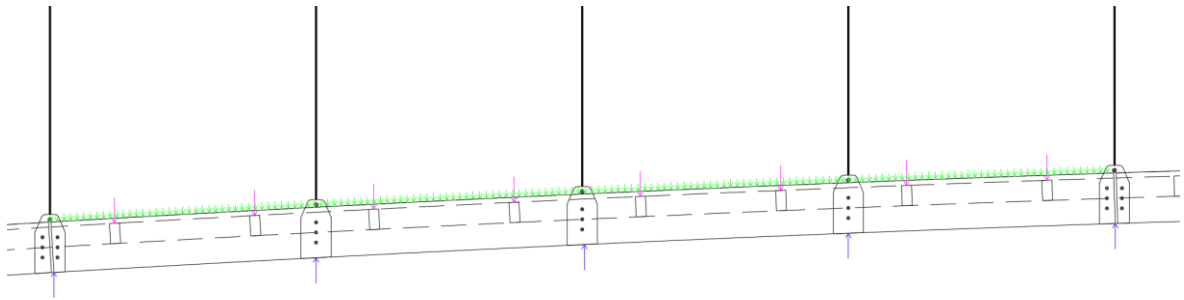


Figure 60: Structural Level 2 - Graphical Representation of the Force Distribution

- Structural Level 3: Structural Arches of the Bridge** – Connected to the deck through vertical steel tension rods, the arches are loaded with point loads at an approximately constant spacing of 5.3 meters, corresponding to the tensile reactions from the deck transferred through the rods (*Figure 61*).

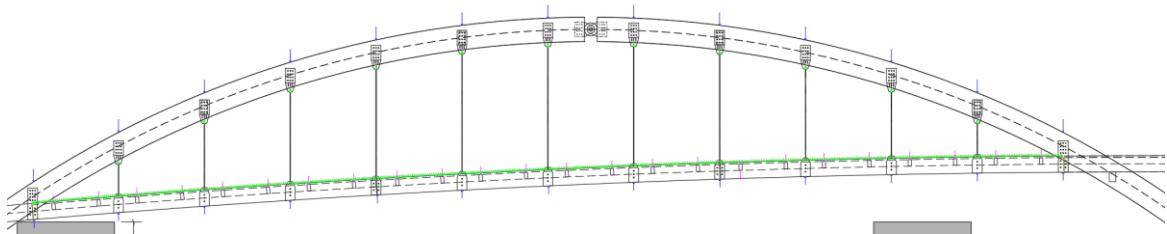


Figure 61: Structural Level 3 - Graphical Representation of the Force Distribution

- Structural Level 4: Central Primary Beams between the two Structural Arches** – The configuration of the deck changes in the area between the first two structural arches (ideally located on the left) and the subsequent two arches (ideally located on the right). In this zone, the deck section is composed of primary beams arranged longitudinally, all simply supported at both ends by transverse beams, which serve as connecting elements to the structural arches. In this way, the loads from the decking system are distributed among the longitudinal primary beams, which, in turn, transfer them as point reactions to the transverse beams, behaving as simply supported elements. The transverse beams are therefore loaded by the reactions of the

primary beams, which - by approximation - can be treated as distributed loads on the transverse beams (by dividing the point reactions by the spacing between the primary beams). At this point, the transverse beams generate two-point reactions onto the body of the structural arches, which are added to the loads already considered in Structural Level 3 (*Figure 62*).

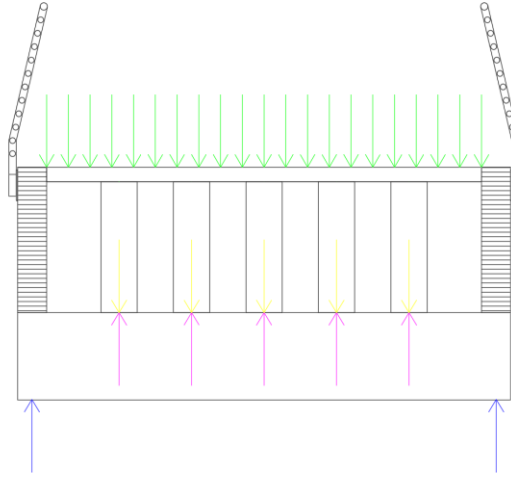


Figure 62: Structural Level 4- Graphical Representation of the Force Distribution

6.2 LOAD EVALUATION

With the aim of making the steps followed as clear as possible, a schematic description of the loads considered during the analysis is provided. The load categories are grouped into general macro-areas, within which the specific types of loads are detailed with their respective values and units.

6.2.1 PERMANENT LOADS

The analysis of permanent loads is divided into structural and non-structural permanent loads.

6.2.1.1 PERMANENT STRUCTURAL LOADS – MATERIAL PROPERTIES DEFINITION

Structural permanent loads are strictly related to the type of structural material selected. In the case under analysis, the entire structure is conceived and designed as entirely made of glued laminated timber (GLT), except for the steel connections, vertical tension rods, and stabilization diagonals, which are designed in S275 steel.

The structural elements are further divided into primary and secondary structural components. For the primary structural elements, GLT26h is selected, while for the secondary structural elements, GLT24h is adopted. It should be noted that this distinction is based on static considerations, particularly with respect to vertical loads and the self-weight of the structure.

The properties of the two selected GLT types are summarized in the following *Table 4*.

TIMBER ELEMENT PROPERTIES		
GLT	SECONDARY ELEMENTS	PRIMARY ELEMENTS
	GL24h	GL26h
fm,g,k [N/mm ²]	24	26
ft,0,g,k [N/mm ²]	19.2	20.8
ft,90,g,k [N/mm ²]	0.5	0.5
fc,0,g,k [N/mm ²]	24	26
fc,90,g,k [N/mm ²]	2.5	2.5
f,v,g,k [N/mm ²]	3.5	3.5
f,r,g,k [N/mm ²]	1.2	1.2
E0,g,mean [Mpa]	11500	12100
E0,g,05 [Mpa]	9600	10100
E90,g,mean [Mpa]	300	300
E90,g,05 [Mpa]	250	250
Gg,mean [Mpa]	650	650
Gg,05 [Mpa]	540	540
Gr,g,mean [Mpa]	65	65
Gr,g,05 [Mpa]	54	54
pg,k	385	405
pg,mean	420	445

Table 4: Timber Properties - (NBN EN 10480, 2013)

The loads, individually calculated for each element, are summarized in the following Table 5.

STRUCTURAL PERMANENT LOADS			
ELEMENT	DIMENSIONS [m]	MATERIAL	q [kg/m]
Primary Beams Deck	0.2x1.0	GL26h	89
Central Primary Beams	0.25x0.9	GL26h	100.13
Primary Beams Arches	0.25x1.5	GL26h	166.88
Transversal Beams	0.4x0.6	GL26h	106.80
Secondary Beams	0.2x0.4	GL24h	33.60

Table 5: Structural Permanent Loads - q [kg/m]

6.2.1.2 PERMANENT NON - STRUCTURAL LOADS

Non-structural permanent loads include the self-weight of all elements considered fixed but that do not contribute to structural stability. These loads comprise the weight of the lateral barrier (handrail), the wooden decking system, and the six DN200 pipes placed beneath the deck section.

These loads are summarized in the following Table 6³⁶.

³⁶ In the table, the loads are reported either in kg/m or in kg/m², depending on the case and the type under consideration. The load related to the piping system has been calculated based on a generic pipe with a weight of 10.91 kg/m, containing a generic liquid initially assumed to be water (considering a total of six pipes per cross-section). As previously described in the earlier chapters, a nominal load of 50 kg/m² is adopted for the decking system; this value is then multiplied by the relevant span during the analysis phase, since the primary direction of the decking changes depending on its position along the deck layout. The load associated with the lateral barriers is derived from the corresponding technical datasheet.

PERMANENT NON -STRUCTURAL LOADS	
ELEMENT	LOAD
Pipes (6xDN200) [kg/m]	220.09
Deck Pavement [kg/m ²]	50.00
Lateral Barrier [kg/m]	15.00

Table 6: Permanent Non- Structural Loads - Values in kg/m and kg/m²

6.2.2 PEDESTRIAN LOADS

The pedestrian load is derived from the provisions of *EN 1991-2:2003*, Section 4.3.5³⁷. A vertical pedestrian traffic load of $q_{fk} = 5 \text{ kN/m}^2$ is defined, along with a concentrated horizontal load Q_{fk} equal to 10% of the vertical load considered. These loads cannot be treated as separate actions and are therefore combined within the same loading conditions.

6.2.3 SNOW LOADS

Based on the provisions of Eurocode *EN 1991-1-3:2003*³⁸ regarding the calculation of snow load, and with reference to the Belgian National Annex for considerations concerning the exposure zone and the values to be adopted, the load is calculated according to the map (*Figure 63*) and the table (*Figure 64*) reported below, as follows:

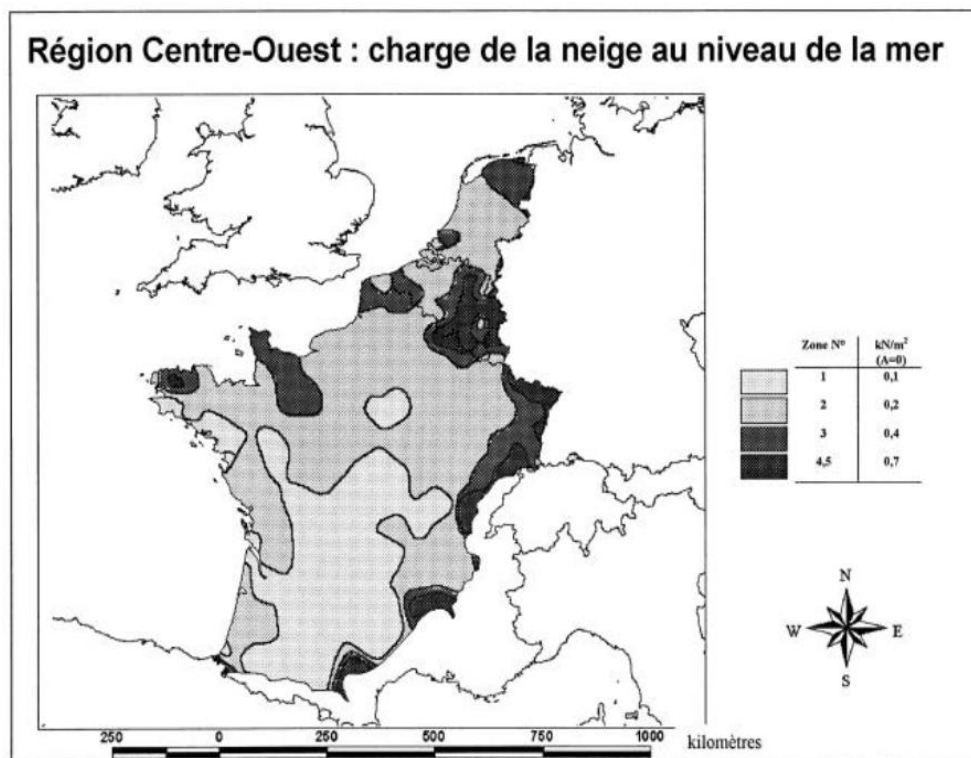


Figure 63: Exposure Zone Map - Snow Load for Belgium - National Belgian Annex

³⁷ (EN 1991 - Eurocode 1: Actions on structures & Relevant Annexes, 2003)

³⁸ (EN 1991 - Eurocode 1: Actions on structures & Relevant Annexes, 2003)

Tableau 5.1 — Valeurs recommandées de C_e en fonction de la topographie

Topographie	C_e
<u>Site balayé par les vents</u> : zone plate, sans obstacles et exposée de tous côtés, pas ou peu protégée par le terrain, par des constructions plus élevées ou par des arbres	0,8
<u>Site normal</u> : zone où il n'y a pas de balayage important de la neige par le vent, à cause de la configuration du terrain, de la présence d'autres constructions ou d'arbres	1,0
<u>Site protégé</u> : zone où la construction considérée est beaucoup plus basse que le terrain environnant, ou entourée de grands arbres ou encore de constructions plus élevées	1,2

Figure 64: Recommended C_e Values - Selection of the Most Conservative Value

$$s = \mu_i * C_e * C_t * s_K [kN/m^2]$$

A (altitude ASL) [m]	180
Z (region param.)	4.5
$s_K [kN/m^2]$	0.916135
μ_i	0.8
C_e^{39}	1.2
C_t	1
S [kN/m²]	0.88

Table 7: Snow Weight Computation [kN/m²]

6.2.4 WIND LOADS

The wind action load is calculated in accordance with the provisions of Eurocode EN 1991-1-5:2005⁴⁰.

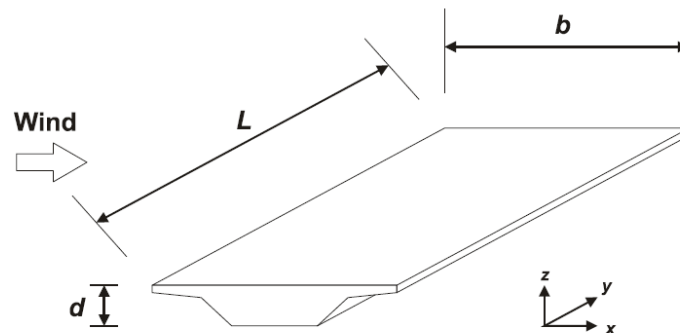


Figure 65: Description of the Dimensions and Directions in the Wind Calculation - EN 1991-1-5

It is important to note that, in the present case, the reference axes are used with an orientation different from that shown in Figure 65. Specifically, the y-axis is adopted to indicate the horizontal direction transverse to the generic cross-section of the deck, while the z-axis refers to the vertical direction. For

³⁹ The selection of $C_e = 1.2$ follows a conservative design approach.

⁴⁰ (EN 1991 - Eurocode 1: Actions on structures & Relevant Annexes, 2003)

the sake of calculation simplicity, the wind effect in the x-direction, parallel to the longitudinal axis of the deck, is neglected.

6.2.4.1 WIND FORCE IN HORIZONTAL y-DIRECTION: DECK ELEMENTS

The wind force in the horizontal direction is evaluated according to the following formula.

$$F_{w,y} = \frac{1}{2} * \rho_{air} * v_b^2 * C_y * A_{ref,y}$$

Where:

- ρ_{air} is the density of the air: 1.25 [kg/m³].
- $A_{ref,y}$ is the exposed area to the wind in y-direction. In the case under analysis, $A_{ref,y}$ is represented by the height of the primary beam of the deck multiplied by the influence length of each segment, which is assumed to be equal to the spacing between the secondary beams, approximately 2.6 meters.
- v_b is the reference wind velocity.
- $C_y = c_e * c_{f,y}$ is the wind load factor.
- c_e is the wind exposure coefficient.
- $c_{f,y}$ is the wind action coefficient.

All the aforementioned factors are subsequently calculated based on the location of the structure, which is assumed to be situated in a “*Ground Class II*” area, with corresponding values of $z_o = 0.05m$ and $z_{min} = 2m$.

Determination of the Reference Wind Velocity

The wind velocity formula is presented as follows:

$$v_b = c_{prob} * c_{dir} * c_{season} * v_{b,0}$$

With $v_{b,0} = 24$ m/s. Considering a return period of 50 years, the probability factor is set to $c_{prob} = 1$. In the absence of a prevailing wind direction ($c_{dir} = 1$) and without reference to a dominant season ($c_{season} = 1$), the reference wind velocity v_b is assumed to be equal to $v_{b,0} = 24$ m/s.

Wind Exposure Coefficient

The calculation height for the deck is equal to the maximum height of the deck above the level considered zero, to which the effective height of the deck profile (i.e., the height of the primary beam, equal to 1 meter) is added. Consequently, considering that the lower intrados of the deck is located at a height of 6.5 meters, the reference height used for the calculation is: $z = 7.5$ m. Comparing this value with the previously defined minimum height ($z_{min} = 2$ m), the condition $z > z_{min}$ is satisfied, and therefore:

Wind Force in the y-Direction

Based on the evaluations above, the wind force is calculated as follows:

$$F_{w,y} = \frac{1}{2} * \rho_{air} * v_b^2 * C_y * A_{ref,y} = 3.25 [kN]$$

The force, expressed as a concentrated value in the simplified procedure, is converted into an area pressure by dividing it by the previously calculated value of $A_{ref,y}$. The resulting value is therefore:

$$F_{w,y} = 1.25 [kN/m^2]$$

6.2.4.2 WIND FORCE IN VERTICAL z – DIRECTION: DECK ELEMENTS

The calculation of the wind action in the z-direction follows the same procedure as that adopted for the y-direction; the only difference lies in the reference dimensions used for the area calculation. In this case, the reference area is no longer the lateral surface but the bottom surface of the deck, which is calculated using a base width of $b = 3000$ mm and a reference segment length of $L = 2600$ mm.

A further point of difference is the calculation of the coefficient $c_{f,z}$, which is obtained empirically, again with reference to the ratio $b/d_{tot} = 3$, from the graph shown in the *Figure 67*:

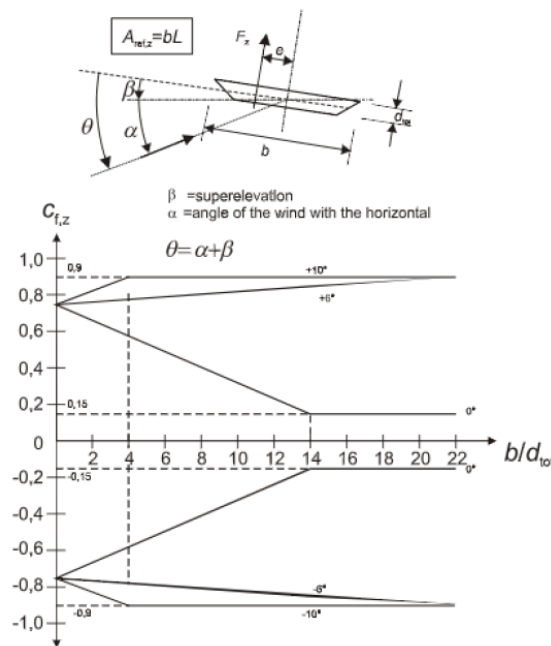


Figure 67: Empirical Computation of the $c_{f,z,0}$ Factor in Relation to the “b/d” Ratio - EN 1991-1-5

The coefficient $c_{f,z}$ is assumed to be equal to 0.6.

Wind Load Factor

$$C_z = c_e * c_{f,z} = \pm 1.303$$

Wind Force in the z-Direction

Based on the evaluations above, the wind force is calculated as follows:

$$F_{w,z} = \frac{1}{2} * \rho_{air} * v_b^2 * C_z * A_{ref,z} = \pm 3.66[kN]$$

The force, expressed as a concentrated value in the simplified procedure, is converted into an area pressure by dividing it by the previously calculated value of $A_{ref,z}$. The resulting value is therefore:

$$F_{w,z} = \pm 0.469 [kN/m^2]^{42}$$

6.2.4.3 WIND FORCE IN y & z – DIRECTION: ARCH ELEMENTS

The same procedure is applied for the calculation of the wind action acting on the structural arches. It is important to note that, due to the reduced base width of the arch cross-section, the wind action is considered only in the horizontal y-direction, while the vertical z-direction component is neglected.

Following the same procedure, but with a reference height of $z = 15 \text{ m}$ (13.5 m^{43} from the intrados to the reference level plus 1.5 m for the height of the arch section), and by obtaining the correct wind coefficients based on a ratio of $b/d_{tot} = 0.33$ (with $b = 500 \text{ mm}$ and $d_{tot} = 1500 \text{ mm}$), the following value of horizontal pressure is obtained:

$$F_{w,y} = 2.26 [kN/m^2]^{44}$$

6.2.5 TEMPERATURE LOADS

The reference temperature is taken as $T_o = +20^\circ\text{C}$, at which the bridge geometry is completed. A variation of $\pm 20^\circ\text{C}$ is considered, resulting in a maximum temperature of $T_{max} = 40^\circ\text{C}$ and a minimum temperature of $T_{min} = -0^\circ\text{C}$.

The application of the temperature gradient is performed in a separate analysis, which is in fact presented in a subsequent subchapter. This analysis was carried out with the aim of verifying the structural stability under thermal loading and understanding the resulting deformations.

A detailed examination of this aspect is provided in the following chapters.

⁴² The wind action in the z-direction is considered as potentially acting in both the positive and negative directions with respect to the reference z-axis.

⁴³ The reference height of 13.5 meters corresponds to the top of the taller of the two consecutive arches. This choice is conservative in terms of calculating the horizontal wind action, as the pressure is proportional to the height above the reference level. For this reason, the calculation is carried out with reference to the taller arch, and the same pressure is applied to the lower one as well.

⁴⁴ It is important to note that, since the structural arches develop vertically with a height difference of 13.5 meters between the base section and the top section, the wind pressure in the horizontal direction would not be uniformly distributed, but rather trapezoidal, reaching its maximum value at the top, as just calculated. However, adopting a conservative approach, the wind action at the top is considered as a uniform pressure applied along the entire height of the structural arch.

6.3 LOAD COMBINATIONS

To limit state verifications, the following combinations of actions are defined, In accordance with the provisions of Eurocode EN 1990:2002⁴⁵ (paragraphs 6.4.3.2 & 6.5.3):

Fundamental Combination, used for Ultimate Limit States (ULS):

$$\sum_{j \geq i} \gamma_{G,j} * G_{k,j} + \gamma_{Q,1} * Q_{k,1} + \sum_{i > 1} \gamma_{Q,i} * \psi_{0,i} * Q_{k,i}$$

Characteristic (Rare) Combination, used for irreversible Serviceability Limit States (SLS):

$$\sum_{j \geq i} G_{k,j} + Q_{k,1} + \sum_{i > 1} \psi_{0,i} * Q_{k,i}$$

Frequent Combination, used for reversible Serviceability Limit States (SLS):

$$\sum_{j \geq i} G_{k,j} + \sum_{i > 1} \psi_{1,i} * Q_{k,i}$$

Where:

- $\gamma_{G,j}$ = partial factor for permanent actions.
 $\gamma_{G,j} = 1.35$ if permanent action is unfavorable.
 $\gamma_{G,j} = 1.00$ if permanent action is favorable.
- $G_{k,j}$ = characteristic value of the j-th permanent action.
- $\gamma_{Q,i}$ = partial factor for variable actions.
 $\gamma_{Q,i} = 1.35$ if the variable action is due to pedestrian traffic and is unfavorable.
 $\gamma_{Q,i} = 1.50$ if the variable action is due to snow, wind (excluding traffic) and is unfavorable.
 $\gamma_{Q,i} = 0.00$ if the variable action is favorable.
- $Q_{k,i}$ = characteristic value of the i-th variable action.
- $Q_{k,1}$ = characteristic value of the principal (leading) variable action.
- $\psi_{0,i}$ & $\psi_{1,i}$ are the combination factor accounting for the non-simultaneous statistical occurrence of loads acting on a structure.

The factors $\psi_{0,i}$ & $\psi_{1,i}$ shall be assumed according to the values given in the following table (*Figure 68*), which refers to the design of pedestrian bridges (ref. EN 1990 – Table A2.2⁴⁶).

⁴⁵ (EN 1990 - Eurocode 0: Basis of Structural Design & Relevant Annexes, 2002).

⁴⁶ (EN 1990 - Eurocode 0: Basis of Structural Design & Relevant Annexes, 2002) – With reference to the Belgian Annex.

Tableau A2.2 ANB – Valeurs des coefficients ψ pour les passerelles

Action	Symbole	ψ_0	ψ_1	ψ_2
Charges de trafic	gr1	0,40	0,40	0
	$Q_{f,wk}$	0	0	0
	gr2	0	0	0
Actions du vent	F_{wk} - situations de projet durables	0,6 ²⁾	0,2	0
	- exécution	0,8 ²⁾	-	0
Actions de la température	T_k	0,6 ^{1,2)}	0,6	0,5
Charges de neige	$Q_{Sn,k}$ - pendant l'exécution	0,8 ²⁾	-	0
	- pour les passerelles couvertes pour situations de projet durables	0,5 ²⁾	-	0
Charges de construction	Q_c	1,0	-	1,0

1) La valeur recommandée ψ_0 pour les actions dues à la température peut dans la plupart des cas être réduite à zéro pour les états-limites ultimes EQU, STR et GEO. Voir aussi les Eurocodes de projet.

2) Lorsqu'une action de courte durée (inférieure à 1 mois), par ex. charge d'exploitation, charge de neige, action du vent, action de la température, est suivie dans une combinaison par une autre action de courte durée, une valeur $\psi_0 = 0,3$ peut être utilisée pour la seconde action variable lorsque celle-ci est une charge de neige, une action du vent ou action due à une variation de la température de l'air. Voir aussi A1.1 ANB (3) pour la justification de cette disposition.

Figure 68: Table A2.2 - Recommended Values of ψ Factors for Footbridges

It is important to note that snow is considered as acting only during the construction phases, as it is deemed incompatible with pedestrian traffic. For this reason, in the combinations described below, snow is never combined with pedestrian traffic.

In the manual calculation phases, however, the load combination adopted for the manual evaluation of structural effects - aimed at performing both ultimate and serviceability limit state verifications - is deliberately overestimated and does not follow the assumption of incompatibility between snow and pedestrian traffic. In fact, the snow load was combined with the pedestrian load as a secondary variable action, to intentionally overestimate the effects on the structure during its service life.

Clearly, this overestimation of stresses and internal forces also serves the purpose of manually validating the calculations⁴⁷, allowing for a higher approximation margin. All internal forces calculated under this specific load combination are then compared - expressed as a percentage - with the critical maximum envelope values derived from Eurocode combinations. In this way, a note concerning any possible overdesign is generated, allowing for further considerations on the potential reduction of some of the calculated cross-sections.

To summarize the coefficients used in the analysis, they are presented in the following *Table 8*:

⁴⁷ The structural calculations were initially carried out manually, following the overestimation of the actions. After completing the manual analysis of loads and their effects, including the calculation and verification of the cross-sections, a FEM model was developed, which is described in the following chapters. This model was loaded with the defined actions, and the appropriate loading conditions were applied. As already stated in the body of the text, the manual calculation serves as a verification tool for the automated FEM analysis. This approach aims to ensure the reliability of the results and to detect any modelling errors that may become evident through significant discrepancies between manual and automated calculations.

LOAD COMBINATION FACTORS						
	unf.	fav.	SLS	ψ_0	ψ_1	ψ_2
Self-Weight	1.35	1	1.00	-	-	-
Traffic Pedestrian	1.35	0	1.00	0.4	0.4	0
Wind	1.5	0	1.00	0.3	0.2	0
Temperature	1.5	0	1.00	0.6	0.6	0.5
Snow	1.5	0	1.00	0.8	-	0
Construction	1.5	0	1.00	1	-	1

Table 8: Loads Combination Factors

6.3.1 LOAD ZONING

With the aim of generating load combinations as effectively as possible for structural analysis purposes, the deck was divided into five influence zones: Two located under the first structural arch, two under the second structural arch, and one in the area between the two arches, as shown in the following *Figure 69*:

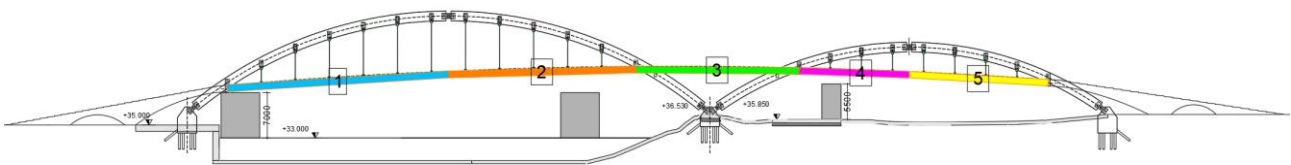


Figure 69: Five Deck Zones for Load Combination Analysis

For these five load zones, six different load position conditions were defined and subsequently applied to each load combination under analysis. In this way, the six load conditions are repeated as many times as there are action combinations considered in the analysis.

The different load conditions are illustrated in the following figures:

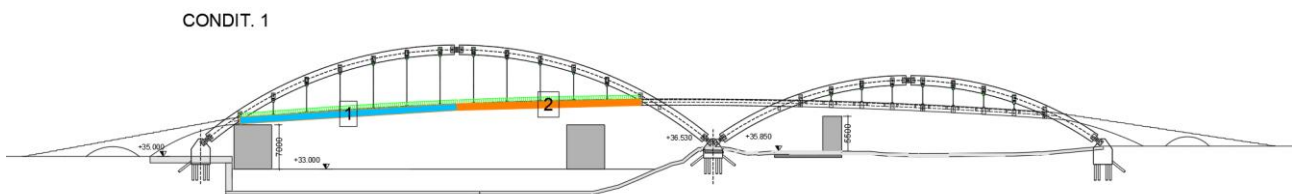


Figure 70: Load Position - Condition 1 - Applied Loads on Deck Segments 1 & 2

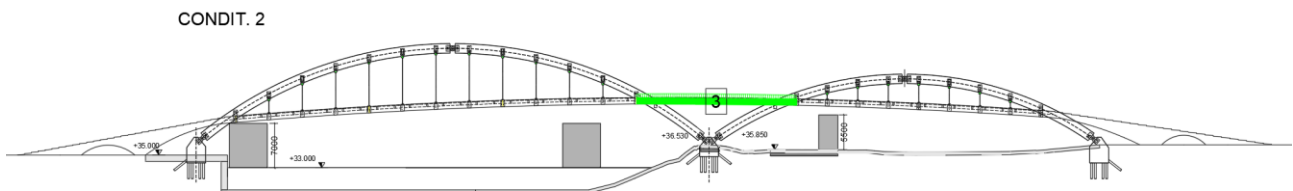


Figure 71: Load Position - Condition 2 - Applied Loads on Deck Segment 3

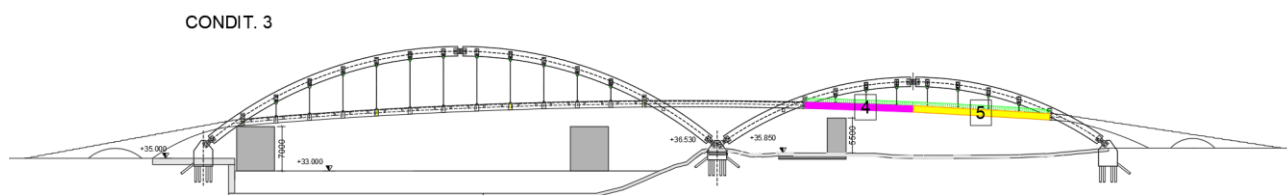


Figure 72: Load Position - Condition 3 - Applied Loads on Deck Segments 4 & 5

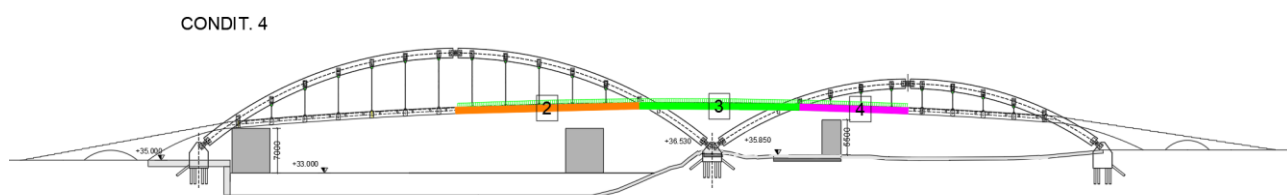


Figure 73: Load Position - Condition 4 - Applied Loads on Deck Segments 2 & 3 & 4

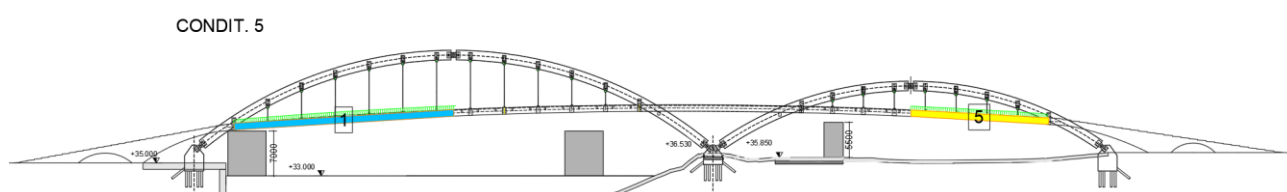


Figure 74: Load Position – Condition 5 - Applied Loads on Deck Segments 1 & 5

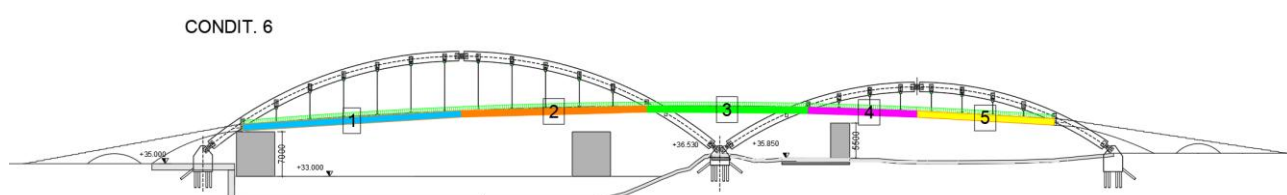


Figure 75: Load Position - Condition 6 - Applied Loads on All Deck Segments

It is important to note that all load conditions, although illustrated as vertical loads, are also replicated in the horizontal direction wherever deemed necessary.

6.3.2 ULTIMATE LIMIT STATE (ULS) COMBINATIONS - EN 1990 (6.4.3.2)

LOADS COMBINATIONS TO THE ULTIMATE LIMIT STATE EN 1990 6.4.3.2							
SNOW ACTION	SSz	0	0	0	0	0	0
	YQ	1.5	1.5	1.5	1.5	1.5	1.5
WIND ACTION	ψ0	0	0	0	0	0	0
	SWy	0	0	0	0	0	0
	SWz	0	0	0	0	0	0
	YQ	1.5	1.5	1.5	1.5	1.5	1.5
	ψ0	0	0	0	0	0	0
	SVx5	0	1.35	0	0	1.35	1.35
	SVz5	0	1.35	0	0	1.35	1.35
TRAFFIC LOADS qfk & Qfk	SVx4	0	1.35	0	1.35	0	1.35
	SVz4	0	1.35	0	1.35	0	1.35
	SVx3	0	0	1.35	1.35	0	1.35
	SVz3	0	0	1.35	1.35	0	1.35
	SVx2	1.35	0	0	1.35	0	1.35
	SVz2	1.35	0	0	1.35	0	1.35
	SVx1	1.35	0	0	1.35	1.35	1.35
	SVz1	1.35	0	0	1.35	1.35	1.35
	ψ0	1	1	1	1	1	1
	PERMANENT LOADS	PP+SP	1.35	1.35	1.35	1.35	1.35
DEAD		1.35	1.35	1.35	1.35	1.35	1.35
	SLU_1	SLU_2	SLU_3	SLU_4	SLU_5	SLU_6	

0	0	0	0	0	0	0	0	0	0	0	0
1.5	1.5	1.5	1.5	1.5	1.5	1.5	1.5	1.5	1.5	1.5	1.5
0	0	0	0	0	0	0	0	0	0	0	0
0	0	0	0	0	0	0.45	0.45	0.45	0.45	0.45	0.45
0	0	0	0	0	0	0.45	0.45	0.45	0.45	0.45	0.45
0	0	0	0	0	0	0.45	0.45	0.45	0.45	0.45	0.45
1.5	1.5	1.5	1.5	1.5	1.5	1.5	1.5	1.5	1.5	1.5	1.5
0	0	0	0	0	0	0.3	0.3	0.3	0.3	0.3	0.3
0	-1.35	0	0	-1.35	-1.35	0	1.35	0	0	1.35	1.35
0	1.35	0	0	0	1.35	0	1.35	0	0	1.35	1.35
0	-1.35	0	-1.35	0	-1.35	0	1.35	0	1.35	1.35	0
0	1.35	0	1.35	0	1.35	0	1.35	0	1.35	1.35	0
0	0	-1.35	0	-1.35	-1.35	0	0	1.35	1.35	0	0
0	1.35	0	1.35	0	1.35	0	1.35	0	1.35	1.35	0
0	0	-1.35	-1.35	0	-1.35	0	0	1.35	1.35	0	0
0	0	1.35	1.35	0	1.35	0	1.35	1.35	1.35	0	0
-1.35	0	0	-1.35	0	-1.35	1.35	0	0	1.35	1.35	0
1.35	0	0	1.35	0	1.35	1.35	0	0	1.35	1.35	0
-1.35	0	0	0	-1.35	-1.35	1.35	0	0	1.35	1.35	0
1.35	0	0	1.35	0	1.35	1.35	0	0	1.35	1.35	0
1.35	0	0	0	1.35	1.35	1.35	0	0	1.35	1.35	0
1	1	1	1	1	1	1	1	1	1	1	1
1.35	1.35	1.35	1.35	1.35	1.35	1.35	1.35	1.35	1.35	1.35	1.35
1.35	1.35	1.35	1.35	1.35	1.35	1.35	1.35	1.35	1.35	1.35	1.35
SLU_7	SLU_8	SLU_9	SLU_10	SLU_11	SLU_12	SLU_13	SLU_14	SLU_15	SLU_16	SLU_17	

0	0	0	0	0	0	0	0	0	0	0
1.5	1.5	1.5	1.5	1.5	1.5	1.5	1.5	1.5	1.5	1.5
0	0	0	0	0	0	0	0	0	0	0
0.45	0.45	0.45	0.45	0.45	0.45	1.5	1.5	1.5	1.5	1.5
0.45	-0.45	-0.45	-0.45	-0.45	-0.45	1.5	1.5	1.5	1.5	1.5
1.5	1.5	1.5	1.5	1.5	1.5	1.5	1.5	1.5	1.5	1.5
0.3	0.3	0.3	0.3	0.3	0.3	1	1	1	1	1
1.35	0	1.35	0	0	1.35	0	0.54	0	0	0
1.35	0	1.35	0	0	1.35	0	0.54	0	0	0
1.35	0	1.35	0	1.35	0	0	0.54	0	0	0.54
1.35	0	1.35	0	1.35	0	0	0.54	0	0	0.54
1.35	0	1.35	0	1.35	0	0	0.54	0	0	0.54
1.35	0	0	1.35	1.35	0	0	0	0	0	0.54
1.35	0	0	1.35	1.35	0	0	0	0	0	0.54
1.35	0	0	1.35	1.35	0	0	0	0	0	0.54
1.35	0	0	0	1.35	0	0.54	0	0	0	0.54
1.35	1.35	0	1.35	1.35	0	0.54	0	0	0	0.54
1.35	1.35	0	0	1.35	0	0.54	0	0	0	0
1	1	1	1	1	1	0.4	0.4	0.4	0.4	0.4
1.35	1.35	1.35	1.35	1.35	1.35	1.35	1.35	1.35	1.35	1.35
1.35	1.35	1.35	1.35	1.35	1.35	1.35	1.35	1.35	1.35	1.35
SLU_18	SLU_19	SLU_20	SLU_21	SLU_22	SLU_23	SLU_24	SLU_25	SLU_26	SLU_27	SLU_28

0	0	0	0	0	0	0	0	1.2	1.5
1.5	1.5	1.5	1.5	1.5	1.5	1.5	1.5	1.5	1.5
0	0	0	0	0	0	0	0	0.8	1
1.5	1.5	1.5	1.5	1.5	1.5	1.5	1.5	1.5	0.45
1.5	1.5	-1.5	-1.5	-1.5	-1.5	-1.5	-1.5	-1.5	-0.45
1.5	1.5	1.5	1.5	1.5	1.5	1.5	1.5	1.5	1.5
1	1	1	1	1	1	1	1	1	0.3
0.54	0.54	0	0.54	0	0	0.54	0.54	0	0
0.54	0.54	0	0.54	0	0	0.54	0.54	0	0
0	0.54	0	0.54	0	0.54	0	0.54	0	0
0	0.54	0	0.54	0	0.54	0	0.54	0	0
0	0.54	0	0	0.54	0.54	0	0.54	0	0
0	0.54	0	0	0.54	0.54	0	0.54	0	0
0	0.54	0	0	0.54	0.54	0	0.54	0	0
0	0.54	0.54	0	0	0.54	0	0.54	0	0
0.54	0.54	0.54	0	0	0.54	0.54	0.54	0	0
0.54	0.54	0.54	0	0	0.54	0.54	0.54	0	0
0.4	0.4	0.4	0.4	0.4	0.4	0.4	0.4	0	0
1.35	1.35	1.35	1.35	1.35	1.35	1.35	1.35	1	1
1.35	1.35	1.35	1.35	1.35	1.35	1.35	1.35	1	1
SLU_29	SLU_30	SLU_31	SLU_32	SLU_33	SLU_34	SLU_35	SLU_36	SLU_37	SLU_38

Table 9: Combination Matrix for the 6 Loads Conditions – ULS

6.3.2.1 EXPLANATION OF THE LOAD COMBINATIONS AT THE ULS

- **SLU-1 TO SLU-12:** Combinations possible in absence of wind. When SV_x has a negative sign, the pedestrian traffic goes in the opposite direction of the x axis.
- **SLU-13 TO SLU-24:** Pedestrian traffic as principal variable load and wind at 30% ($\psi_0 \cdot \gamma_Q = 0.30 \cdot 1.50 = 0.45$). When SW_z is in negative sign, the direction is opposite to the principal direction of the z-axis. All the wind combinations in SW_z and SW_y are applied simultaneously because the vertical component comes from the horizontal one.
- **SLU-25 TO SLU-36:** Pedestrian traffic at 40% ($(\psi_0 \cdot \gamma_Q = 0.40 \cdot 1.35 = 0.54)$) and wind assumed as principal variable load.
- **SLU-37 & SLU-38:** Pedestrian traffic absent and wind as principal variable action (SLU-37) or snow as principal variable action (SLU-38). Wind is only considered as negative in z-direction to maximize the possibility of load inversion on the structural elements. For this reason, self-weight and non-structural permanent loads are combined with coefficient = 1.

6.3.3 SERVICEABILITY LIMIT STATE (SLS) – CHARACTERISTIC COMBINATION – EN 1990 (6.5.3)

LOADS COMBINATIONS TO THE SERVICE LIMITE STATE - CHARACTERISTIC COMBINATION - EN 1990 6.5.3	SNOW ACTION	SSz	0	0
		YQ	1.00	1.00
		ψ0	0	0
	WIND ACTION	SWy	0	0
		SWz	0	0
		YQ	1.00	1.00
		ψ0	0	0
	TRAFFIC LOADS qtk & Qfk	SVx5	0	1
		SVz5	0	1
		SVx4	0	1
		SVz4	0	1
		SVx3	0	0
		SVz3	0	0
		SVx2	1	0
		SVz2	1	0
	PERMANENT LOADS	SVx1	1	0
		SVz1	1	0
ψ0		1	1	
PP+SP		1.00	1.00	
DEAD	1.00	1.00		
SLS_1		SLS_2		

0	0	0	0	0	0	0	0	0	0	1	
1.00	1.00	1.00	1.00	1.00	1.00	1.00	1.00	1.00	1.00	1.00	
0	0	0	0	0	0	0	0	0	0	1.00	
1	1	1	1	1	1	1	1	1	1	0.3	
1	1	1	1	1	-1	-1	-1	-1	-1	0.3	
1.00	1.00	1.00	1.00	1.00	1.00	1.00	1.00	1.00	1.00	1.00	
1	1	1	1	1	1	1	1	1	1	0.3	
0.4	0	0	0.4	0.4	0	0.4	0	0	0.4	0	
0.4	0	0	0.4	0.4	0	0.4	0	0	0.4	0	
0.4	0	0.4	0	0.4	0	0.4	0	0	0.4	0	
0	0.4	0.4	0	0.4	0	0.4	0.4	0	0.4	0	
0	0	0.4	0	0.4	0.4	0	0.4	0	0.4	0	
0	0	0	0.4	0.4	0.4	0	0	0	0.4	0	
0	0	0	0.4	0.4	0.4	0	0	0	0.4	0	
0	0	0	0.4	0.4	0.4	0	0	0	0.4	0	
0.4	0.4	0.4	0.4	0.4	0.4	0.4	0.4	0.4	0.4	0	
1.00	1.00	1.00	1.00	1.00	1.00	1.00	1.00	1.00	1.00	1.00	
1.00	1.00	1.00	1.00	1.00	1.00	1.00	1.00	1.00	1.00	1.00	
SLS_14	SLS_15	SLS_16	SLS_17	SLS_18	SLS_19	SLS_20	SLS_21	SLS_22	SLS_23	SLS_24	SLS_25

6.3.4 SERVICEABILITY LIMIT STATE (SLS) – FREQUENT COMBINATION – EN 1990 (6.5.3)

LOADS COMBINATIONS TO THE SERVICE LIMIT STATE - FREQUENT COMBINATION - EN 1990 6.5.3									
	SNOW ACTION	SSz	0	0	0	0	0	0	0
		YQ	1.00	1.00	1.00	1.00	1.00	1.00	1.00
	ψ0	0	0	0	0	0	0	0.00	0.00
WIND ACTION	SWy	0	0	0	0	0	0	0.2	0.2
	SWz	0	0	0	0	0	0	0.2	-0.2
	YQ	1.00	1.00	1.00	1.00	1.00	1.00	1.00	1.00
	ψ0	0	0	0	0	0	0	0.2	0.2
	SVx5	0	0.4	0	0	0.4	0.4	0	0
TRAFFIC LOADS qfk & Qfk	SVz5	0	0.4	0	0	0.4	0.4	0	0
	SVx4	0	0.4	0	0.4	0	0.4	0	0
	SVz4	0	0.4	0	0.4	0	0.4	0	0
	SVx3	0	0	0.4	0.4	0	0.4	0	0
	SVz3	0	0	0.4	0.4	0	0.4	0	0
	SVx2	0.4	0	0	0.4	0	0.4	0	0
	SVz2	0.4	0	0	0.4	0	0.4	0	0
	SVx1	0.4	0	0	0.4	0.4	0	0	0
PERMANENT LOADS	SVz1	0.4	0	0	0.4	0.4	0	0	0
	ψ0	0.4	0.4	0.4	0.4	0.4	0	0	0
	PP+SP	1.00	1.00	1.00	1.00	1.00	1.00	1.00	1.00
	DEAD	1.00	1.00	1.00	1.00	1.00	1.00	1.00	1.00
		SLSF_1	SLSF_2	SLSF_3	SLSF_4	SLSF_5	SLSF_6	SLSF_7	SLSF_8

Table 11: Combination Matrix for the 6 Loads Conditions – SLS Frequent Combination

7 FINITE ELEMENT MODELLING (FEM) AND STRUCTURAL RESULTS

To implement the analyzed load combinations and proceed with the verification of sections and structural elements, a detailed FEM model is developed.

For this purpose, the software *MasterSap 4U*, developed by the Italian company AMV, is selected.

The structure is initially idealized as a composition of points and vector coordinates arranged in space; all structural elements are subsequently generated and connected to their respective nodes, with the objective of creating the complete Finite Element Model (*Figure 76*).

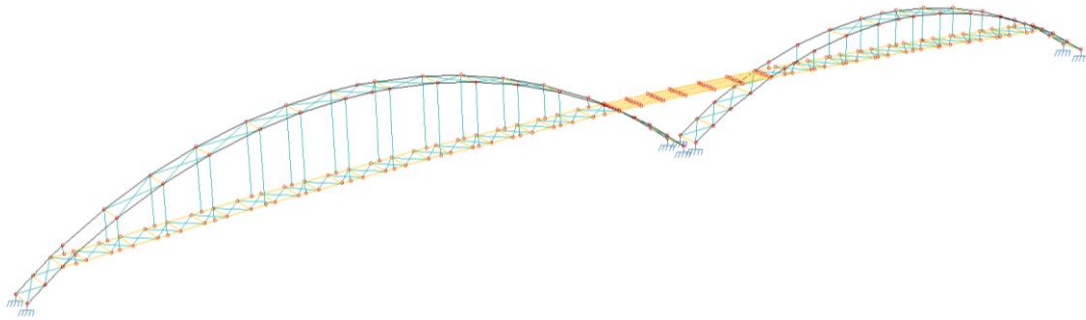


Figure 76: FEM Model: Structural Elements, Nodes and Nodal Connections

The meshing of the structural elements leads to the generation of intermediate nodes along with the linear development of the individual constituent elements. In this regard, to restore the structural completeness and continuity of the components, internal connection properties are assigned to the constituent nodes. In this way, the nodes located within the structural elements are provided with continuity stiffness; all nodes at the ends of the elements are instead defined with properties that reflect their respective boundary conditions:

- For simply supported elements, the start and end nodes are released in the M_z and M_y rotational directions (with respect to the reference axes of the model).
- The same principle applies to fully restrained elements, which are kept rigid.
- At the bases of the structural arches, external fixed supports are initially assigned and then modified into internal properties of the arch beams by releasing the appropriate rotational degrees of freedom, to reproduce the three-hinged arch base condition and maintain the isostatic structural system.

Each element is assigned the appropriate cross-section and material properties, dividing the structure into structural levels and individual structural elements. In this way, each element is associated with a list of geometric and structural properties that can be independently modified during the analysis of the results. In the following figures (*Figure 77 & Figure 78*) a global view of the bridge, with a color-coded graphical representation distinguishing between materials and section geometries, is represented. Each view is appropriately accompanied by a legend.

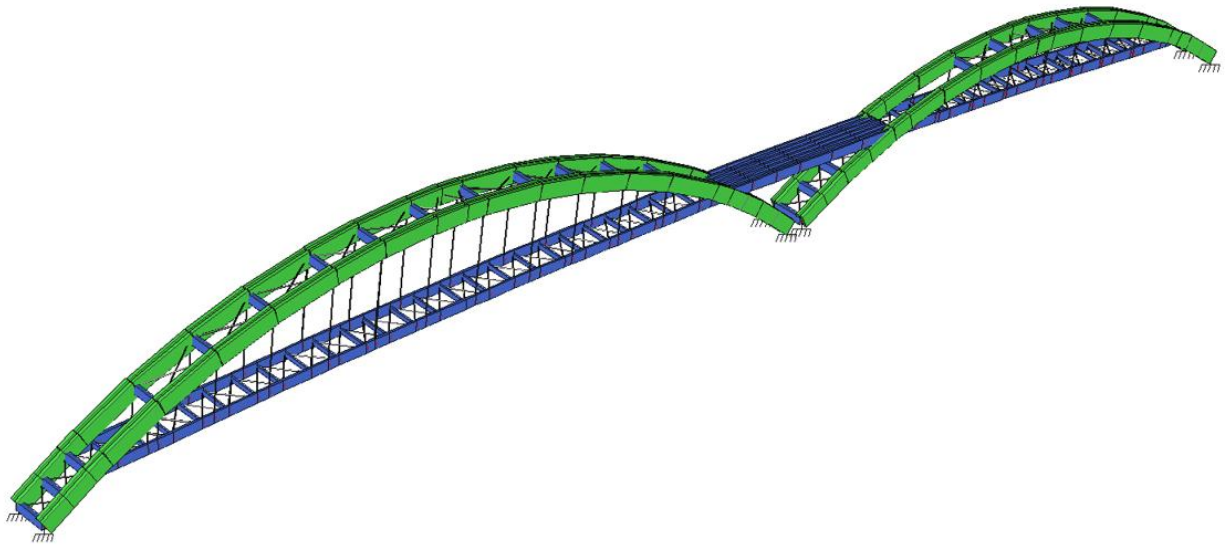


Figure 77: Global Structural View - Elements Grouped by Color⁴⁸

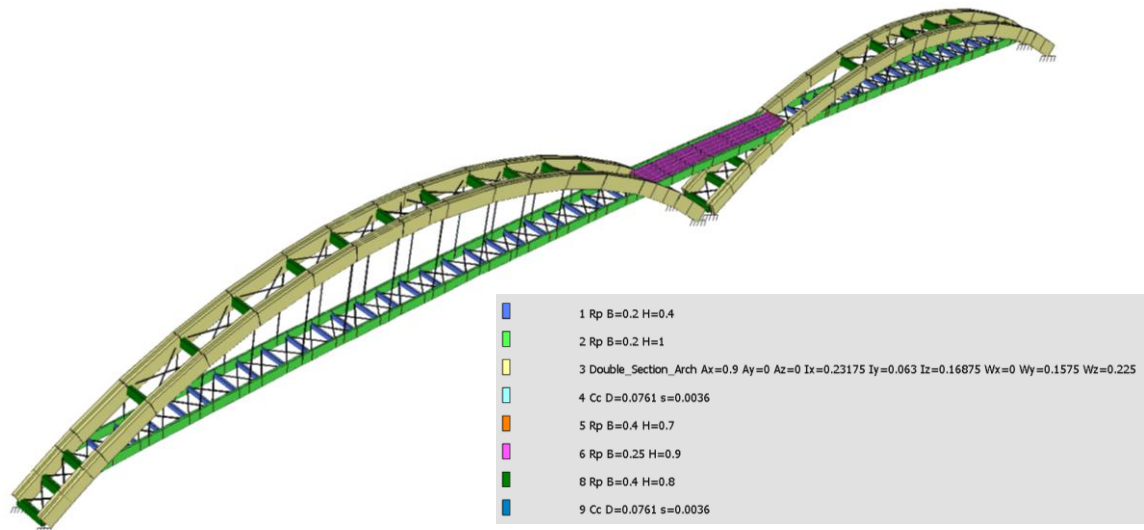


Figure 78: Global Structural View: (a) Analysis of the Cross-Sections of Structural Elements – (b) Color Scale

Cross-Section Group 3, represented in yellow in *Figure 78* and corresponding to the structural arch sections, consists of composite cross-sections. For this group, the composite section was specifically designed and developed, and its moment of inertia properties were calculated based on the characteristics of its constituent components (*Figure 79*).

⁴⁸ Blue for Timber Elements in GLT with Regular Geometric Cross-Section, Green for Timber Elements in GLT with Composite Geometric Cross-Section, Yellow for Steel Elements (Vertical Hangers, Deck Stabilizing Diagonals, etc.)

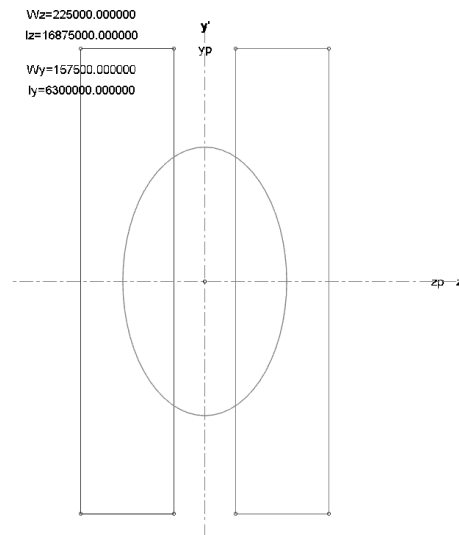


Figure 79: Properties of the Composite Cross-Section of the Structural Arch⁴⁹

The structure is then verified at the level of its defining elements through a dual verification procedure: All elements are independently oriented in the same analysis direction, to obtain a consistent distribution and representation of the results across the entire bridge (Figure 80).

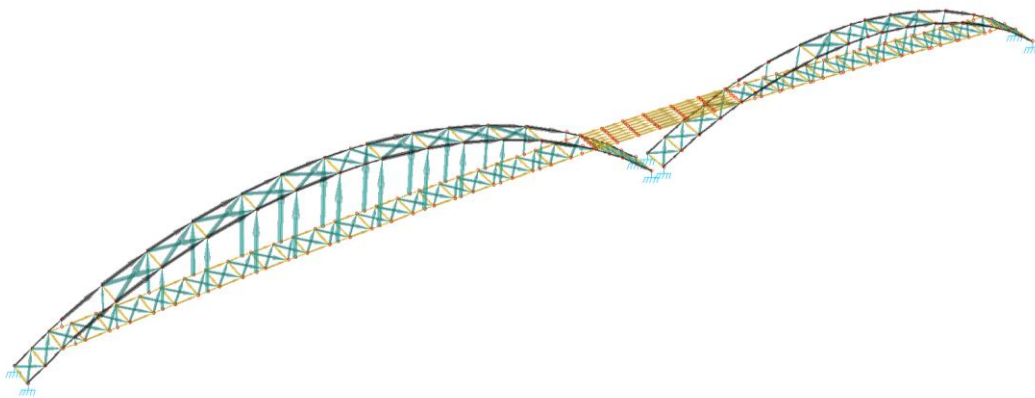


Figure 80: Orientation of Structural Elements - Directional Arrows with Respect to the Local Axes of Element Orientation

Subsequently, the software allows verification through an automatic design analyzer: The latter performs checks on structural instabilities and verifies the matrices for the presence of potential singularities. The automatic diagnostic analyzer also highlights individual warnings and points of interest within the structure, such as areas of greater displacement under critical load envelopes.

⁴⁹ It is important to note that the images and the corresponding properties of the cross-sections presented in this paragraph have already been verified through cross-section analyses and internal stress evaluations according to ultimate limit state procedures. In fact, some of these properties have been modified with respect to the assumptions made during the pre-design phase. A primary example is the composite section of the structural arches, which, although initially assumed to consist of two rectangles measuring 0.25×1.5 m, was modified to 0.3×1.5 m to satisfy global stability and buckling verification requirements.

7.1 LOAD APPLICATION ON STRUCTURAL ELEMENTS

The next step consists of applying loads to the structural elements. The loads are categorized according to their type: The values – as already described and presented in the previous chapters - are entered into and stored as areal and/or linear load codes.

In the subsequent analysis, slab areas are identified in relation to the longitudinal development of the bridge deck: The loads are assigned to these slab areas and automatically distributed to the corresponding structural elements, based on their respective influence areas and the principal direction of the slab.

In *Figure 81*, the slab areas are highlighted in blue. Although it may visually appear that some areas are disconnected or overlapping, this is merely a representational limitation. All loads have been appropriately verified in terms of their distribution with respect to the individual elements falling within each defined slab area.

Some loads, such as those related to the lateral barriers, have instead been directly applied to the primary elements, following the correct load distribution across the various structural levels as described in the preceding chapters.

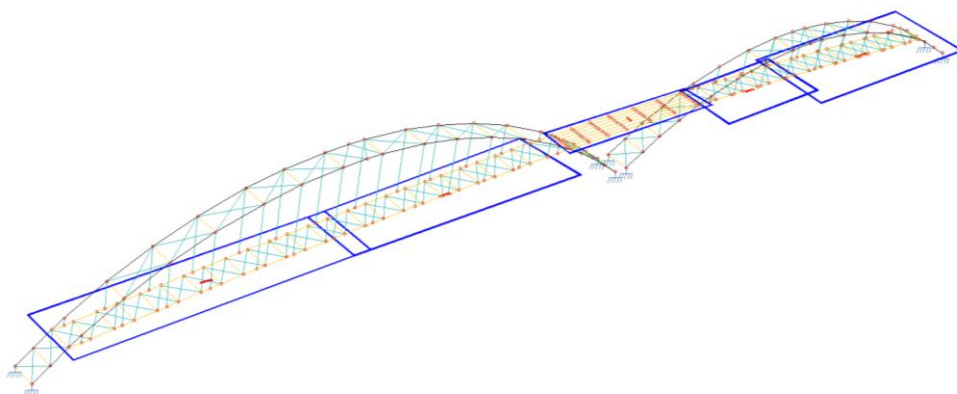


Figure 81: Slab Areas - Definition of Slab Areas (in Blue) and Principal Layout Directions (in Bidirectional Red Arrows⁵⁰)

The division of loads according to this analysis leads to their effective distribution across the structural elements. A graphical representation of the vertical loads applied to the structure is therefore provided (*Figure 82*), using monochromatic polygons. This representation is amplified by a factor of 10 to allow for the proper visualization of the vertical load distribution across the structure. It is important to note that, particularly with reference to the secondary deck elements, the dimensions of

⁵⁰ The principal direction of the slabs varies according to the development of the deck. Specifically, in the deck elements located directly beneath the structural arches, the direction follows the global x-axis. In contrast, for the deck elements located in the central portion between the two arches - where there is a substantial change in the geometry of the structural system - the principal direction corresponds to the global y-axis. The general rule is that the slab elements rest on the supporting structural elements, always oriented orthogonally to them; therefore, when the direction of the supporting elements changes, the principal slab layout direction changes accordingly.

the load representation polygons are not uniform. This is due to slight differences in the influence areas of the secondary beams which, given the curved and non-linear configuration of the deck, result in slightly different total loads (a difference further emphasized by the representation scale).

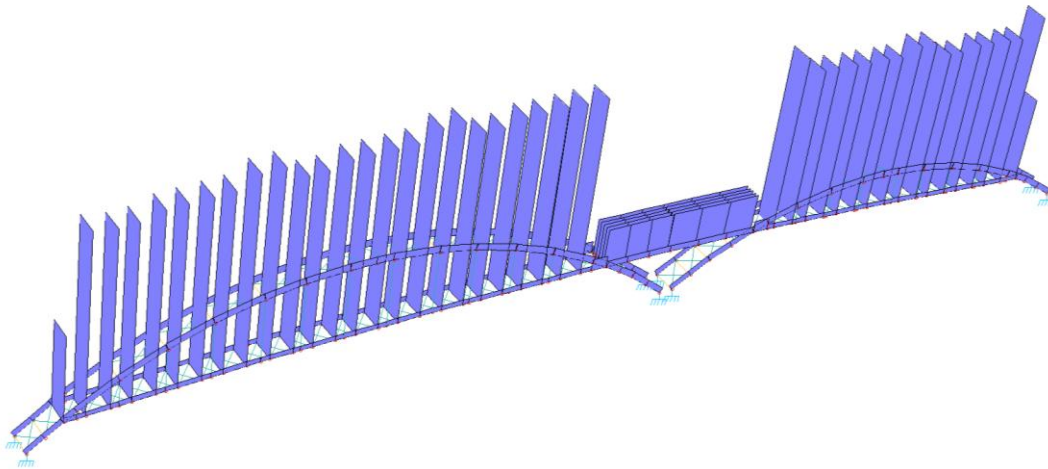


Figure 82: Representation of Vertical Forces Applied to the Structure – Monochromatic Polygons for the Distributed Loads on Structural Elements⁵¹

The assigned loads are then divided into the loading conditions previously described and applied within the generated load combinations. The load combinations are manually entered into the software, with appropriate adjustment of the combination factors for the various ultimate and serviceability limit state combinations.

7.2 STATIC DEFORMATION ANALYSIS

The structure is analyzed according to finite element analysis criteria, and static deformations are generated as a result of the structural resolution. Deformation shapes are produced for each load combination applied to the structure, but not in a critical envelope format. This outcome is since the structure is not divided into structural shells (as it is not a building with perimeter and internal walls), and the software is therefore unable to produce a critical envelope by directly comparing all deformation shapes resulting from the load combinations under analysis.

To study and make optimal use of the generated deformation shapes, specific load combinations based on individual load cases were created. These combinations allow for the analysis of structural behavior under isolated loading scenarios, with the aim of assessing their consistency with the initial structural design assumptions.

⁵¹ The same type of graphical representation can also be generated for the loads in the other two global loading directions, "x" and "z"; however, these are not included in the present document.

Accordingly, four static deformation shapes are presented below (*Figure 83, Figure 84, Figure 85, Figure 86*), corresponding to the individual application of structural and non-structural permanent loads, snow load, wind load, and pedestrian load.

All deformation shapes are presented with an axonometric side view to clearly display structural deformations. To enhance the clarity of the visual representation, all deformations have been amplified by a factor of 100.

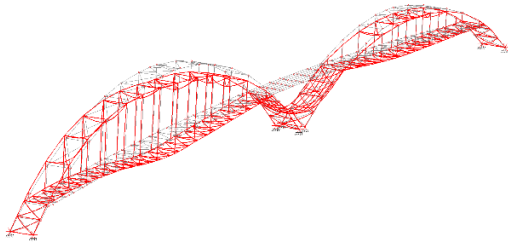


Figure 83: Static Deformation – Permanent Loads

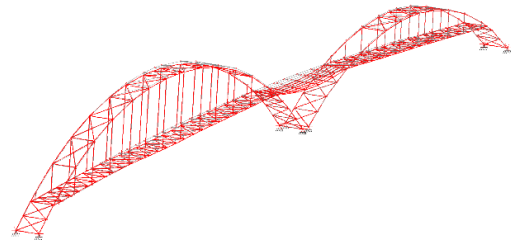


Figure 84: Static Deformation – Snow Load

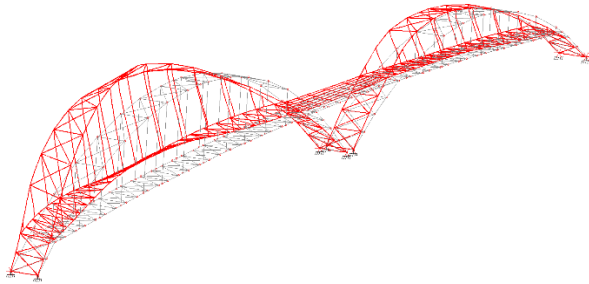


Figure 85: Static Deformation – Wind Load

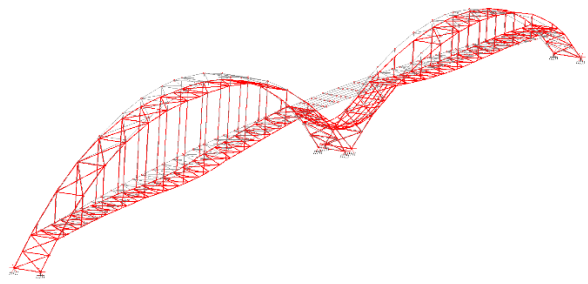


Figure 86: Static Deformation – Traffic Pedestrian Loads

It is necessary to provide some clarifications to accurately explain the shape assumed by the static deformation patterns.

In *Figure 85*, the deformation corresponds to the application of wind load on the structure: This load is applied horizontally on the right side of the bridge (*Figure 87*), with the addition of vertical components (where calculated). This explains the shape of the static deformation, which is consistent with the structural design assumptions and the boundary conditions applied to the structure. Moreover, it is important to highlight that the maximum horizontal displacement in this deformation occurs at the upper node of the main structural arch, reaching a value of 7.4 cm.

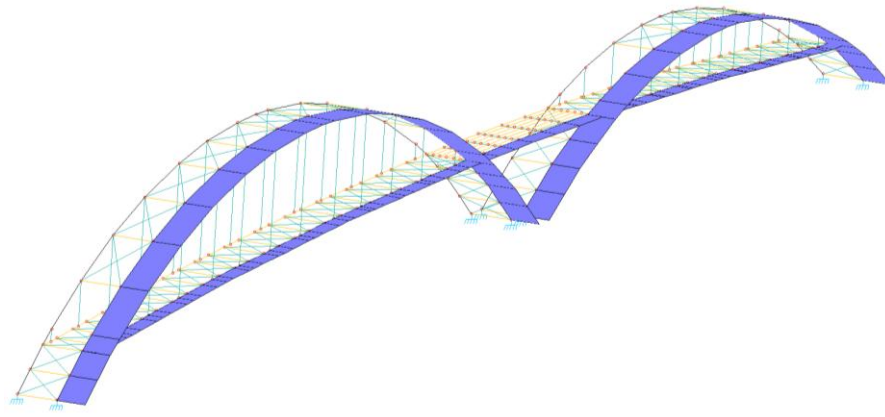


Figure 87: Explanatory Representation of the Direction of Application of the Wind Lateral Force on the Structural “Right” Facade

In Figure 86, the static deformation represents a displacement in the direction parallel to the longitudinal axis of the deck. This is caused by the application of the horizontal component of the pedestrian traffic load, as previously described and appropriately analyzed. The maximum displacement in the x-direction corresponds to 3 cm.

From the analysis of these deformation shapes, it can be concluded that the structural response to the loads applied in the principal directions is consistent with the structural design.

Additionally, a final explanatory view is provided below, showing the deformation under vertical loads with a front view (Figure 88): This has been included to better highlight the structural deformation of the three-hinged arches under vertical loading. The deformation is not symmetrical, due to the presence of concentrated loads at the sides of the arches resulting from the support of the deck beams in the central portion.

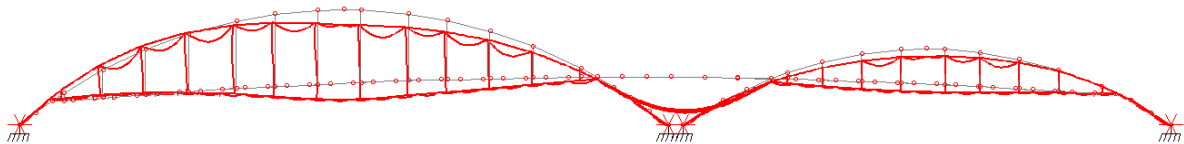


Figure 88: Structural Front View: Deformation Under Permanent Loads – Asymmetrical Deflection of the Structural Arches

In conclusion, the maximum deformation values were extracted individually from all load conditions and subsequently compared with those obtained through manual calculations. Since the manual verifications are conservative in terms of deformation, the values derived from hand calculations were used for the serviceability limit state deformation checks. This approach was adopted not only to exaggerate the structural deformations of a complex structure, but also to properly account for the effects of creep by applying the appropriate deformation contributions. This topic will be addressed in detail in the following chapters.

7.3 INTERNAL STRESS AND FORCE DISTRIBUTION

The analysis of the model proceeds with the identification of internal stresses for all structural elements. These are derived from the critical envelopes: The selected load combinations (in this case, corresponding to ultimate limit states) are superimposed, and the maximum values for each structural element are extracted.

To present these results in the most schematic and intuitive manner possible, a series of figures is provided, illustrating the structural elements divided by structural level, with representations of axial force, shear force, and bending moment in the “z” and “y” directions. A graphical color scale is used for the representation of internal forces: This scale varies for each element and each force diagram, depending on the maximum and minimum values encountered. For each element and each internal force, the maximum value and the corresponding location along the element are clearly highlighted.

It is important to note that in the color scales used for axial forces, indicated as F_x with respect to the local axes of the elements, negative values represent compression, while positive values indicate tension.

7.3.1 SECONDARY BEAMS – DECK

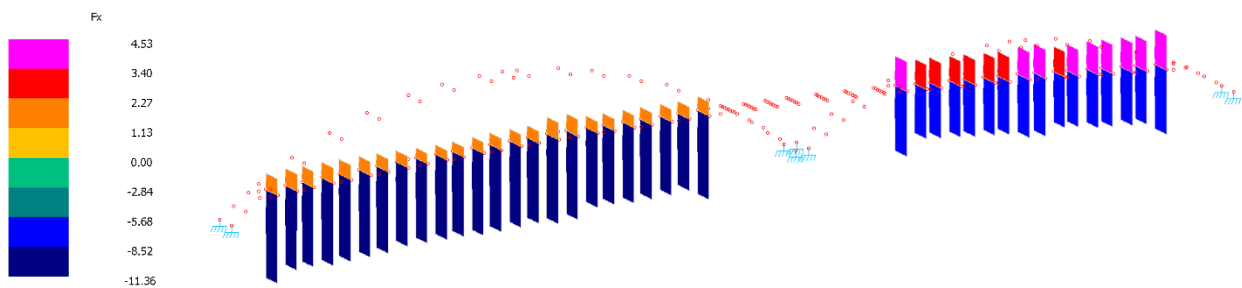


Figure 89: Axial Force F_x – Secondary Deck Beams. Maximum Compression: 11.36 kN, Maximum Tension: 4.53 kN

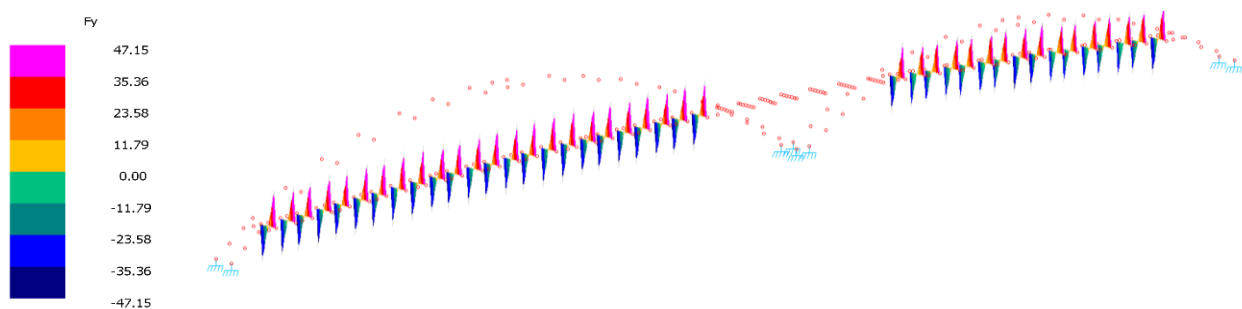


Figure 90: Shear Force F_y – Secondary Deck Beams. Maximum Shear Force: 47.15 kN

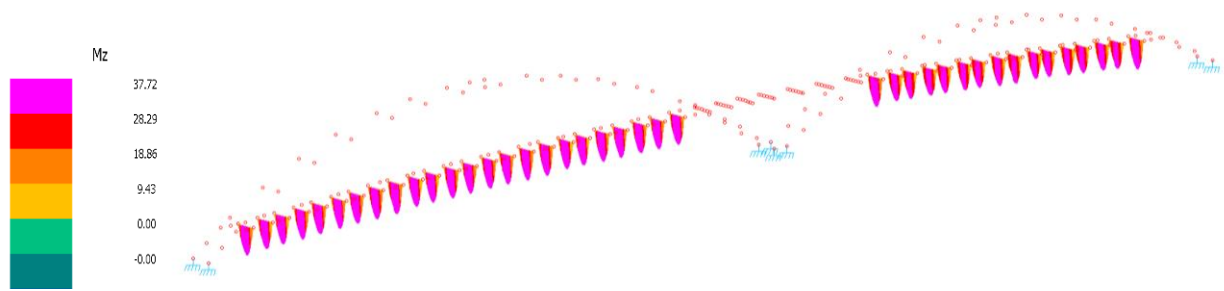


Figure 91: Bending Moment M_z —Secondary Deck Beams. Maximum Bending Moment: 37.72 kNm

7.3.2 PRIMARY BEAMS – DECK

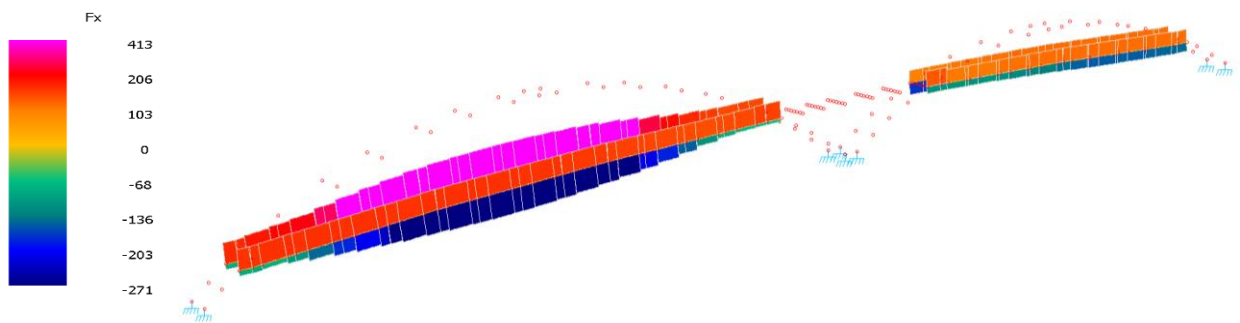


Figure 92: Axial Force F_x —Primary Deck Beams. Maximum Compression: 271 kN, Maximum Tension: 413 kN

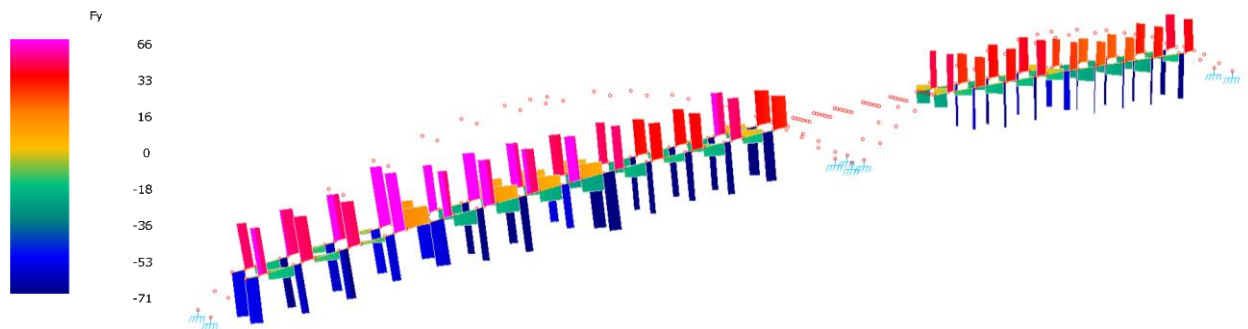


Figure 93: Shear Force F_y —Primary Deck Beams. Maximum Shear Force: 71 kN

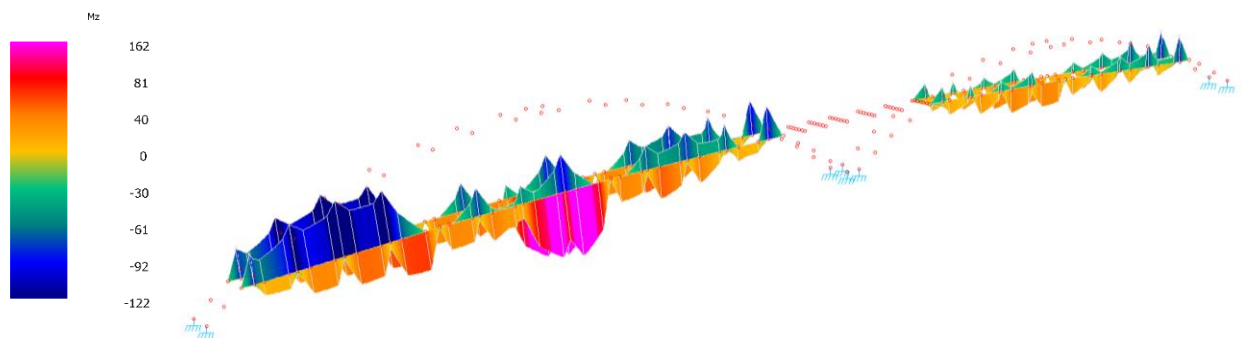


Figure 94: Bending Moment M_z —Primary Deck Beams. Maximum Bending Moment: 162 kNm

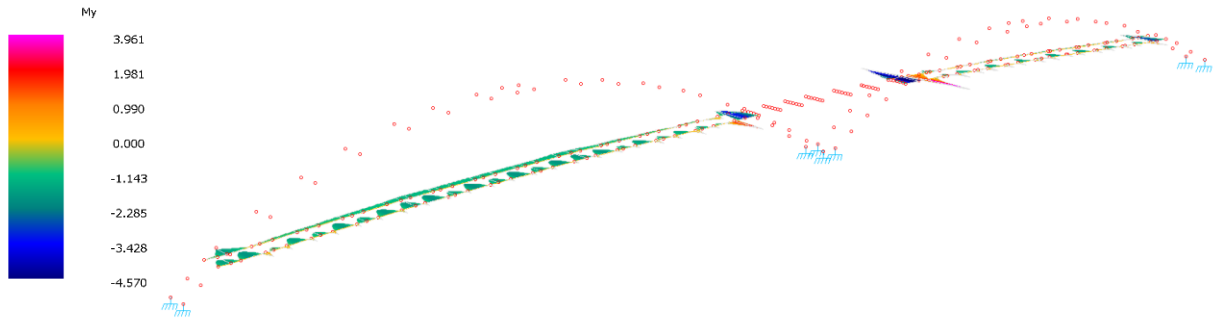


Figure 95: Bending Moment M_y – Primary Deck Beams. Maximum Lateral Bending Moment: 4.57 kNm

7.3.3 PRIMARY BEAMS – CENTRAL DECK ZONE

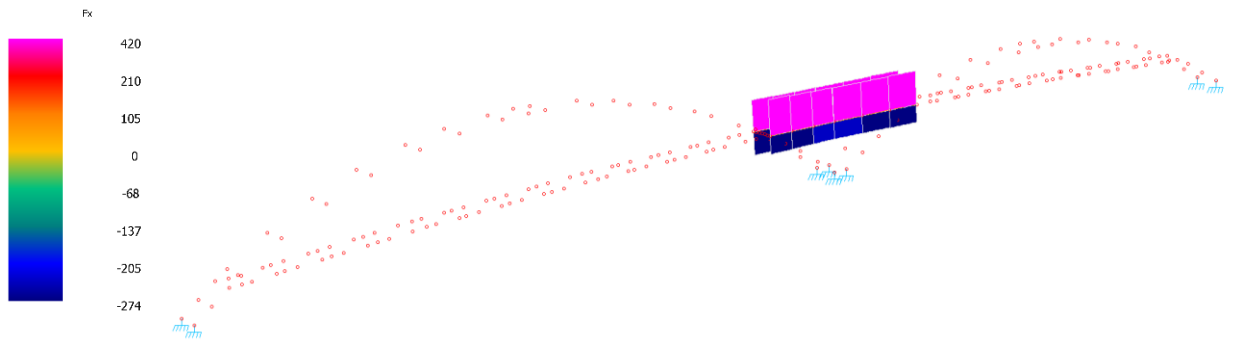


Figure 96: Axial Force F_x – Primary Central Deck Beams. Maximum Compression: 274 kN, Maximum Tension: 420 kN

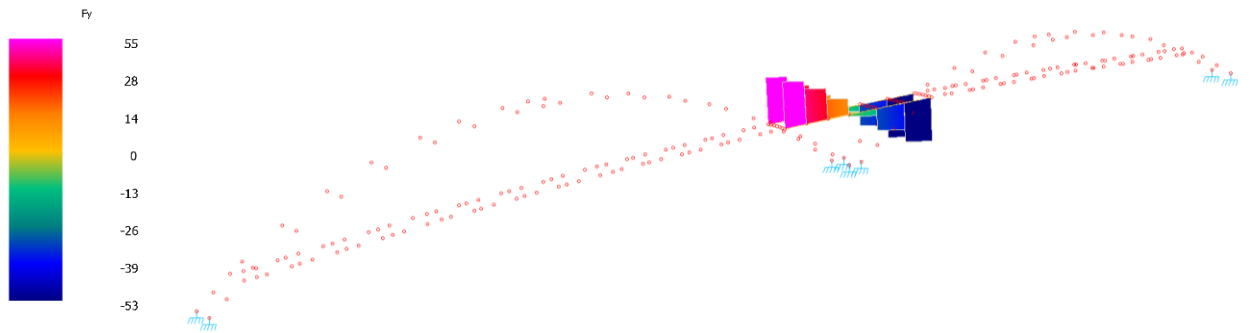


Figure 97: Shear Force F_y – Primary Central Deck Beams. Maximum Shear Force: 55 kN

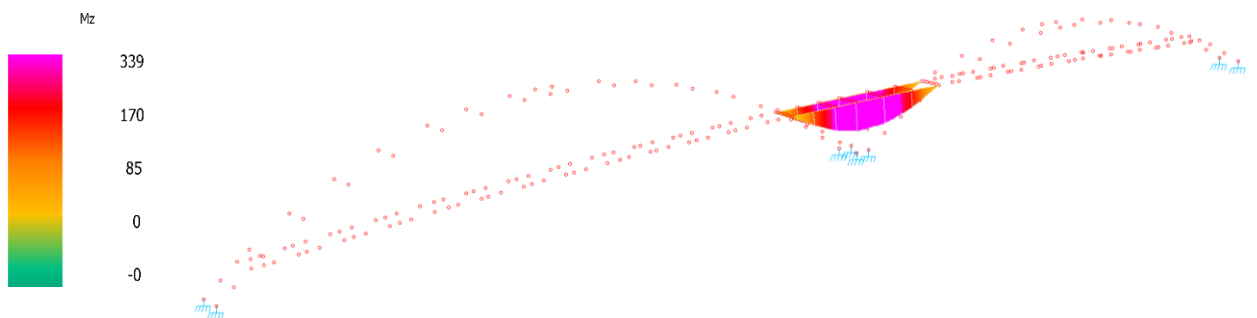


Figure 98: Bending Moment M_z – Primary Central Deck Beams. Maximum Bending Moment: 339 kNm

7.3.4 CENTRAL BEAMS – CENTRAL DECK ZONE

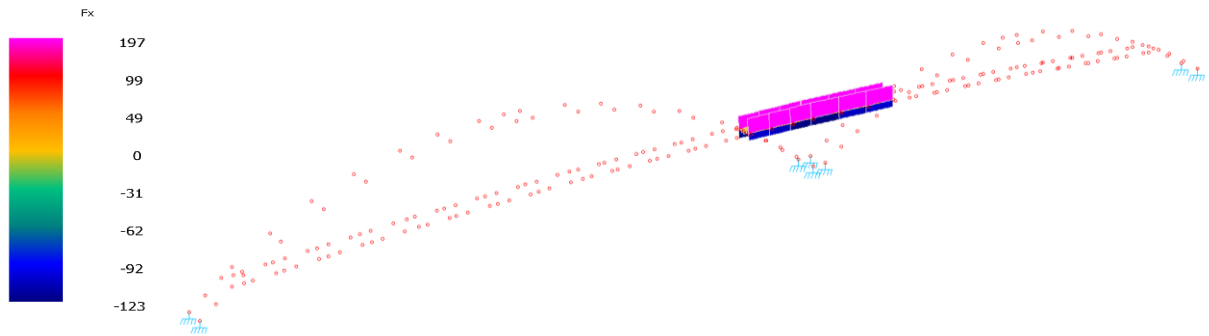


Figure 99: Axial Force F_x – Central Deck Beams. Maximum Compression: 123 kN, Maximum Tension: 197 kN

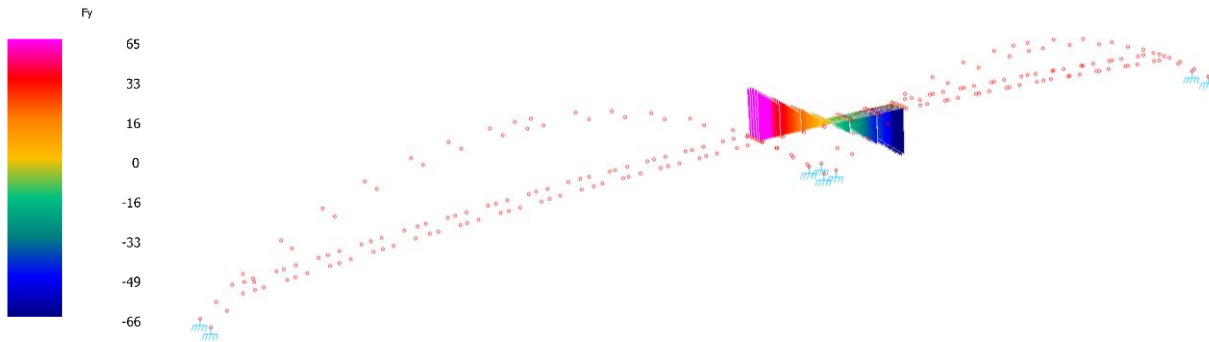


Figure 100: Shear Force F_y – Central Deck Beams. Maximum Shear Force: 66 kN

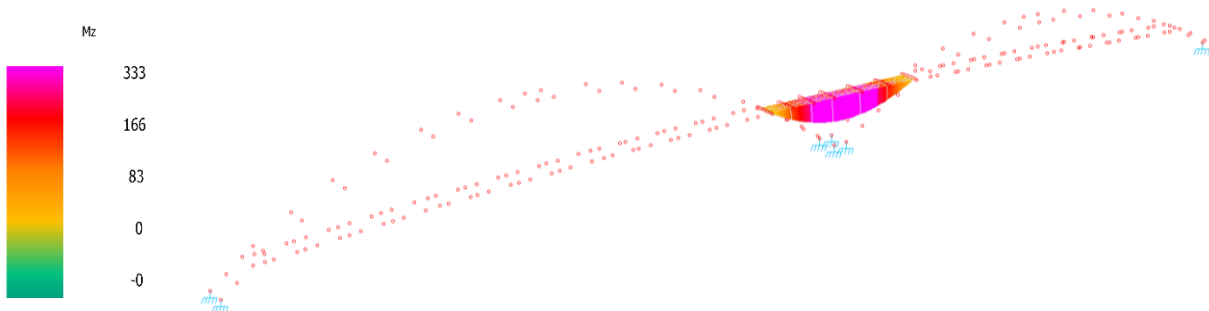


Figure 101: Bending Moment M_z – Central Deck Beams. Maximum Bending Moment: 333 kNm

7.3.5 TRANSVERSAL BEAMS – DECK-TO-ARCH CONNECTION

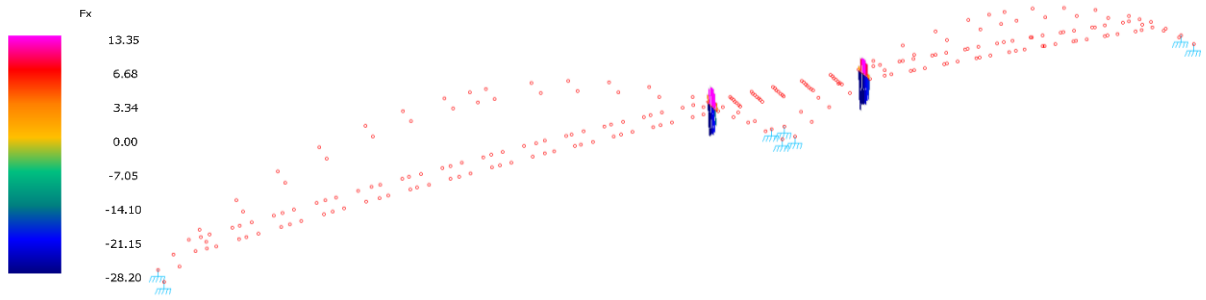


Figure 102: Axial Force F_x – Transversal Beams. Maximum Compression: 28.20 kN, Maximum Tension: 13.35 kN

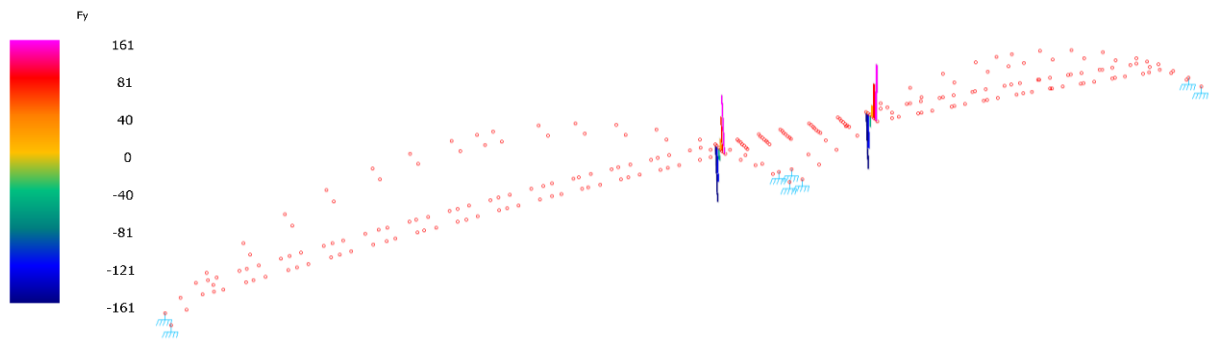


Figure 103: Shear Force F_y – Transversal Beams. Maximum Shear Force: 161 kN

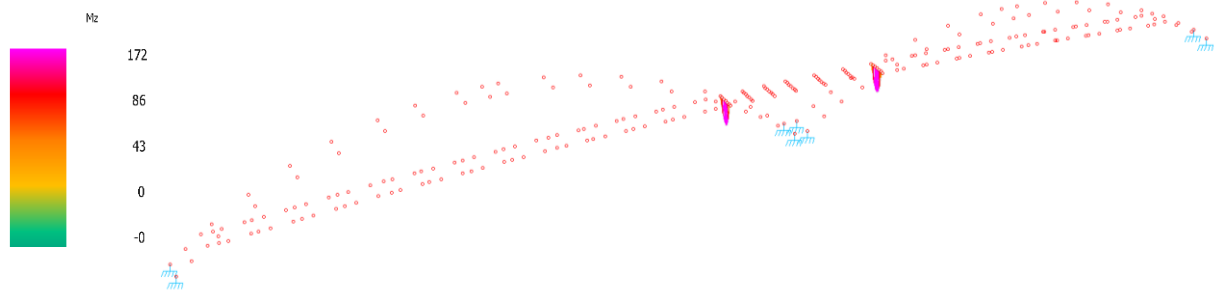


Figure 104: Bending Moment M_z – Transversal Beams. Maximum Bending Moment: 172 kNm

7.3.6 ARCH BEAMS

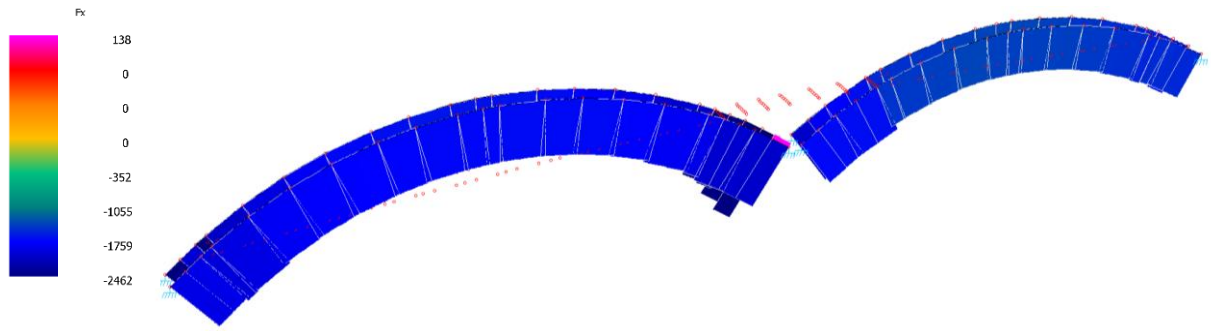


Figure 105: Axial Force F_x – Arch Beams. Maximum Compression: 2462 kN

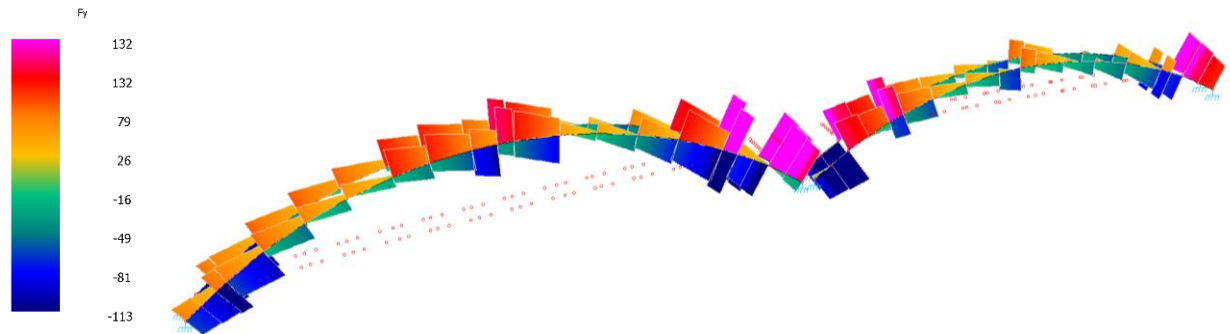


Figure 106: Shear Force F_y – Arch Beams. Maximum Shear Force: 132 kN

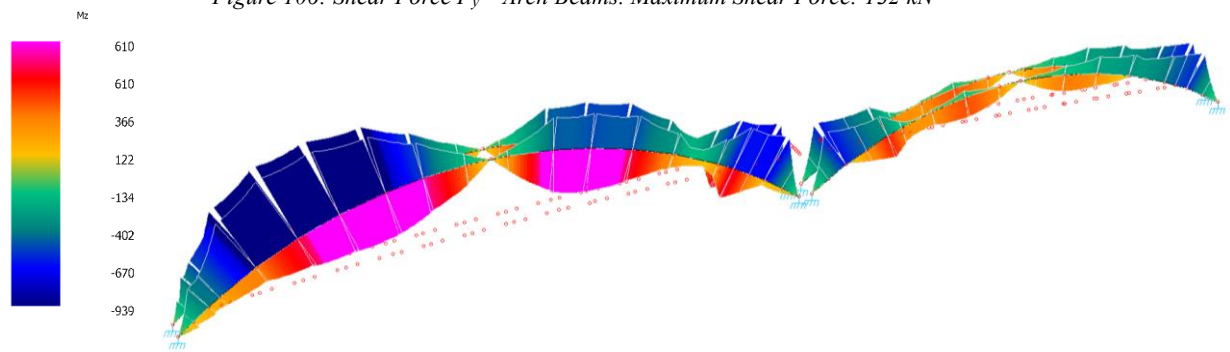


Figure 107: Bending Moment M_z – Arch Beams. Maximum Bending Moment: 939 kNm

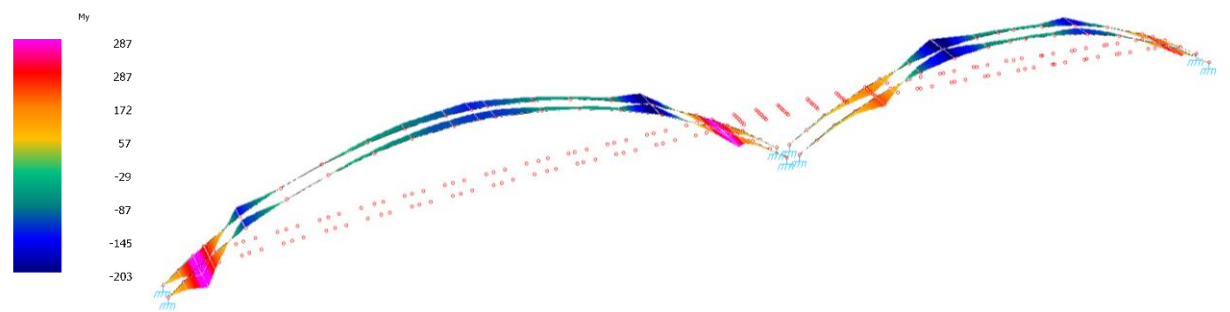


Figure 108: Bending Moment M_y – Arch Beams. Maximum Lateral Bending Moment: 287 kNm

7.3.7 VERTICAL HANGERS

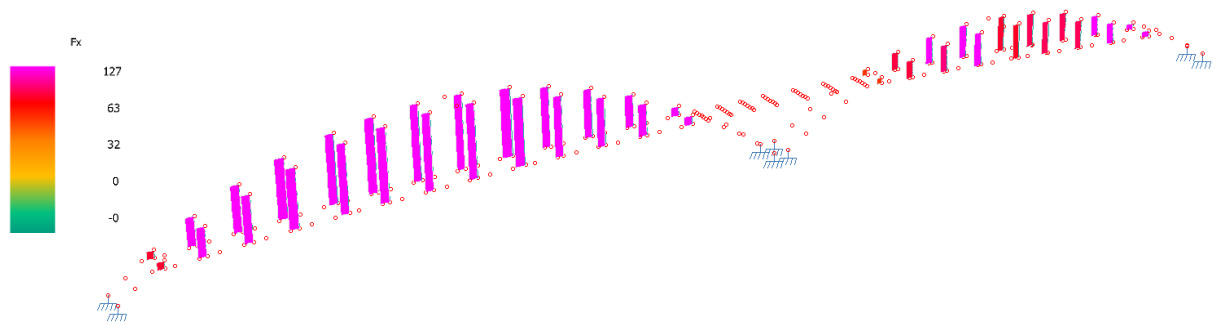


Figure 109: Axial Force F_x – Vertical Hangers. Maximum Tension: 127 kN

7.3.8 SUMMARY TABLE OF STRUCTURAL RESULTS

A summary table of the results follows (*Table 12*), divided by type of internal force and corresponding structural element. The values correspond to those shown in the figures representing the internal forces, except for some not displayed, as they were considered less relevant for the purposes of the analysis.

SUMMARY TABLE OF RESULTS – FEM MODEL					
ELEMENT	TYPE OF INTERNAL FORCES – ELEMENTS				
	AXIAL FORCE - COMPRESSION $-F_x$ [kN]	AXIAL FORCE - TENSION $+F_x$ [kN]	SHEAR FORCE - F_y [kN]	BENDING MOMENT M_z [kNm]	BENDING MOMENT M_y [kNm]
SECONDARY BEAMS	11.36	4.53	47.15	37.72	2.36
PRIMARY BEAMS	271	413	71.1	162	4.57
PRIMARY BEAMS - CENTRAL DECK	274	420	55.2	339	6.8
CENTRAL BEAM - CENTRAL DECK	123	197	66	333	29.8
TRANSVERSAL BEAMS	28.2	13.35	161	172	98.9
ARCH BEAMS	2462	138	132	939	287
VERTICAL HANGERS	-	127	-	-	-

Table 12: Summary Table of Results - FEM Model - MasterSap 4U

These results are incorporated into the limit state verifications, as described in the following chapter.

8 VERIFICATION TO ULS AND SLS – EN 1995 – 1-1 COMPLIANCE

Based on the defined load combinations, the analysis of internal forces obtained from the FEM model, and the considerations derived from the manual calculations used to validate the numerical results, the following verifications at the Serviceability and Ultimate Limit States are performed. The verifications are carried out in strict accordance with the provisions of Eurocode EN 1995-1-1⁵² and the relevant national annexes.

8.1 SERVICE CLASS DEFINITION

According to the procedures set out in Eurocode NBN EN 1995 for timber structures, it is necessary to define a service class for the structure. Given the structural typology and its location, the structure is classified as *Service Class 3*, as it is fully exposed to direct moisture and weather conditions. This classification influences the parameters and partial factors used for the verifications of both short-term and long-term effects on the structure, as well as the coefficients applied in the ultimate limit state stress checks.

8.2 DEFORMATION FACTOR k_{def}

The k_{def} deformation factor is used for the evaluation of the creep deformation of each component, considering the service class. The service class affects each component, and the materials of each component have already been identified. According to NBN EN 1995, for Glued Laminated Timber and Service Class 3, the deformation factor is $k_{def} = 2$ (Figure 110).

Table 3.2 – Values of k_{def} for timber and wood-based materials

Material	Standard	Service class		
		1	2	3
Solid timber	EN 14081-1	0,60	0,80	2,00
Glued Laminated timber	EN 14080	0,60	0,80	2,00
LVL	EN 14374, EN 14279	0,60	0,80	2,00
Plywood	EN 636			
	Part 1	0,80	–	–
	Part 2	0,80	1,00	–
	Part 3	0,80	1,00	2,50
OSB	EN 300			
	OSB/2	2,25	–	–
	OSB/3, OSB/4	1,50	2,25	–
Particleboard	EN 312			
	Part 4	2,25	–	–
	Part 5	2,25	3,00	–
	Part 6	1,50	–	–
	Part 7	1,50	2,25	–
Fibreboard, hard	EN 622-2			
	HB.LA	2,25	–	–
	HB.HLA1, HB.HLA2	2,25	3,00	–
Fibreboard, medium	EN 622-3			
	MBH.LA1, MBH.LA2	3,00	–	–
	MBH.HLS1, MBH.HLS2	3,00	4,00	–
Fibreboard, MDF	EN 622-5			
	MDF.LA	2,25	–	–
	MDF.HLS	2,25	3,00	–

Figure 110: Values of k_{def} for Timber and Wood-Based Material - (EN 1995 - Eurocode 5: Design of timber structures & Relative Annexes, 2004) Table 3.2

⁵² (EN 1995 - Eurocode 5: Design of timber structures & Relative Annexes, 2004)

8.3 DEFLECTION CONTROL

The simplification of structural elements as isostatic members from the perspective of structural analysis leads to the following considerations regarding the deflection verifications of the elements themselves.

The calculation of long-term deflection includes considerations of both instantaneous deflection and creep deflection. To perform a correct evaluation, and in accordance with EN 1995-1-1, paragraph 7.2⁵³, both deflection components were calculated for variable and permanent loads. The results were then summed, taking proper account of the deformation factor k_{def} - which directly affects the elastic properties of the materials - and the partial safety factors ψ_i .

To provide a reference value for the admissible structural deformation, the total deflection (i.e., the sum of the long-term and short-term components) was limited to $L/250$ ⁵⁴.

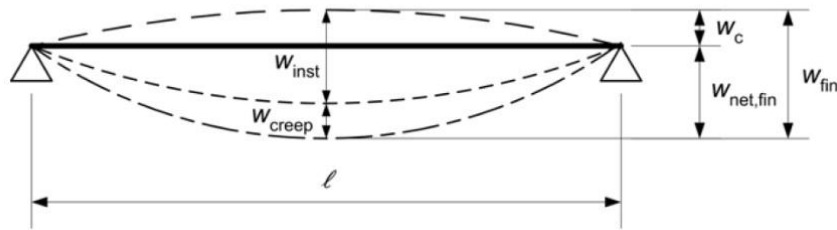


Figure 111: Components of Deflection - EN 1995 - 1 - 1 Figure 7.1

According to what is shown in the Figure 111, the elements considered in the deflection calculation are:

- w_c is the pre-camber (if applied).
- w_{inst} is the instantaneous deflection.
- w_{creep} is the creep deflection.
- w_{fin} is the final deflection.
- $w_{net, fin}$ is the net final deflection.

As previously mentioned, the calculation for each load type followed the following formulation:

For Permanent Load G	For Main Variable Load Q_1	For other Variable Loads Q_i
$w_{fin} = w_{inst,G} * (1 + k_{def})$	$w_{fin} = w_{inst,Q1} * (1 + \psi_{2,1} * k_{def})$	$w_{fin} = w_{inst,Qi} * (\psi_{0,i} + \psi_{i,1} * k_{def})$

Table 13: Formulas for the Computation of the w_{fin}

⁵³ (EN 1995 - Eurocode 5: Design of timber structures & Relative Annexes, 2004)

⁵⁴ It is important to note that this reference value is purely indicative: Since the structure under analysis is not a building with doors, windows, or other elements whose integrity and function directly depend on structural deformation, exceeding the suggested deflection limit would not pose a structural problem. While a larger deformation would indeed alter the overall geometry of the structure, it would not affect its load-bearing capacity or proper structural functioning. However, the situation is different when considering the performance of the structure in relation to pedestrian comfort. Excessive deformations could negatively impact walking comfort, to the extent that further analysis would become necessary.

From the formulas presented in *Table 13*, it follows that creep effects are considered for all variable actions included in the analysis. However, this is only valid when the combination factors $\psi_{i,1}$, which are multiplied by the k_{def} values, are different from zero. In the present case, the variable actions - such as pedestrian traffic, wind, and snow - all have $\psi_{i,1}=0$; therefore, creep deformation is considered only for permanent actions.

The calculation of instantaneous deformation was carried out both for bending moment - $w_{m,inst}$ - (following beam theory) and for shear deformation - $w_{v,inst}$ -, since timber has a relatively low shear modulus G compared to the longitudinal elastic modulus E_0 . The resulting deflections were then summed up.

For distributed loads, the described deformations can be calculated as follows:

$$w_{v,inst} = \frac{q_{Ed} * L^2}{8 * G * \frac{5}{6} * A}; \quad w_{m,inst} = \frac{5}{384} * \frac{q_{Ed} * L^4}{E * I}$$

Where:

- q_{Ed} is the distributed load.
- A is the cross-section area.
- E is the Young modulus (in mean value).
- I is the inertia of the cross section.
- L is the span of the considered elements.

The calculated w_{inst} values, derived from shear and bending actions, were inserted into the appropriate formulas for the evaluation of w_{fin} , and each of these was then summed to determine the total net deformation $w_{net,fin}$, compared to the selected deflection limitation $L/250$.

In some elements, a pre-camber w_c was introduced to make the instantaneous deformation resulting from permanent structural and non-structural loads equal to zero, effectively resetting the element's axis to zero before the application of variable loads.

It is important to note, however, that the bridge deck under analysis was already designed with an initial pre-camber, following an overall slope of 4%, with elements that are not horizontal and slightly curved.

This leads to the final consideration that, although a calculated pre-camber was applied, the initial geometric camber given to the structural elements is greater than any expected downward deformation. As a result, from a purely theoretical verification standpoint, the deck should not experience excessive additional negative deflection.

8.4 STRENGTH VERIFICATION – MODIFICATION FACTOR k_{mod}

For the calculation of design strengths, it is essential to consider the moisture content and the duration of the applied loads, to consider the effects of creep (long-term effects). In this regard, the design strength to be used for ULS verifications is calculated as follows:

$$R_d = k_{mod} * \frac{R_k}{\gamma_M}$$

Where γ_M is the partial factor for timber, whose value is fixed at 1.25 according to Eurocode 2, and k_{mod} is the coefficient accounting for the strength reduction due to increased moisture content and long-term loading duration.

The k_{mod} coefficient takes on different values depending on the material under analysis, the service class, and the load duration. The values used in the analysis phase - considering GLT material in Service Class 3 under permanent and short-term loads - are obtained from the following table (*Figure 112*), extracted from EN 1995-1-1:

Table 3.1 – Values of k_{mod}

Material	Standard	Service class	Load-duration class				
			Permanent action	Long term action	Medium term action	Short term action	Instantaneous action
Solid timber	EN 14081-1	1	0,60	0,70	0,80	0,90	1,10
		2	0,60	0,70	0,80	0,90	1,10
		3	0,50	0,55	0,65	0,70	0,90
Glued laminated timber	EN 14080	1	0,60	0,70	0,80	0,90	1,10
		2	0,60	0,70	0,80	0,90	1,10
		3	0,50	0,55	0,65	0,70	0,90
LVL	EN 14374, EN 14279	1	0,60	0,70	0,80	0,90	1,10
		2	0,60	0,70	0,80	0,90	1,10
		3	0,50	0,55	0,65	0,70	0,90
Plywood	EN 636 Type EN 636-1 Type EN 636-2 Type EN 636-3	1	0,60	0,70	0,80	0,90	1,10
		2	0,60	0,70	0,80	0,90	1,10
		3	0,50	0,55	0,65	0,70	0,90
OSB	EN 300 OSB/2 OSB/3, OSB/4 OSB/3, OSB/4	1	0,30	0,45	0,65	0,85	1,10
		1	0,40	0,50	0,70	0,90	1,10
		2	0,30	0,40	0,55	0,70	0,90
Particle-board	EN 312 Type P4, Type P5 Type P5 Type P6, Type P7 Type P7	1	0,30	0,45	0,65	0,85	1,10
		2	0,20	0,30	0,45	0,60	0,80
		1	0,40	0,50	0,70	0,90	1,10
		2	0,30	0,40	0,55	0,70	0,90
Fibreboard, hard	EN 622-2 HB.LA, HB.HLA 1 or 2 HB.HLA1 or 2	1	0,30	0,45	0,65	0,85	1,10
		2	0,20	0,30	0,45	0,60	0,80
Fibreboard, medium	EN 622-3 MBH.LA1 or 2 MBH.HLS1 or 2 MBH.HLS1 or 2	1	0,20	0,40	0,60	0,80	1,10
		1	0,20	0,40	0,60	0,80	1,10
		2	–	–	–	0,45	0,80
Fibreboard, MDF	EN 622-5 MDF.LA, MDF.HLS MDF.HLS	1	0,20	0,40	0,60	0,80	1,10
		2	–	–	–	0,45	0,80

Figure 112: Value of k_{mod} - EN 1995-1-1 Table 3.1

This results in $k_{mod} = 0.5$ for permanent actions and $k_{mod} = 0.7$ for short-term actions.

In general, the k_{mod} value to be considered corresponds to the short-term action. However, it is possible that the dominant action on the structure - the one exerting the greatest long-term effect - is the permanent action. Therefore, it is necessary to define a degree of dominant loading, to determine which action is predominant (whether variable or permanent). The criterion for selecting the predominant action and the corresponding k_{mod} value is expressed by the following formula:

$$r = \frac{\frac{\gamma_G * G}{k_{mod,G}}}{\frac{\gamma_G * G + \gamma_Q * Q}{k_{mod,Q}}} \rightarrow \begin{cases} < 1 \rightarrow \text{Effects of variable loads are dominant} \\ > 1 \rightarrow \text{Effects of permanent loads are dominant} \end{cases}$$

In a case where permanent loads come out as predominant, additional checks concerning permanent loads alone must be conducted⁵⁵.

8.5 SIZE EFFECT FACTOR k_h

Along with load duration and moisture effects, tensile and flexural strength in timber requires to account for the size effects⁵⁶ using the amplification coefficient k_h for Glued Laminated Timber as:

$$k_h = \min \left\{ \left(\frac{600}{h} \right)^{0.1} \text{ if } h \leq 600 [mm] \text{ and } k_h = 1 \text{ if } h \geq 600 [mm] \right.$$

Where h is the height of the considered cross-section.

It is important to note that the value of k_h cannot be lower than 1, as this would not represent an economic solution and would lead to an underestimation of the section's strength.

Except for the secondary deck beams, which have a cross-sectional height of 0.4 m, all other structural elements under analysis have a cross-sectional height greater than or equal to 600 mm. For this reason, the k_h factor is assumed to be equal to 1 for these elements.

8.6 SYSTEM FACTOR k_{sys}

Structural systems composed of members connected through elements capable of redistributing internal forces exhibit enhanced global stiffness and, therefore, increased load-bearing capacity. This collective behavior, known as the group effect, is typically achieved through the implementation of continuous sheathing panels or purlins spanning over multiple supports. The phenomenon is accounted for in structural design by means of the coefficient k_{sys} , which allows for a 10% increase in the design strength of timber elements.

In the present analysis, this multiplicative coefficient is applied exclusively to the secondary beams and to the primary beams located in the central zone between the two arches. It is therefore considered

⁵⁵ In the case under analysis, for all elements, the variable loads constitute the predominant action, with the ratio r always less than 1. Nonetheless, it remains important to state this condition of predominant variable loading, in view of any future modifications to the project.

⁵⁶ Testing timber with different sizes varies the results: The smaller are the elements the more the properties will vary.

only in those areas where the structural elements are interconnected by the deck planking spanning over multiple supports. For these elements, the value of $k_{sys}=1.1$ is adopted.

8.7 CROSS-SECTIONAL RESISTANCE CHECKS

To prevent local failure of the elements, the following strength criteria are verified. A descriptive list of the individual verifications is presented below. These checks are selected for each structural member and subsequently carried out, with the corresponding values and verification results summarized in a dedicated table.

Compression Parallel to the Grain (σ_c)

$$\sigma_{c,0,d} \leq f_{c,0,d} \text{ with } \sigma_{c,0,d} = \frac{N_{Ed}}{A}$$

Where A is the area of the cross section under analysis and N_{Ed} is the compression in the member.

Tension Perpendicular to the Grain ($\sigma_{t,90}$)

$$\sigma_{t,90,d} \leq k_{dis} * k_{Vol} * f_{t,90,d} \text{ with } \sigma_{t,90,d} = \frac{T_{Ed}}{A}$$

Where:

- $k_{dis} = \begin{cases} 1.4 & \rightarrow \text{for Double Tapered and Curved Beams} \\ 1.7 & \rightarrow \text{for Pitched Cambered Beams} \end{cases} \rightarrow \text{Stress distribution factor}$
- $k_{Vol} = \begin{cases} 1.0 & \rightarrow \text{for Solid Timber} \\ \left(\frac{0.01}{V}\right)^{0.2} & \rightarrow \text{for GLT and Laminated Veneer} \end{cases} \rightarrow \text{Volume factor}^{57}$

Compression Perpendicular to the Grain ($\sigma_{c,90}$)

$$\sigma_{c,90,d} \leq k_{c,90} * f_{c,90,d}$$

Where:

- $k_{c,90} = \begin{cases} 1.50 & \text{for a Continuous Support } [l1 \geq 2h] \\ 1.75 & \text{for a Discrete Support } [l1 \geq 2h \text{ and } l \leq 400mm] \\ 1 & \text{for all the Other Cases} \end{cases} \rightarrow \text{Factor considering the loading configuration, possibility of splitting and degree of compressive deformation.}$

⁵⁷ $V[m^3]$ as stressed volume

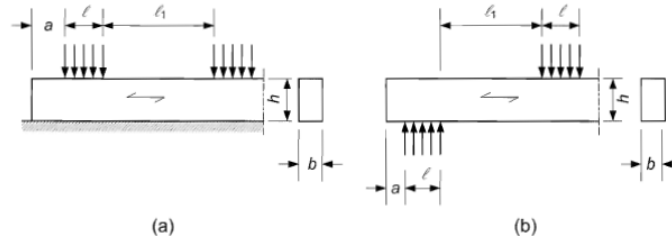


Figure 113: Member on (a) Continuous and (b) Discrete Support - EN 1995-1-1 Figure 6.2

$$- \sigma_{c,90,d} = \frac{F_{c,90,d}}{A_{ef}}, \quad A_{ef} = b * (l + \Delta_{right} + \Delta_{left}) \quad \text{and} \quad \Delta_i = \min(30\text{mm}; l; a \text{ or } \frac{l_{1,i}}{2})$$

Uniaxial Bending ($\sigma_{m,y}$ or $\sigma_{m,z}$)

$$\sigma_{m,d} \leq k_h * f_{m,d} \quad \text{with} \quad \sigma_{m,d} = \frac{M_{Ed} * d}{I}$$

Where d is the height of the cross section neutral axis, I is the inertia and M_{Ed} is the applied bending moment.

Biaxial Bending

$$\frac{\sigma_{m,y,d}}{f_{m,y,d}} + k_m * \frac{\sigma_{m,z,d}}{f_{m,z,d}} \leq 1 \quad \text{with} \quad \sigma_{m,y,d} = \frac{M_{Ed} * h_y}{I_y}$$

$$k_m * \frac{\sigma_{m,y,d}}{f_{m,y,d}} + \frac{\sigma_{m,z,d}}{f_{m,z,d}} \leq 1 \quad \text{with} \quad \sigma_{m,z,d} = \frac{M_{Ed} * h_z}{I_z}$$

Where:

$$- k_m = \begin{cases} 0.7 & \text{for Rectangular CS of Solid Timber, GLT and LVL} \\ 1.0 & \text{for othe CS geometries of Solid Timber, GLT, LVL and} \end{cases} \rightarrow \text{Factor for the re-}$$

other wood based strctural products

distribution of stresses and the effect of inhomogeneities of the material in a cross-section.

Shear

$$\tau_d \leq f_{v,d} \quad \text{with} \quad \tau_{max,d} = \frac{3}{2} * \frac{V_{Ed}}{A}$$

Where A is the area of the cross-section under analysis and V_{Ed} is the design shear.

Combined Internal Forces, Compression and Bending

$$\left(\frac{\sigma_{c,0,d}}{f_{c,0,d}}\right)^2 + \frac{\sigma_{m,y,d}}{f_{m,y,d}} + k_m * \frac{\sigma_{m,z,d}}{f_{m,z,d}} \leq 1$$

$$\left(\frac{\sigma_{c,0,d}}{f_{c,0,d}}\right)^2 + k_m * \frac{\sigma_{m,y,d}}{f_{m,y,d}} + \frac{\sigma_{m,z,d}}{f_{m,z,d}} \leq 1$$

8.8 ADDITIONAL RULES FOR CURVED BEAMS – ARCH ELEMENTS

The structural arches supporting the deck are elements with an initial construction curvature. The presence of this curvature induces internal forces and stresses that are not negligible and must be accounted for through specific computational approaches. Furthermore, the curved geometry of these elements requires the verification of internal forces using procedures that, in certain cases, differ from those previously described in earlier sections.

Beams With Apex – Relevant Geometric Dimensions

The structural arches must comply with specific geometric parameters concerning the outer and inner radii, the section height, and the positioning of the apex zone.

According to the configuration shown in *Figure 114*, the geometric parameters of the arches are verified as follows: The actual inner radius is compared, in the final stage, with the reference value prescribed by the code, and a deviation of less than 10% (within the order of a few centimeters) is considered acceptable.

The verification is briefly carried out for both structural arch sequences of the structure, with reference to the geometric properties of the arches themselves. The results are summarized in the following tables (*Table 14 & Table 15*).

RELEVANT GEOMETRIC DIMENSIONS – ARCH 1		
r_{int} [m]	61.825	OK
h_{ap} [m]	1.5	
r [m]	62.575	
r_{eff} [m]	62.583	

Table 14: Verification of the Geometric Dimensions - Arch 1

RELEVANT GEOMETRIC DIMENSIONS – ARCH 2		
r_{int} [m]	51.547	OK
h_{ap} [m]	1.5	
r [m]	52.297	
r_{eff} [m]	52.29	

Table 15: Verification of the Geometric Dimensions - Arch 2

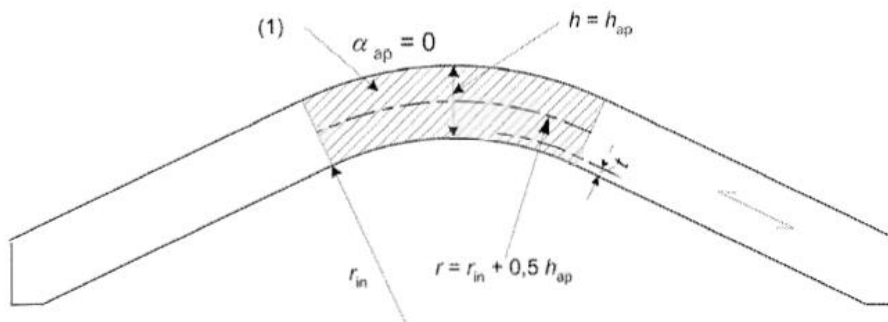


Figure 114: Curved Beam with the Fiber Direction Parallel to the Lower Edge of the Beam - Geometrical Dimensions for the Curved Elements and Definition of the Apex Zone - EN 1995-1-1 Figure 6.9

Beams with Apex – Bending Stresses ($\sigma_{m,d}$)

$$\sigma_{m,d} \leq k_r * f_{m,d}$$

Where:

- $k_r = \begin{cases} 1 & \text{for } \frac{r_{in}}{t} \geq 240 \\ 0.76 + 0.001 * \frac{r_{in}}{t^{58}} & \text{for } \frac{r_{in}}{t} < 240 \end{cases} \rightarrow \text{For Curved and Pitched Beams}$
- $\sigma_{m,d} = k_l * \frac{6 * M_{ap}}{b * h_{ap}^2}$
- M_{ap} is the bending moment in the Apex
- $k_l = k_1 + k_2 * \left(\frac{h_{ap}}{r}\right) + k_3 * \left(\frac{h_{ap}}{r}\right)^2 + k_4 * \left(\frac{h_{ap}}{r}\right)^3$
- $k_1 = 1 + 1.4 * \tan(a_{ap}) + 5.4 * \tan^2(a_{ap})$
- $k_2 = 0.35 - 8 * \tan(a_{ap})$
- $k_3 = 0.6 + 8.3 * \tan(a_{ap}) - 7.8 * \tan^2(a_{ap})$
- $k_4 = 6 * \tan^2(a_{ap})$

Beams with Apex – Tension Stresses Perpendicular to the Grain ($\sigma_{t,90,d}$)

$$\sigma_{t,90,d} \leq k_{dis} * k_{Vol} * f_{t,90,d}$$

Where:

- $k_{dis} = \begin{cases} 1.4 & \rightarrow \text{for Double Tapered and Curved Beams} \\ 1.7 & \rightarrow \text{for Pitched Cambered Beams} \end{cases} \rightarrow \text{Stress Apex distribution factor}$
- $k_{Vol} = \begin{cases} 1.0 & \rightarrow \text{for Solid Timber} \\ \left(\frac{0.01}{V}\right)^{0.2} & \rightarrow \text{for GLT and Laminated Veneer} \end{cases} \rightarrow \text{Volume Factor (V[m}^3\text{] as stressed volume)}$
- $V \leq \frac{2}{3} * V_b$ with V_b Beam Volume
- $\sigma_{t,90,d} = k_p * \frac{6 * M_{ap,d}}{b * h_{ap}^2}$
- $k_p = k_5 + k_6 * \left(\frac{h_{ap}}{r}\right) + k_7 * \left(\frac{h_{ap}}{r}\right)^2$
- $k_5 = 0.2 * \tan(a_{ap})$
- $k_6 = 0.25 - 1.5 * \tan(a_{ap}) + 2.6 * \tan^2(a_{ap})$
- $k_7 = 2.1 * \tan - 4 * \tan^2(a_{ap})$

⁵⁸ “t” corresponds to the lamellae thickness: In the case study is assumed as equal to 40mm (hypothesis that could be changed in possible future considerations).

8.9 MEMBER VERIFICATION – BUCKLING AND LATERAL-TORSIONAL INSTABILITY

The individual structural components are verified with respect to their stability under axial compression and lateral-torsional buckling, as well as under the combined effect of both. Connection elements aimed at increasing overall stability and reducing the effective buckling lengths are incorporated into the structure.

Flexural Buckling

The buckling verification of the individual elements must be carried out when, based on their relative slenderness, the following condition is met:

$$\lambda_{rel,y} = \frac{\lambda_y}{\pi} * \sqrt{\frac{f_{c,0,k}}{E_{0.05}}} \leq 0.3 \text{ or } \lambda_{rel,z} = \frac{\lambda_z}{\pi} * \sqrt{\frac{f_{c,0,k}}{E_{0.05}}} \leq 0.3$$

Where λ_y and λ_z are the relative slenderness for strong and weak axis of the element under analysis and they are defined as:

$$\lambda_y = \frac{L_{b,y}}{i_y} \text{ with } i_y = \frac{\sqrt{I_y}}{A}$$

$$\lambda_z = \frac{L_{b,z}}{i_z} \text{ with } i_z = \frac{\sqrt{I_z}}{A}$$

If the previously described condition is not met - $\lambda_{rel,i} \leq 0.3$ - the verification proceeds by checking the following stress limitation under compression:

$$\sigma_{c,0,d} \leq k_{c,y} * f_{c,0,d} \text{ and } \sigma_{c,0,d} \leq k_{c,z} * f_{c,0,d}$$

Where:

- $k_{c,y}$ & $k_{c,z}$ are the buckling reductions factors (buckling curves) and are computed as follows:

$$k_{c,y} = \frac{1}{k_y + \sqrt{k_y^2 - \lambda_{rel,y}^2}} \rightarrow k_y = 0.5 * (1 + \beta_c * (\lambda_{rel,y} - 0.3) + \lambda_{rel,y}^2)$$

$$k_{c,z} = \frac{1}{k_z + \sqrt{k_z^2 - \lambda_{rel,z}^2}} \rightarrow k_z = 0.5 * (1 + \beta_c * (\lambda_{rel,z} - 0.3) + \lambda_{rel,z}^2)$$

- $\beta_c = \begin{cases} 0.2 & \text{for Solid Timber} \\ 0.1 & \text{for GLT and LVL} \end{cases} \rightarrow \text{Factor for straightness within the limits of EN 1995-1-1}^{59}$

⁵⁹ (EN 1995 - Eurocode 5: Design of timber structures & Relative Annexes, 2004)

Lateral Torsional Buckling

When lateral-torsional buckling occurs in the elements under analysis, the deformation develops out of plane. Reference is made to the critical moment, and an out-of-plane instability mechanism is considered. This is verified by following the steps outlined below:

$$\sigma_{m,d} \leq k_{crit} * f_{m,d}$$

Where:

- $k_{crit} = \begin{cases} 1 & \text{if } \lambda_{rel,m} \leq 0.75 \\ 1.56 - 0.75 * \lambda_{rel,m} & \text{if } 0.75 \leq \lambda_{rel,m} \leq 1.4 \\ \frac{1}{\lambda_{rel,m}^2} & \text{if } \lambda_{rel,m} > 1.4 \end{cases} \rightarrow \text{LTB Reduction Factor}$
- $\lambda_{rel,m} = \sqrt{\frac{f_{m,k}}{\sigma_{m,crit}}}$
- $\sigma_{m,crit} = \frac{M_{y,crit} * h_y}{W_y} = \frac{\pi * \sqrt{E_{0.05} * I_z * G_{0.05} * I_{tor}}}{L_{LTB} * W_y}$
- $I_{tor} = \frac{h * b^3}{3}$ for a regular cross section
- $L_{LTB} = m * L$
- m is the equivalent uniform bending moment factor, which values come from the following table (Figure 115) of the EN 1995-1-1:

Beam type	Loading type	ℓ_{ef}/ℓ^a
Simply supported	Constant moment	1,0
	Uniformly distributed load	0,9
	Concentrated force at the middle of the span	0,8
Cantilever	Uniformly distributed load	0,5
	Concentrated force at the free end	0,8

^a The ratio between the effective length ℓ_{ef} and the span ℓ is valid for a beam with torsionally restrained supports and loaded at the centre of gravity. If the load is applied at the compression edge of the beam, ℓ_{ef} should be increased by $2h$ and may be decreased by $0,5h$ for a load at the tension edge of the beam.

Figure 115: Effective Length as Ratio of the Span - EN 1995-1-1 Table 6.1

Lateral Torsional Buckling & Flexural Buckling

This verification is a combination of two independent checks:

- Verification against buckling under the combined action of compression and biaxial bending:

$$\begin{cases} \frac{\sigma_{c,0,d}}{k_{c,y} * f_{c,0,d}} + \frac{\sigma_{m,y,d}}{f_{m,y,d}} + k_m * \frac{\sigma_{m,z,d}}{f_{m,z,d}} \leq 1 \\ \frac{\sigma_{c,0,d}}{k_{c,z} * f_{c,0,d}} + k_m * \frac{\sigma_{m,y,d}}{f_{m,y,d}} + \frac{\sigma_{m,z,d}}{f_{m,z,d}} \leq 1 \end{cases}$$

- Verification against buckling and lateral-torsional buckling under the combined action of compression and uniaxial flexion:

$$\begin{cases} \frac{\sigma_{c,0,d}}{k_{c,z} * f_{c,0,d}} + \left(\frac{\sigma_{m,y,d}}{k_{crit} * f_{m,y,d}} \right)^2 \leq 1 \\ \frac{\sigma_{c,0,d}}{k_{c,y} * f_{c,0,d}} + \left(\frac{\sigma_{m,z,d}}{k_{crit} * f_{m,z,d}} \right)^2 \leq 1 \end{cases}$$

8.10 DESIGN CHECKS

All the verifications described and theoretically computed are summarized below in result tables, organized for each individual structural element considered. The design analysis, for each element, includes the checks related to deflections under serviceability limit states and those related to ultimate limit states, with the appropriate verification criteria selected according to the specific characteristics of the element under analysis.

Each of the following subsections begins with a descriptive image of the static scheme under analysis, featuring an approximate graphical representation of the distributed loads considered as applied to the structural element in question. A summary table of the element's cross-sectional geometry and geometric properties is also included.

8.10.1 SECONDARY BEAMS – DECK

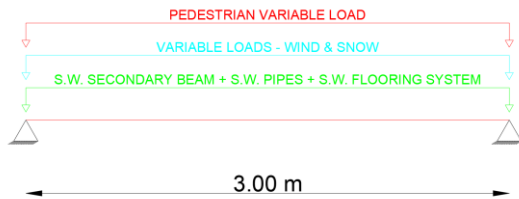


Figure 116: Static Scheme Description - Secondary Beams - Geometry and Applied Loads

DIMENSION OF SECONDARY ELEMENTS			
b [m]	0.2	A [m ²]	0.08
h [m]	0.4	I [m ⁴]	0.001067
L [m]	3.0	Rho mean [kg/m ³]	420
Self-Weight [kg/m]		33.6	

Table 16: Summary Table of Geometric Dimensions - Secondary Beams

8.10.1.1 SLS VERIFICATIONS

DEFLECTION CONTROL [m]								
PERMANENT	W _{m,inst,G}	3.30E-04	W _{inst,G}	W _{fin,G}	W _{net,fin} [m]	w _c [m]	W _{net,lim,fin} [m]	CHECK
	W _{v,inst,G}	9.96E-05	4.30E-04	1.29E-03	3.00E-03	0.00E+00	1.20E-02	OK
VARIABLE	W _{m,inst,Q1}	1.12E-03	W _{inst,Q1}	W _{fin,Q1}				
	W _{v,inst,Q1}	3.38E-04	1.46E-03	1.46E-03				
	W _{m,inst,Q2}	1.97E-04	W _{inst,Q2}	W _{fin,Q2}				
	W _{v,inst,Q2}	5.94E-05	2.56E-04	2.05E-04				
	W _{m,inst,Q3}	1.21E-04	W _{inst,Q3}	W _{fin,Q3}				
	W _{v,inst,Q3}	3.65E-05	1.58E-04	4.73E-05				

Table 17: Vertical Deflections Control - SLS Verifications - Secondary Beams – Deck

8.10.1.2 ULS VERIFICATIONS

SIZE EFFECT		SYSTEM FACTOR	
TENSION OR BENDING		ksys	1.1
k_h	1.04		
COMPRESSION PARALLEL TO GRAIN		LIMIT	CHECK
$\sigma_{c,0,d}$	0.14	13.44	<OK
UNIAXIAL BENDING		LIMIT	CHECK
$\sigma_{m,d}$	7.07	13.44	<OK
SHEAR		LIMIT	CHECK
T_d	1.32	1.96	<OK
LATERAL TORTIONAL BUCKLING		LIMIT	CHECK
$\sigma_{m,d}$	7.07	13.44	<OK
COMBINED COMPRESSION AND BENDING		LIMIT	CHECK
$(\sigma_{c,0,d}/f_{c,0,d})^2 + (\sigma_{m,y,d}/f_{m,y,d}) + k_m \cdot (\sigma_{m,z,d}/f_{m,z,d})$	0.53	1	<OK
$(\sigma_{c,0,d}/f_{c,0,d})^2 + k_m \cdot (\sigma_{m,y,d}/f_{m,y,d}) + (\sigma_{m,z,d}/f_{m,z,d})$	0.37	1	<OK

Table 18: ULS Verifications - Secondary Beams – Deck

8.10.2 PRIMARY BEAMS – DECK

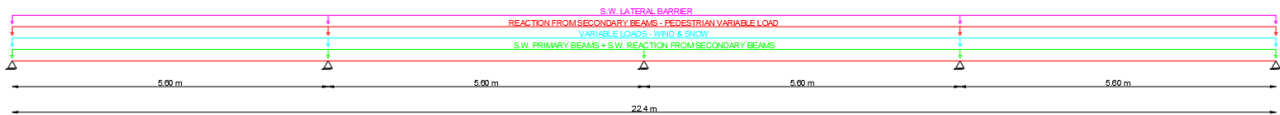


Figure 117: Static Scheme Description – Primary Beams - Geometry and Applied Loads

DIMENSION OF PRIMARY ELEMENTS			
b [m]	0.2	A [m ²]	0.20
h [m]	1.0	I [m ⁴]	0.016667
L [m]	5.6	Rho mean [kg/m ³]	445
Self-Weight [kg/m]	89		

Table 19: Summary Table of Geometric Dimensions - Primary Beams

8.10.2.1 SLS VERIFICATIONS

DEFLECTION CONTROL [m]								
PERMANENT	$w_{m,inst,G}$	1.67E-04	$w_{inst,G}$	$w_{fin,G}$	$w_{net,fin}$ [m]	w_c [m]	$w_{net,lim,fin}$ [m]	CHECK
	$w_{v,inst,G}$	1.06E-04	2.73E-04	8.18E-04				
VARIABLE	$w_{m,inst,Q1}$	3.82E-04	$w_{inst,Q1}$	$w_{fin,Q1}$				
	$w_{v,inst,Q1}$	2.43E-04	6.25E-04	6.25E-04				
	$w_{m,inst,Q2}$	6.66E-05	$w_{inst,Q2}$	$w_{fin,Q2}$				
	$w_{v,inst,Q2}$	4.24E-05	1.09E-04	8.72E-05				
	$w_{m,inst,Q3}$	4.31E-05	$w_{inst,Q3}$	$w_{fin,Q3}$				
	$w_{v,inst,Q3}$	2.74E-05	7.05E-05	2.12E-05				

Table 20: Vertical Deflections Control - SLS Verifications – Primary Beams – Deck

8.10.2.2 ULS VERIFICATIONS

SIZE EFFECT		SYSTEM FACTOR	
TENSION OR BENDING		ksys	1
k_h	1		
TENSION PARALLEL TO THE GRAIN		LIMIT	CHECK
$\sigma_{t,0,d}$	2.07	11.648	<OK
COMPRESSION PARALLEL TO GRAIN		LIMIT	CHECK
$\sigma_{c,0,d}$	1.36	14.56	<OK
COMPRESSION PERPENDICULAR TO GRAIN		LIMIT	CHECK
$\sigma_{c,90,d}$	0.83	1.4	<OK
UNIAXIAL BENDING		LIMIT	CHECK
$\sigma_{m,d}$	4.86	14.56	<OK
SHEAR		LIMIT	CHECK
T_d	0.80	1.96	<OK
LATERAL TORSIONAL BUCKLING		LIMIT	CHECK
$\sigma_{m,d}$	4.86	14.56	<OK
COMBINED COMPRESSION AND BENDING		LIMIT	CHECK
$(\sigma_{c,0,d}/f_{c,0,d})^2 + (\sigma_{m,y,d}/f_{m,y,d}) + k_m * (\sigma_{m,z,d}/f_{m,z,d})$	0.34	1	<OK
$(\sigma_{c,0,d}/f_{c,0,d})^2 + k_m * (\sigma_{m,y,d}/f_{m,y,d}) + (\sigma_{m,z,d}/f_{m,z,d})$	0.24	1	<OK

Table 21: ULS Verifications – Primary Beams – Deck

8.10.3 PRIMARY BEAMS – CENTRAL DECK ZONE

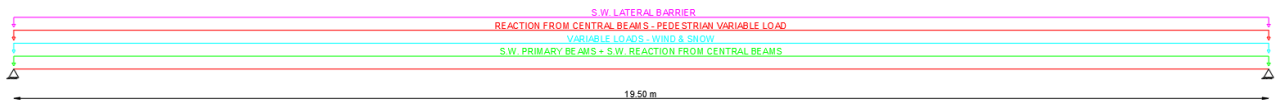


Figure 118: Static Scheme Description – Primary Beams – Deck Central Position - Geometry and Applied Loads

DIMENSION OF PRIMARY ELEMENTS – DECK CENTRAL			
b [m]	0.2	A [m²]	0.20
h [m]	1	I [m⁴]	0.01667
L [m]	19.5	Rho mean [kg/m³]	445
Self-Weight [kg/m]	89		

Table 22: Summary Table of Geometric Dimensions - Primary Beams – Deck Central Position

8.10.3.1 SLS VERIFICATIONS

DEFLECTION CONTROL [m]								
PERMANENT	$W_{m,inst,G}$	1.07E-02	$W_{inst,G}$	$W_{fin,G}$	$w_{net,fin}$ [m]	w_c [m]	$w_{net,lim,fin}$ [m]	CHECK
	$W_{v,inst,G}$	5.10E-04	1.12E-02	3.36E-02				
VARIABLE	$W_{m,inst,Q1}$	1.25E-02	$W_{inst,Q1}$	$W_{fin,Q1}$	5.05E-02	0.00E+00	7.75E-02	OK
	$W_{v,inst,Q1}$	5.95E-04	1.31E-02	1.31E-02				
	$W_{m,inst,Q2}$	3.80E-03	$W_{inst,Q2}$	$W_{fin,Q2}$				
	$W_{v,inst,Q2}$	1.81E-04	3.98E-03	3.18E-03				
	$W_{m,inst,Q3}$	2.03E-03	$W_{inst,Q3}$	$W_{fin,Q3}$				
	$W_{v,inst,Q3}$	9.65E-05	2.12E-03	6.37E-04				

Table 23: Vertical Deflections Control - SLS Verifications – Primary Beams – Deck Central Position

8.10.3.2 ULS VERIFICATIONS

SIZE EFFECT		SYSTEM FACTOR	
TENSION OR BENDING		ksys	1
k_h	1		
TENSION PARALLEL TO THE GRAIN		LIMIT	CHECK
$\sigma_{t,0,d}$	2.10	11.648	<OK
COMPRESSION PARALLEL TO GRAIN		LIMIT	CHECK
$\sigma_{c,0,d}$	1.37	14.56	<OK
UNIAXIAL BENDING		LIMIT	CHECK
$\sigma_{m,d}$	10.17	14.56	<OK
SHEAR		LIMIT	CHECK
T_d	0.62	1.96	<OK
LATERAL TORSIONAL BUCKLING		LIMIT	CHECK
$\sigma_{m,d}$	10.17	14.56	<OK
COMBINED COMPRESSION AND BENDING		LIMIT	CHECK
$(\sigma_{c,0,d}/f_{c,0,d})^2 + (\sigma_{m,y,d}/f_{m,y,d}) + k_m \cdot (\sigma_{m,z,d}/f_{m,z,d})$	0.71	1	<OK
$(\sigma_{c,0,d}/f_{c,0,d})^2 + k_m \cdot (\sigma_{m,y,d}/f_{m,y,d}) + (\sigma_{m,z,d}/f_{m,z,d})$	0.50	1	<OK

Table 24: ULS Verifications – Primary Beams – Deck Central Position

8.10.4 CENTRAL BEAMS – CENTRAL DECK ZONE

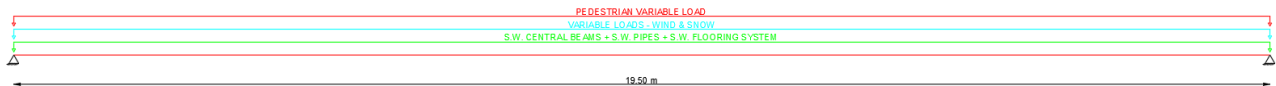


Figure 119: Static Scheme Description – Central Beams – Deck Central Position - Geometry and Applied Loads

DIMENSION OF CENTRAL PRIMARY ELEMENTS			
b [m]	0.25	A [m ²]	0.225
h [m]	0.9	I [m ⁴]	0.0151875
L [m]	19.5	Rho mean [kg/m ³]	445
Self-Weight [kg/m]		100.125	

Table 25: Summary Table of Geometric Dimensions – Central Beams – Deck Central Position

8.10.4.1 SLS VERIFICATIONS

DEFLECTION CONTROL [m]								
PERMANENT	$W_{m,inst,G}$	2.12E-02	$W_{inst,G}$	$W_{fin,G}$	$W_{net,fin}$ [m]	w_c [m]	$W_{net,lim,fin}$ [m]	CHECK
	$W_{v,inst,G}$	8.17E-04	2.20E-02	6.60E-02				
VARIABLE	$W_{m,inst,Q1}$	2.74E-02	$W_{inst,Q1}$	$W_{fin,Q1}$	3.33E-02	6.60E-02	7.75E-02	OK
	$W_{v,inst,Q1}$	1.06E-03	2.85E-02	2.85E-02				
	$W_{m,inst,Q2}$	4.82E-03	$W_{inst,Q2}$	$W_{fin,Q2}$				
	$W_{v,inst,Q2}$	1.86E-04	5.01E-03	4.01E-03				
	$W_{m,inst,Q3}$	2.57E-03	$W_{inst,Q3}$	$W_{fin,Q3}$				
	$W_{v,inst,Q3}$	9.93E-05	2.67E-03	8.02E-04				

Table 26: Vertical Deflections Control - SLS Verifications – Central Beams – Deck Central Position

8.10.4.2 ULS VERIFICATIONS

SIZE EFFECT		SYSTEM FACTOR	
TENSION OR BENDING		ksys	1.1
k_h	1		
TENSION PARALLEL TO THE GRAIN		LIMIT	CHECK
$\sigma_{t,0,d}$	0.88	11.65	<OK
COMPRESSION PARALLEL TO GRAIN		LIMIT	CHECK
$\sigma_{c,0,d}$	0.55	14.56	<OK
UNIAXIAL BENDING		LIMIT	CHECK
$\sigma_{m,d}$	9.87	14.56	<OK
SHEAR		LIMIT	CHECK
T_d	0.65	1.96	<OK
LATERAL TORSIONAL BUCKLING		LIMIT	CHECK
$\sigma_{m,d}$	9.87	14.56	<OK
COMBINED COMPRESSION AND BENDING		LIMIT	CHECK
$(\sigma_{c,0,d}/f_{c,0,d})^2 + (\sigma_{m,y,d}/f_{m,y,d}) + k_m \cdot (\sigma_{m,z,d}/f_{m,z,d})$	0.68	1	<OK
$(\sigma_{c,0,d}/f_{c,0,d})^2 + k_m \cdot (\sigma_{m,y,d}/f_{m,y,d}) + (\sigma_{m,z,d}/f_{m,z,d})$	0.48	1	<OK

Table 27: ULS Verifications – Central Beams – Deck Central Position

8.10.5 TRANSVERSAL BEAMS – DECK-TO-ARCH CONNECTIONS

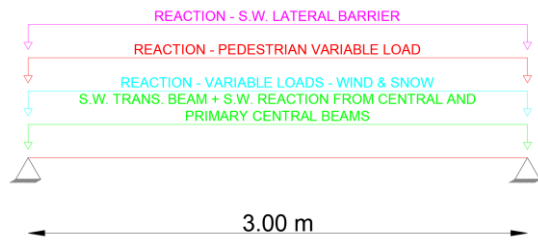


Figure 120: Static Scheme Description – Transversal Beams – Connection Deck-Arches - Geometry and Applied Loads

DIMENSION OF TRASVERSAL ELEMENT			
b [m]	0.4	A [m ²]	0.28
h [m]	0.7	I [m ⁴]	0.0114
L [m]	3.0	Rho mean [kg/m ³]	445
Self-Weight [kg/m]		124.6	

Table 28: Summary Table of Geometric Dimensions – Transversal Beams – Connection Deck-Arches

8.10.5.1 SLS VERIFICATIONS

DEFLECTION CONTROL [m]								
PERMANENT	W _{m,inst,G}	3.87E-04	W _{inst,G}	W _{fin,G}	3.24E-03	0.00E+00	1.28E-02	OK
	W _{v,inst,G}	3.31E-04	7.19E-04	2.16E-03				
VARIABLE	W _{m,inst,Q1}	4.93E-04	W _{inst,Q1}	W _{fin,Q1}				
	W _{v,inst,Q1}	4.21E-04	9.14E-04	9.14E-04				
	W _{m,inst,Q2}	9.72E-05	W _{inst,Q2}	W _{fin,Q2}				
	W _{v,inst,Q2}	8.31E-05	1.80E-04	1.44E-04				
	W _{m,inst,Q3}	5.19E-05	W _{inst,Q3}	W _{fin,Q3}				
	W _{v,inst,Q3}	4.43E-05	9.62E-05	2.89E-05				

Table 29: Vertical Deflections Control - SLS Verifications – Transversal Beams – Connection Deck-Arches

8.10.5.2 ULS VERIFICATIONS

SIZE EFFECT		SYSTEM FACTOR	
TENSION OR BENDING		ksys	1
k_h	1		
TENSION PARALLEL TO THE GRAIN		LIMIT	CHECK
$\sigma_{t,0,d}$	0.05	11.65	<OK
COMPRESSION PARALLEL TO GRAIN		LIMIT	CHECK
$\sigma_{c,0,d}$	0.10	14.56	<OK
UNIAXIAL BENDING		LIMIT	CHECK
$\sigma_{m,d}$	5.27	14.56	<OK
SHEAR		LIMIT	CHECK
T_d	1.29	1.96	<OK
LATERAL TORSIONAL BUCKLING		LIMIT	CHECK
$\sigma_{m,d}$	5.27	14.56	<OK
COMBINED COMPRESSION AND BENDING		LIMIT	CHECK
$(\sigma_{c,0,d}/f_{c,0,d})^2 + (\sigma_{m,y,d}/f_{m,y,d}) + k_m \cdot (\sigma_{m,z,d}/f_{m,z,d})$	0.36	1	<OK
$(\sigma_{c,0,d}/f_{c,0,d})^2 + k_m \cdot (\sigma_{m,y,d}/f_{m,y,d}) + (\sigma_{m,z,d}/f_{m,z,d})$	0.25	1	<OK

Table 30: ULS Verifications – Transversal Beams – Connection Deck-Arches

8.10.6 ARCH BEAMS

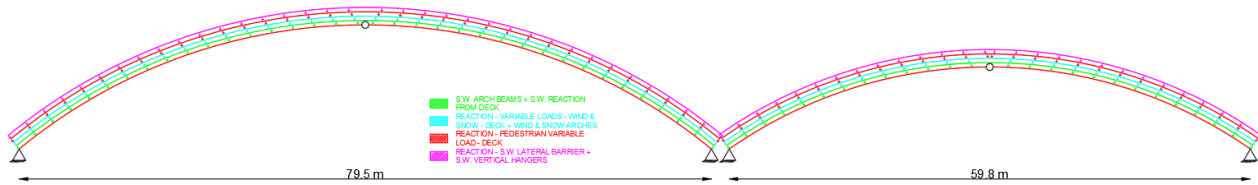


Figure 121: Static Scheme Description – Three-Hinged-Arch – Structural Arches - Geometry and Applied Loads

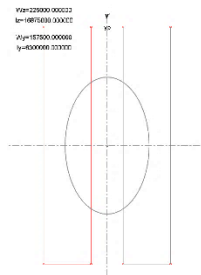


Figure 122: Composed Cross-Section - Arch

DIMENSION OF ARCH ELEMENTS - COMPOSED CROSS-SECTION			
b[m] (x2)	0.3	$W_z [m^3]$	0.1575
h [m]	1.5	$I_z [m^4]$	0.063
L [m] (x2)⁶⁰	43	$W_y [m^3]$	0.225
Ax [m²]	0.9	$I_y [m^4]$	0.16875

Table 31: Summary Table of Geometric Dimensions – Arch Beams

8.10.6.1 SLS VERIFICATIONS

Given the complexity of the structure and its structural relationships, it is not possible to perform a direct manual calculation of the maximum deformations of the arches based on simplified loading

⁶⁰ The symbol (x2) indicates the presence of duplicate elements with the same dimensions: In the case of the base of the section, the composite section consists of two rectangular elements each with a base of 0.3 m; as for the length, Arch 1 is composed of two simply supported arches, each 43 m long, resulting in a total axial length of 86 m.

It should be noted that, since both arches are subjected to identical loading conditions and have the same cross-sectional dimensions, but Arch 2 has a shorter span, the verifications were carried out on Arch 1. This is, of course, a conservative decision, as Arch 2, being smaller in size, could have been verified and designed with a reduced cross-section.

assumptions and standard schemes. In fact, the deformation of the arches was theoretically verified through an assumed deformation shape, considering the superposition of two effects: A load - approximated as distributed - originating from the deck directly beneath the arch, and a load - considered as concentrated - resulting from the lateral support of the portion of the deck located between the two arches.

At this stage, after having understood the probable deformation shape of the arch under such loading conditions, the static deformations are analyzed under the four load categories: Permanent (structural and non-structural), variable - wind, variable - snow, and variable - pedestrian load. The maximum deformation values are considered as the sum of all contributions from the various internal forces of the structure elements and are therefore regarded as w_{inst} .

The images corresponding to the static deformations under these loading conditions are therefore presented⁶¹, along with the respective maximum deformation values.

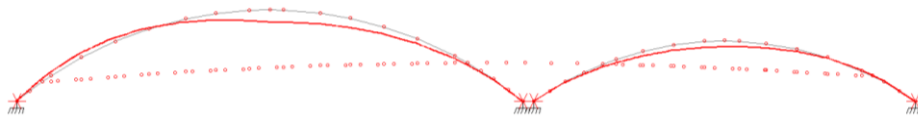


Figure 123: Arch Deformation – Permanent Loads G – Front View – $dz_{max} = 1.8 \text{ cm}$

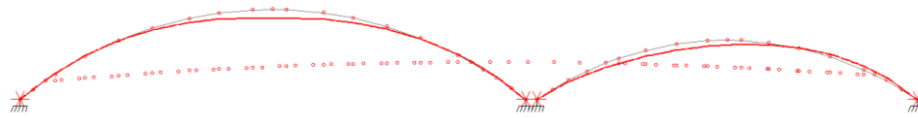


Figure 124: Arch Deformation – Variable Load Pedestrian Traffic Q1 – Front View – $dz_{max} = 1.34 \text{ cm}$

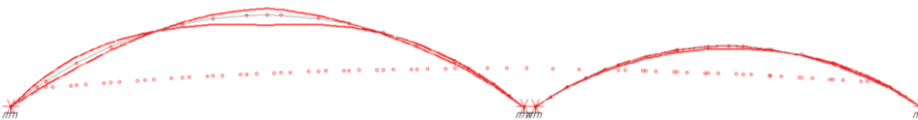


Figure 125: Arch Deformation – Variable Load Wind Q2 – Front View – $dz_{max} = 1.54 \text{ cm}$

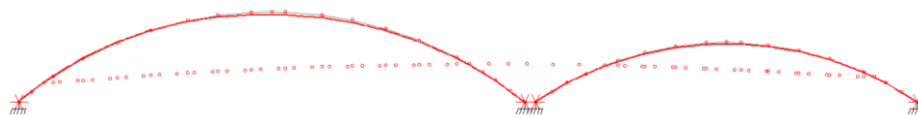


Figure 126: Arch Deformation – Variable Load Snow Q3 – Front View – $dz_{max} = 0.4 \text{ cm}$

The values reported in the description are therefore used as the w_{inst} for the corresponding load action. The deflection calculations are then carried out, including considerations related to creep, as previously done for the other structural elements (Table 32).

⁶¹ All deformation shapes are, once again, plotted using a graphical scale aimed at maximizing the visual representation of the deformation; in fact, a magnification factor of 100 has been applied to the displacements.

DEFLECTION CONTROL [m]						
PERMANENT	$W_{inst,G}$	$W_{fin,G}$	$W_{net,fin}$ [m]	w_c [m]	$W_{net,lim,fin}$ [m]	CHECK
	1.80E-02	5.40E-02	7.52E-02	0.00E+00	3.44E-01	OK
VARIABLE	$W_{inst,Q1}$	$W_{fin,Q1}$				
	1.34E-02	1.34E-02				
	$W_{inst,Q2}$	$W_{fin,Q2}$				
	1.54E-02	4.62E-03				
	$W_{inst,Q3}$	$W_{fin,Q3}$				
	4.00E-03	3.20E-03				

Table 32: Vertical Deflections Control - SLS Verifications – Arch Beams

It is important to note that, also in this case, a reference limit value equal to $L/250$ was introduced: As already explained in previous chapters, this value - particularly with regard to the deformation of the arch - is purely indicative and may serve as a reference threshold to ensure the preservation of the structural design under service loads and over time, considering the effects of creep.

Moreover, in the context of calculating the values reported in the table, a change is made in the order of the variable actions, with wind considered as variable Q2 and snow as Q3. This adjustment stems from the fact that, at least in the case of the structural arches, wind actions result in more critical deformations compared to those caused by snow.

8.10.6.2 ULS VERIFICATIONS

For the ultimate limit state verifications of the structural arch elements, direct reference is made to the formulas previously described, using the appropriate coefficients for curved members with a structural apex. In addition to the verifications (*Table 34*), a summary table of all the coefficients used in these calculations is also provided (*Table 33*).

TABLE OF COEFFICIENTS AND FACTORS	
α_{ap}	0.00
k_1	1.00
k_2	0.35
k_3	0.60
k_4	0.00
k_l	1.01
t - lamellae thickness [mm]	40.00
k_r	1.00
k_5	0.00
k_6	0.25
k_7	0.00
k_p	0.01
k_{dis}	1.40
k_{vol}	0.21

Table 33: Table of Coefficients and Factors – ULS Verifications – Arch Elements with Structural Apex

SIZE EFFECT		SYSTEM FACTOR	
TENSION OR BENDING		ksys	1
k_h	1		
COMPRESSION PARALLEL TO GRAIN		LIMIT	CHECK
$\sigma_{c,0,d}$	2.74	14.56	<OK
TENSION STRESSES PERPENDICULAR TO GRAIN		LIMIT	CHECK
$\sigma_{t,90,d}$	0.03	0.15	<OK
UNIAXIAL BENDING		LIMIT	CHECK
$\sigma_{m,d}$	4.21	26	<OK
SHEAR		LIMIT	CHECK
T_d	0.33	1.96	<OK
COMBINED COMPRESSION AND BENDING		LIMIT	CHECK
$(\sigma_{c,0,d}/f_{c,0,d})^2 + (\sigma_{m,y,d}/f_{m,y,d}) + k_m \cdot (\sigma_{m,z,d}/f_{m,z,d})$	0.32	1	<OK
$(\sigma_{c,0,d}/f_{c,0,d})^2 + k_m \cdot (\sigma_{m,y,d}/f_{m,y,d}) + (\sigma_{m,z,d}/f_{m,z,d})$	0.24	1	<OK

Table 34: ULS Verifications – Arch Beams

8.10.6.3 BUCKLING CONCEPTS OF THE STRUCTURAL ARCHES

Particular attention is given to the buckling behavior of the arch elements. Due to their large span and the significant horizontal force component induced by wind loading, these elements require careful computational treatment and conceptual analysis. It is important to recall the properties of the arch cross-sections: Indeed, these vary significantly depending on the direction of analysis, as a result of the composite nature of the section - an aspect that makes the structure itself more capable of absorbing horizontal loads. Moreover, the presence of diagonal members and transverse connecting elements between the arches, spaced at intervals of 5.6 m, significantly alters the effective buckling length, thereby increasing the flexural-torsional stability of the structure.

A summary table of the results related to the buckling verification formulas, in both the y-direction (parallel to the development axis of the arches) and the z-direction (orthogonal to the development axis of the arches), is presented below (Table 35). It is recalled that these results derive from the theoretical verifications described in the previous chapters, to which the geometric and inertia properties of the structure under analysis have been applied.

DESIGN CRITERION - BUCKLING - Y plane				DESIGN CRITERION - BUCKLING - Z plane			
$\lambda_{rel,y}$		LIMIT	CHECK	$\lambda_{rel,z}$		LIMIT	CHECK
1.60		0.3	<u>Buckling to be considered</u>	0.34		0.3	<u>Buckling to be considered</u>
$\sigma_{c,0,d}$ [kN/m ²]	2.74	6.05	<OK	$\sigma_{c,0,d}$ [kN/m ²]	2.74	21.36	<OK
$\sigma_{m,d,y}$ [kN/m ²]	4.17	14.56	<OK	$\sigma_{m,d,z}$ [kN/m ²]	3.42	14.56	<OK
Buckling + M	0.90	1.00	<OK	Buckling + M	0.56	1.00	<OK
Buckling + LTB	0.51	1.00	<OK	Buckling + LTB	0.21	1.00	<OK

Table 35: Summary Table of Buckling Verifications Under Compression and Bending Moment Actions, in Both Principal Directions “y” and “z” – Actions also Considered in Combination

8.11 DESIGN OF VERTICAL HANGERS

Based on the results presented in the previous chapters concerning the maximum tensile force to which the vertical hangers are subjected, a sectional verification is carried out for the selection of the appropriate cable type and diameter.

In this context, the selected solution is the 7-wire strand, which has a characteristic tensile strength of f_{yk} equal to 1860 MPa.

The calculation of the required cross-sectional area follows the procedure outlined in the following formulas:

$$A_{req,ULS} = 0.66 * (F_{x,ULS} * \frac{\gamma_M}{f_{yk}}) = 130 \text{ mm}^2$$

$$A_{req,SLS} = 0.45 * (F_{x,SLS} * \frac{\gamma_M}{f_{yk}}) = 140 \text{ mm}^2$$

Where:

- A_{req} is the requested minimum area for the vertical hanger's cross-section, computed with reference to the ULS and SLS tensile maximum forces.
- F_x is the maximum tensile force in the cables in the ULS and SLS worst envelope, estimated as $F_{x,ULS} = 127 \text{ kN}$ & $F_{x,SLS} = 93.3 \text{ kN}$.
- γ_M is the resistance reduction factor, imposed as equal to 1.25.
- 0.66 & 0.45 are the reduction factors applied to the calculation with the goal to prevent fatigue problems (SLS) and to consider ULS verifications.

Considering the cross-sectional area of a 7-wire strand as equal to 150 mm^2 , each vertical hanger will consist of a minimum of two 7-wire strands, resulting in a total resistant area of 300 mm^2 ; this also increases the stability of the cables.

8.11.1 CABLE STABILITY UNDER WIND AND RAIN – VORTEX EFFECTS

The combined action of wind and snow generates a non-negligible effect on the vertical hangers themselves. This phenomenon, known as the vortex effect, results from the horizontal wind force (with speeds up to 30 km/h) combined with the action of raindrops, producing significant vibrations.

To enhance structural performance and minimize the effects of wind and rain, the implementation of vortex-shedding reduction mechanisms can be considered. The most influential factor is the external shape of the cables, which should be as smooth as possible to reduce friction and, consequently, vibration. In fact, the hangers can be encased in tubular sheaths that enclose the cables, providing a smooth outer surface and thereby reducing friction caused by wind and rain impact.

In addition, vibration mitigation measures can be introduced through the installation of damping mechanisms. Among the possible solutions, the use of dampers with petroleum wax may be

considered. Alternatively, more cost-effective and practical solutions include connecting the vertical hangers to each other using horizontal hollow elements. These components act as restraints against vibrations and effectively reduce the free buckling length. However, it is essential to ensure the stability of such elements, especially in design configurations like the one under analysis, in which the number of hangers is limited and the spacing between them is not negligible.

8.12 CONSIDERATIONS ON STRUCTURAL CONNECTIONS

When dealing with timber structure, the concepts related to connection types are extensive: The theoretical challenges and calculations involved in this field make it a technically complex topic, often requiring considerable computational effort.

For the purposes of the present design and the scope of this document, the analysis of the connections is limited to a conceptual definition of the main idealized connection types, along with a brief calculation concerning the number and diameter of bolts required for the connections with the vertical hangers.

8.12.1 CONNECTIONS BETWEEN HORIZONTAL ELEMENTS

In the context of horizontal element connections, particular attention must be given to two main components: The connections between secondary and primary beams, and the connections between the linking beams and the arches themselves.

Secondary-to-Primary Beam Connection

The presence of a horizontal force (horizontal component of the pedestrian load) acting eccentrically on the secondary beams with respect to their central axis, generates a torsional moment that must be properly addressed through the design of an appropriate connection type.

Based on the assumption that the secondary beam is idealized as a simply supported element (with pinned connections at both ends), the connection to be designed must exhibit dual behavior: It should act as a hinge with respect to the moment around the z-axis (M_z), while also providing fixed-end restraint in the direction parallel to the longitudinal axis of the primary beams. This is necessary to effectively resist the horizontal loading component and the resulting torsional effects.

To this end, a connection consisting of steel plates and horizontal bolts is idealized, as illustrated in the following *Figure 127*. The shape and dimensions are schematically represented, but no practical or code-based verification calculations are carried out at this stage.

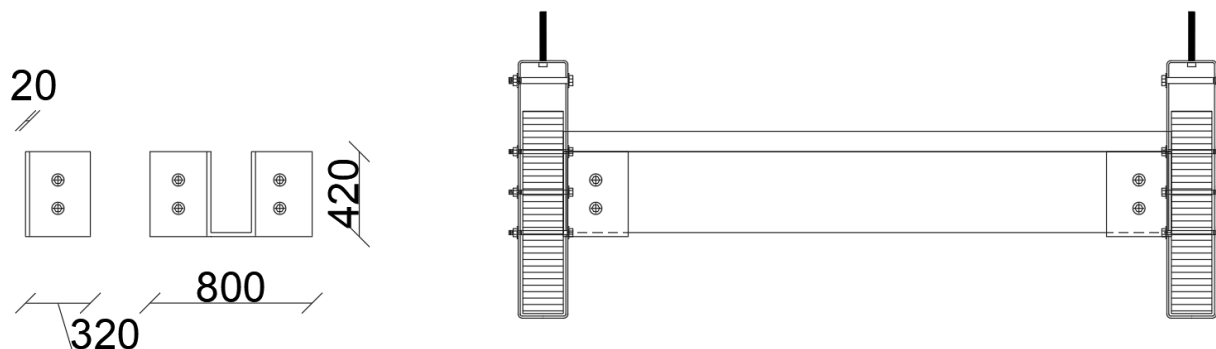


Figure 127: Connection Design Proposal – Secondary to Primary Beams

A steel plate is therefore idealized, composed of segments of varying dimensions (as shown in the *Figure 127*, in millimeters), with a fixed thickness of 2 cm. The insertion of steel bolts is also considered, positioned in such a way as to provide an appropriate reaction to the previously analyzed and described forces. The diameter of the bolts must be carefully verified and accurately defined.

Furthermore, the possibility of introducing slotted holes for the bolts may be considered, to allow for slight deformations induced by thermal loading and long-term structural deformations (structural creep).

Horizontal Beams-to-Structural Arches Connection

Focusing on the connections between the horizontal beams placed between the arches and the arches themselves, the analysis considers not only the applied forces but also the stability of the arch elements. The connection and support system for the linking beams draws upon the same technology adopted for the secondary beams, with the aim of reducing variability among connection types and ensuring greater simplicity and control during on-site construction.

Particular attention, however, must be paid to the type of connection with the arch elements, considering that the arches are composed of built-up sections which are not always fully connected across their components.

To address this requirement, the presence of bolted connections is idealized, crossing both components of the built-up arch sections. In this way, the structural response to horizontal loads - and consequently the lateral stability - is improved by reducing the effective lateral buckling length and increasing the structural reaction inertia.

To make this concept more realistic and easier to understand, a schematic representation is provided in the following *Figure 128*.

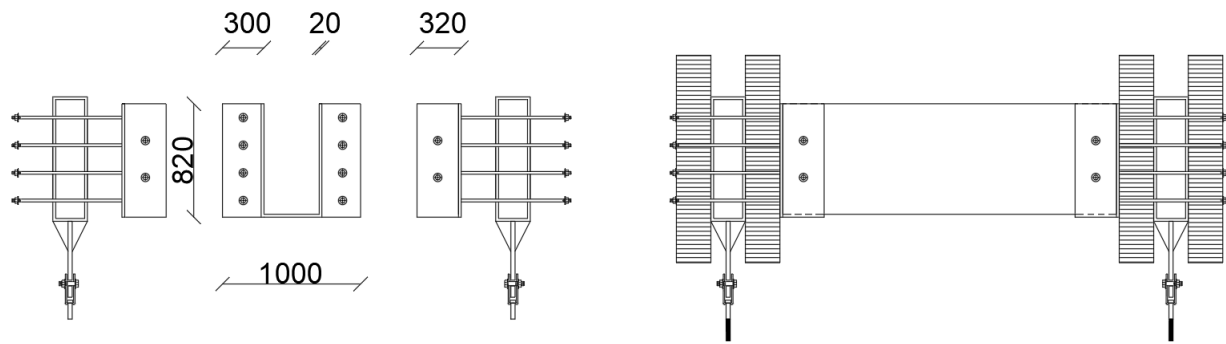


Figure 128: Connection Design Proposal – Horizontal Beams to Structural Arches

Following the proposed geometry, the steel connection plates are designed to form a continuous element between the linking beams and the built-up arch sections, thereby responding to the need for increased horizontal moment of inertia. This configuration also allows the arches to behave more compatibly with a unified section, providing greater inertia and improved structural stability in the horizontal direction.

As in the previous case, the use of bolts is proposed; however, the number of bolts varies depending on the specific plate considered. In the connection to the arches, four bolts are placed on each side of the connection, although their diameter is not computed at this stage.

8.12.2 VERTICAL HANGER-TO-ARCH CONNECTIONS

Another fundamental connection is between the vertical hangers and the structural arches. The design foresees the direct attachment of the vertical hangers to a steel hook, which is itself directly connected to complex-section plates with a hollow rectangular profile.

A representation of this connection is shown in the following *Figure 129*.

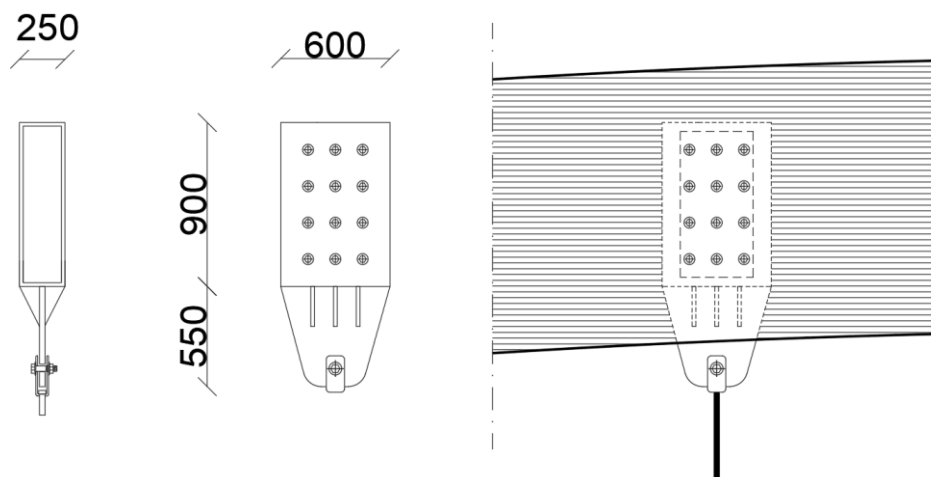


Figure 129: Connection Design Proposal – Vertical Hangers to Structural Arches

The hollow composite-section steel plates are connected to the arch sections through a bolted joint. In the design phase, a total of 12 bolts with a diameter of 10 mm ($\phi 10$) are assumed. These bolts are verified at the ultimate limit state based on the tensile force transmitted by the vertical hangers, as follows.

In accordance with the provisions of Eurocode 3 – EN 1993-1-8⁶², the shear resistance of the described bolted connection is verified. The starting point is the design shear force, which is compared with the shear resistance of the selected bolts.

The shear resistance of a single bolt is calculated as follows:

$$F_{v,Rd} = \frac{\alpha_v * f_{vb} * A_b}{\gamma_{M2}} = 30.22 \text{ kN}$$

Where:

- f_{vb} is the nominal shear strength of the bolt material = 800 N/mm^2 .
- α_v is the reduction factor for long holes and/or type of bolt = 0.6.
- A_b is the tensile stress area of the bolt, computed considering a diameter of 10mm and standard metric coarse thread bolts = 78.54 mm^2 .
- γ_{M2} is the safety factor for resistance = 1.25.

The required total resisting area is defined according to the following expression:

$$A_{req} = \frac{F_{shear,max} * 10^3 * \gamma_{M2}}{\alpha_v * f_{vb}} = 330.73 \text{ mm}^2$$

Considering 12 bolts with the selected diameter, the assumed total resisting area is equal to:

$$A_{supp} = n * A_b = 942.48 \text{ mm}^2$$

Since the assumed resistance area is significantly greater than the required area, the verification is fully satisfied.

It is also appropriate to consider the possibility of adjusting the number and diameter of the bolts: Even 6 bolts with a diameter of 14 mm could prove to be effective. Moreover, the selected configuration provides a resisting capacity that largely exceeds the required limit. This conservative approach is justified by the nature of the structure, which is relatively heavy and subject to variable loads such as pedestrian traffic. Ensuring a wide safety margin in the verification process contributes to enhancing the overall reliability of the connection.

⁶² (EN 1993 - Eurocode 3: Design of steel structures & Relative Annexes, 2005)

8.13 THERMAL GRADIENT EFFECTS ON THE STRUCTURE

With reference to the temperature gradient applied to the structure, as previously described in the chapter on load definition for structural analysis, a study is carried out to evaluate the effects of such a gradient on structural behavior.

This analysis is conducted primarily to assess the stability of the vertical hangers, which must consistently operate under tension. The application of a temperature gradient may, in certain cases, induce compressive forces in these elements, potentially leading to structural instability.

To conduct such considerations, it is essential to understand the behavior of the main structural material used: Glued laminated timber (glulam). Timber exposed to a temperature gradient exhibits anisotropic dimensional variations, due to its fiber-reinforced and hygroscopic nature. When compared to other construction materials, timber's thermal expansion is relatively low; however, it may still cause significant deformations, especially in the presence of rigid constraints.

Glued laminated timber, which is obtained by bonding thin, longitudinally oriented lamellas, demonstrates improved thermal stability. Its layered structure reduces global thermal anisotropy and enhances the distribution of thermal stresses. Moreover, the presence of adhesives improves internal cohesion and limits the propagation of cracks due to differential shrinkage. It is therefore less susceptible to local instabilities such as torsional deformations.

A different consideration must be made for the steel elements, which constitute an integral part of the structure. The stabilizing diagonals, as well as the vertical hangers and the connections, are conceived and verified as steel sections, and the application of a thermal gradient may generate additional stresses in the structure due to the deformation of these elements.

Within the scope of this document, the primary objective remains the assessment of the stability of the vertical hangers under thermal loads and the evaluation of potential structural deformations. For this purpose, static deformation analyses are carried out for the structure subjected to both positive and negative thermal loads. It is important to note that these deformations do not consider the self-weight of the structure or any additional loads: The aim is solely to assess the structural deformation resulting from thermal loading.

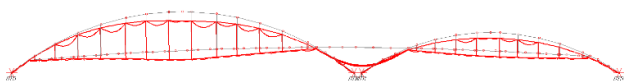


Figure 130: Static Deformation - Structure under Negative Thermal Load

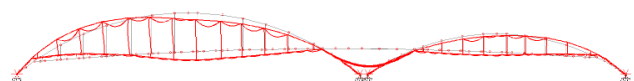


Figure 131: Static Deformation - Structure under Positive Thermal Load⁶³

As shown in *Figure 130*, the structure subjected solely to a negative thermal load behaves as if a uniformly distributed vertical load were applied across its entire surface. The resulting deformation is primarily due to the shrinkage of the vertical hangers. The deformed shape appears more uniform

⁶³ Both figures represent a static deformation amplified by a factor of 100.

compared to that resulting from conventional vertical loading, as it is directly linked to the position and deformation of the hangers.

Figure 131, on the other hand, illustrates the static deformation shape under a positive thermal gradient, which leads to an elongation of the structural elements, particularly those made of steel. In this case, and only in this case, it is possible to observe how the vertical hangers exhibit signs of geometric instability, deforming because of compressive forces acting within them (presence of the deck and the arch elements as a restraint for the elongation of the hangers, causing compression and out-of-plane geometrical deformation).

However, it is important to emphasize that even in this latter case, the deformation pattern merely suggests the theoretical possibility of compression in the vertical hangers. In practice, such a condition does not occur, as the self-weight of the structure is sufficient to keep the hangers in a state of tension.

This conclusion is further confirmed by the analysis of the internal tensile and compressive stresses in the hangers, which remain in tension in all cases, with stress values showing no significant variation.

9 PEDESTRIAN WALKING COMFORT ASSESSMENT

This chapter presents an in-depth analysis of the dynamic behavior of the pedestrian bridge, with particular attention given to the verification of walking comfort as perceived by pedestrians during crossing. This verification is carried out based on two key normative and technical references: The French SETRA⁶⁴ guidelines and Eurocode 5 – Part 2⁶⁵. Both provide specific guidance regarding the behavior and assessment of pedestrian bridges (whether timber or otherwise) subjected to dynamic actions induced by the pedestrian movement.

Detailed analysis is conducted through the development of a MATLAB model, in which the bridge structure is schematized in a simplified two-dimensional finite element representation. This allows for a realistic simulation of the dynamic response of the structure under periodic excitation, enabling the calculation of induced accelerations for different vibration modes and the comparison of these results with prescribed verification thresholds.

This is a detailed study that constitutes a crucial step in the analysis of the pedestrian bridge under consideration: It provides a clear understanding of how the structure responds to dynamic pedestrian traffic loads and how users may perceive structural vibrations, thus helping to prevent the development of dangerous resonance phenomena.

9.1 NUMERICAL MODEL DESCRIPTION

The bridge structure was therefore schematized using a finite element model in which both structural constraints and the overall configuration were accurately represented (*Figure 132*). The arches were discretized with a mesh of 50 elements each, based on coordinates calculated from a parabolic equation centered along their span. The deck, also idealized with a parabolic geometry, was discretized at the anchorage points of the vertical hangers, with the aim of accurately representing the vertical restraints, thereby providing a model that closely reflects the actual support conditions induced by the vertical hangers.

The structural elements were assigned the appropriate geometric and mechanical properties, including elastic moduli, material densities, and cross-sectional dimensions, with due reference to moments of inertia. Particular attention was given to the composite cross-sections of the arches, whose properties were imported from the previously developed FEM model described earlier.

The developed model also adheres to the general design geometry of the bridge, including the same number of vertical hangers. These hangers, to simulate their behavior as realistically as possible, were modelled as rigid springs with a constant stiffness of $k = 10^9$ N/m. The supports were modelled in accordance with the actual degrees of constraint of the structure, simulating restraints in both the

⁶⁴ SETRA (Service d'Études Techniques des Routes et Autoroutes) is a French technical body that has developed specific guidelines for the design and verification of the dynamic comfort of pedestrian walkways, with reference to vibrations induced by walking. The SETRA criterion assesses the acceptability of modal accelerations perceived by pedestrians, establishing comfort thresholds in terms of maximum or RMS (Root Mean Square) acceleration, generally set at 0.7 m/s^2 to ensure the usability and safety of the structure.

⁶⁵ (EN 1995 - Eurocode 5: Design of timber structures & Relative Annexes, 2004), Part 2.

vertical and horizontal directions, such as at the base points of the arches or at the intersections between the deck and the arches.

For each element, the global stiffness (K) and mass (M) matrices were assembled and subsequently integrated into the overall system. Once the degrees of freedom were properly defined, matrix reduction was performed, and modal analysis was carried out. This process yielded natural frequencies and corresponding vibration modes of the structure.

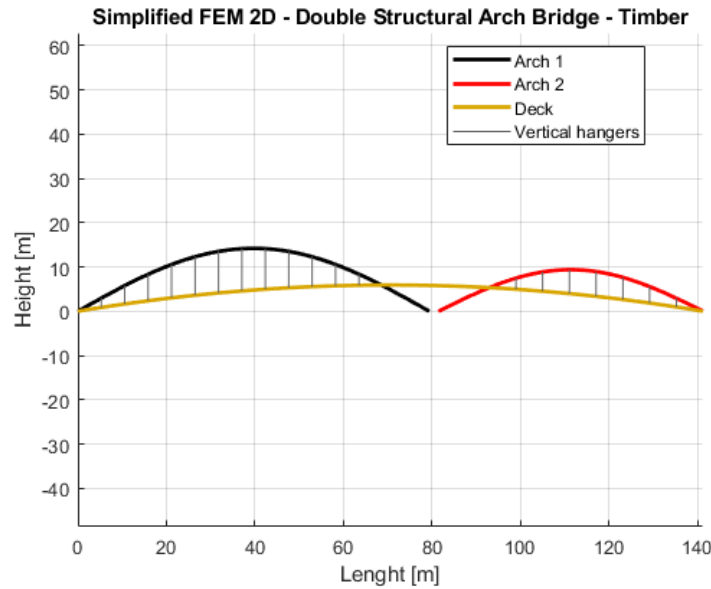


Figure 132: Simplified FEM 2D - Arch Bridge - MATLAB Script

9.2 MODAL ANALYSIS

To achieve a proper understanding of the dynamic behavior of the bridge, a modal analysis is required. This analysis identifies the natural frequencies and the corresponding modal shapes of vibration. It is important to note that the structure is free to vibrate along with the degrees of freedom that are not restrained.

The analysis focuses on the first six vibration modes, as these are the most significantly affected by the dynamic load induced by human walking.

The modes are obtained by solving the eigenvalue problem in the following form:

$$[K] * \phi = \lambda * [M] * \phi$$

Where:

- $[K]$ is the reduced stiffness matrix.
- $[M]$ is the reduced mass matrix.
- ϕ is the vector of modal displacements.
- $\lambda = \omega^2$ is the eigenvalue associated with the angular frequency ω .

From this, the following natural frequencies (in Hz) are obtained (*Table 36*):

MODE	FREQUENCY [Hz]
1	0.56
2	0.82
3	1.55
4	2.27
5	2.84
6	3.52

Table 36: Natural Frequencies – Modes 1–6

The resulting modal shapes are then graphically represented, showing the amplified vertical displacement of the deck (*Figure 133*).

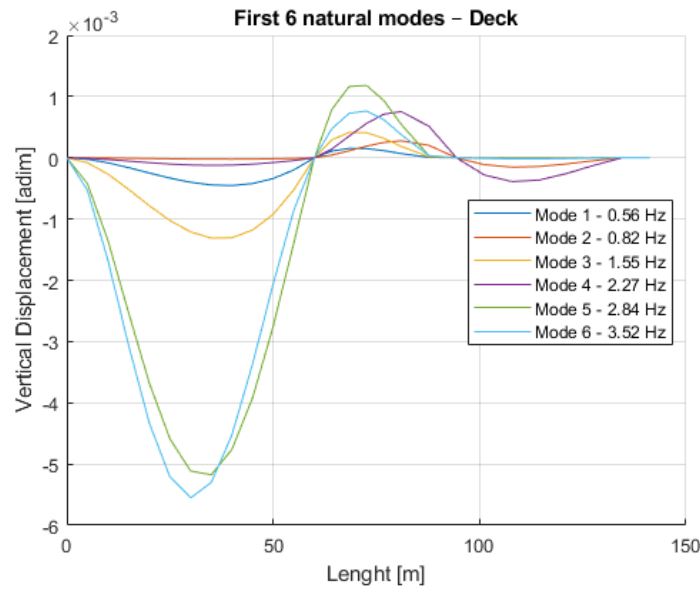


Figure 133: Amplified Deck Displacements - 6 First Natural Modes - MATLAB Script

9.3 COMFORT CHECK ACCORDING TO SETRA GUIDELINES

The SETRA guidelines (*Service d'Études Techniques des Routes et Autoroutes*) are a European reference for the verification and design of dynamic comfort in the context of pedestrian bridges. Their methodology enables the use of a simplified approach to estimate the acceleration perceived by a pedestrian during crossing, by modelling the structure as a single degree of freedom (SDOF) system for each natural mode.

The method is based on the response of a harmonic oscillator subjected to a sinusoidal force:

- Harmonic force: $F(t) = F_0 * \sin(w_{exc} * t)$;
- Excitation frequency: $F_{exc} = 2 \text{ Hz}$, typical of human walking.
- Modal damping ratio: $\xi = 0.01$.

To calculate the maximum value of modal acceleration, the following numerical procedure is followed (*Table 37*):

1.	Calculation of the natural angular frequency of mode “i”	$\omega_i = 2\pi * f_i$
2.	Calculation of the equivalent stiffness for mode “i”	$k_i = m_{mod} \cdot \omega_i^2$
3.	Calculation of the static displacement	$x_{stat} = F_0/k_i$
4.	Calculation of the Dynamic Amplification Factor (DAF)	$A_{dyn} = 1/\sqrt{(1 - (\frac{w_{ecc}}{w_i})^2)^2 + (2 * \xi * \frac{w_{ecc}}{w_i})^2}$
5.	Amplified dynamic displacement	$x_{dyn} = x_{stat} * A_{dyn}$
6.	Acceleration	$\alpha_i = x_{dyn} * w_{ecc}^2$

Table 37: Numerical Procedure – Calculation of the Maximum Value of Modal Acceleration

It is noted that in “Step 2” a mass referred to as m_{mod} is used: This represents the modal mass of the system. Although the modal mass can be calculated, it is assumed to be equal to 10% of the total mass of the system and is therefore set to a value of 15000 kg.

A direct comparison is then made with the threshold established by the standard, set at a value of 0.7 m/s². Exceeding this threshold necessitates the adoption of mitigation measures, such as the implementation of Tuned Mass Dampers (TMD).

From the application of the procedure described above, the following acceleration results are obtained for the first six modes (*Table 38*):

SETRA COMFORT ASSESSMENT			
MODE	FREQUENCY [Hz]	MAXIMUM ACCELERATION [m/s ²]	COMPLIANT
1	0.56	0.0506	YES
2	0.82	0.0561	YES
3	1.55	0.1174	YES
4	2.27	0.1632	YES
5	2.84	0.0461	YES
6	3.52	0.0223	YES

Table 38: SETRA Comfort Assessment - Values of the Maximum Modal Acceleration – Verification of the Criteria (max 0.7m/s²)

9.4 COMFORT CHECK ACCORDING TO EUROCODE 5 - PART 2, ANNEX B

An additional method, more specifically tailored to timber bridges, is provided and analyzed directly in Eurocode 5 - Part 2, Annex B⁶⁶. This method allows for a simplified estimation of the acceleration induced by either a single pedestrian or a continuous pedestrian flow.

Depending directly on the frequency of the first vertical mode, three expressions are examined for the calculation of vertical and horizontal acceleration (*Table 39*):

1.	If $f_1 \leq 2.5$ Hz	$\alpha_{EC5} = 200/(m_{tot} * \xi)$
2.	If $2.5 < f_1 \leq 5.0$ Hz	$\alpha_{EC5} = 100/(m_{tot} * \xi)$
3.	Horizontal Accelerations	$\alpha_{hor} = 50/(m_{tot} * \xi)$

Table 39: Vertical and Horizontal Accelerations Formulas – EC5 Part 2 -Annex B

⁶⁶ (EN 1995 - Eurocode 5: Design of timber structures & Relative Annexes, 2004)

Since $f_1 = 0.56 \text{ Hz}$, formula 1 is selected, obtaining $\alpha_{EC5} = 0.127 \text{ m/s}^2$ and $\alpha_{hor} = 0.0318 \text{ m/s}^2$.

The trend of the vertical acceleration α_{EC5} and the horizontal acceleration α_{hor} as a function of the natural frequencies are plotted in *Figure 134* & *Figure 135*: It is possible to observe a change in the vertical acceleration values corresponding to the transition of the analyzed frequency from a value below 2.5 Hz to a value above.

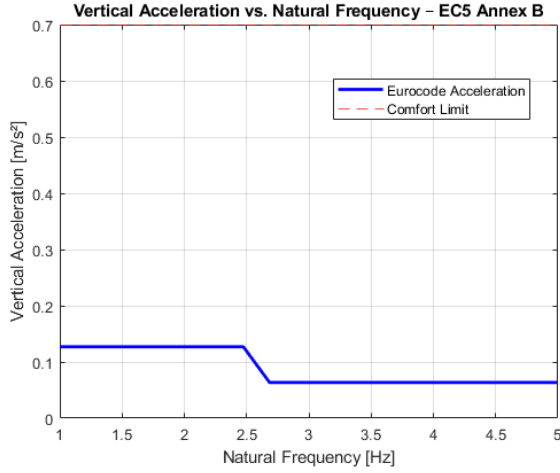


Figure 134: Vertical Acceleration VS Natural Frequency - EC5 Part 2 - Annex B

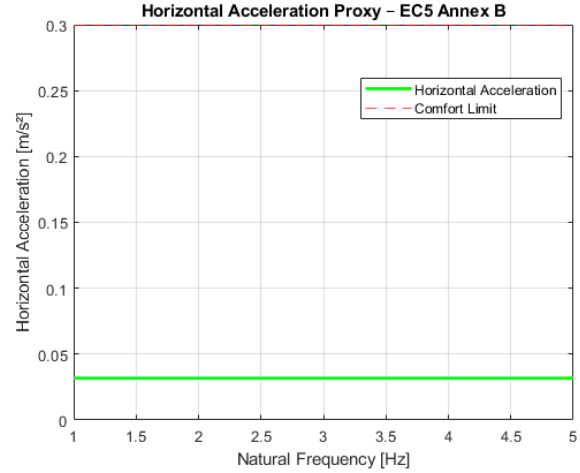


Figure 135: Horizontal Acceleration VS Natural Frequency - EC5 Part 2 - Annex B

9.4.1 ESTIMATION FOR DISTINCT PEDESTRIAN GROUPS AND CONTINUOUS FLOW

According to Annex B, the formula for estimating the vertical acceleration in the presence of several persons crossing the bridge is:

$$a_{vert,n} = 0.23 * a_{EC5} * n * k_{vert}$$

Where:

- n is the number of pedestrians on the bridge:
 $n = 13$ for a distinct group of pedestrians
 $n = 0.6 * A_{pavimentation}$ for a continuous stream of pedestrians.
- k_{vert} is a coefficient obtained from Figure B.1 of Eurocode 5 Part 2 (*Figure 136*), with a corresponding value of approximately 0.33 for $f = 0.56 \text{ Hz}$.

The formula for estimating the horizontal acceleration in the presence of several persons crossing the bridge is:

$$a_{hor,n} = 0.18 * a_{hor} * n * k_{hor}$$

Where:

- n is the number of pedestrians on the bridge (as already specified).

- k_{hor} is a coefficient obtained from Figure B.2 of Eurocode 5 Part 2 (Figure 137), with a corresponding value of 1 for $f = 0.56$ Hz.

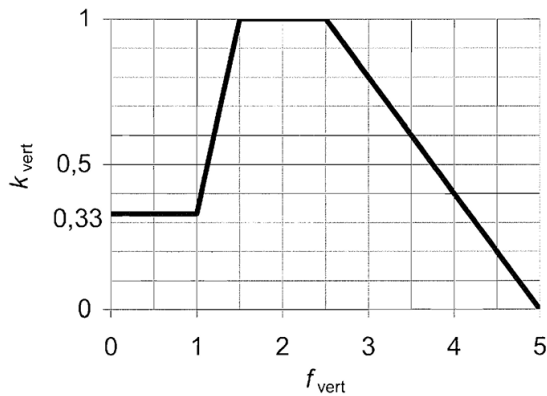


Figure 136: Relationship between the Vertical Fundamental Natural Frequency f_{vert} and the Coefficient k_{vert} - Figure B.1 EC5 Part 2 - Annex B

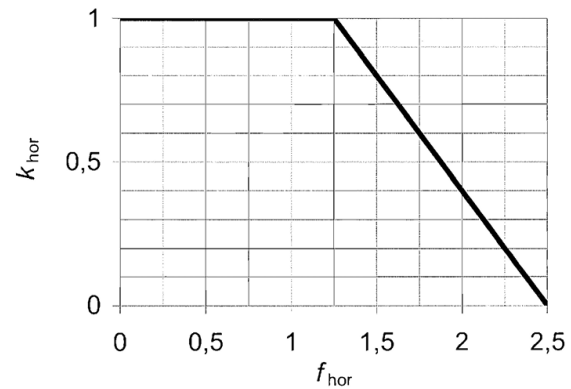


Figure 137: Relationship between the Horizontal Fundamental Natural Frequency f_{hor} and the Coefficient k_{hor} - Figure B.2 EC5 Part 2 - Annex B⁶⁷

The acceleration values obtained using the described formulas, both in the vertical and horizontal directions, as a function of the coefficient n representing the number of people on the bridge, are summarized in the following Table 40:

VERTICAL ACCELERATION UNDER PEDESTRIAN FLOW		
n	$a_{vert,n} [m/s^2]$	COMPLIANT
13	0.1254	YES
271	2.6151	NO
HORIZONTAL ACCELERATION UNDER PEDESTRIAN FLOW		
n	$a_{hor,n} [m/s^2]$	COMPLIANT
13	0.0743	YES
271	1.5504	NO

Table 40: Vertical and Horizontal Acceleration Under Pedestrian Flow – Variation of Values as a Function of n

As can be observed from the acceleration values obtained, both in the vertical and horizontal directions, the verification is satisfied in the case of non-continuous pedestrian occupancy on the bridge ($n=13$) but not verified for full pedestrian occupancy of the bridge ($n=271$). This outcome is consistent with the design assumptions of the bridge itself: The pedestrian bridge was not conceived to accommodate high occupancy classes, as it is not a public structure. Being a private structure, its occupancy is limited to private use related to the bridge's primary function, which is to support the pipes attached to the deck that transport gas and liquids across the riverbanks. In summary, the results reflect the conditions assumed during the design phase.

A graph is plotted below showing the trend of vertical acceleration as a function of the number of people occupying the bridge (Figure 138). As can be observed, the acceleration values remain below the threshold up to an occupancy of approximately $n=75$ people.

⁶⁷ (EN 1995 - Eurocode 5: Design of timber structures & Relative Annexes, 2004) – Part 2, Annex B.

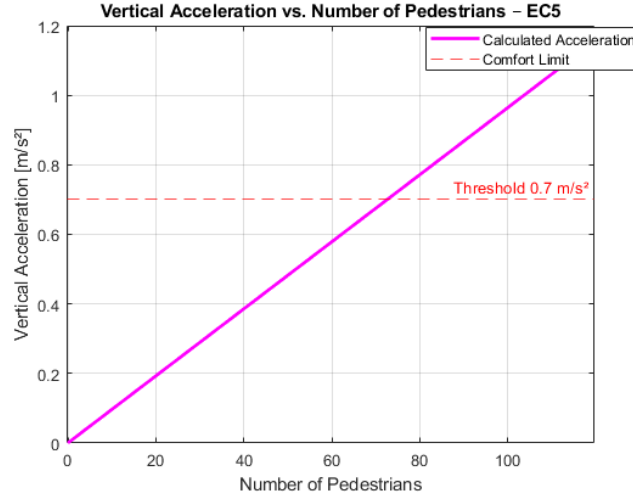


Figure 138: Vertical Acceleration VS Number of Pedestrians – EC5 Part 2 - Annex B

9.5 TIME-DOMAIN DYNAMIC ANALYSIS

When analyzing the structure from a dynamic perspective under pedestrian loading, the definition of the acting force becomes a crucial aspect. The spatial and temporal characteristics of the load can significantly influence the dynamic response of the structure, potentially leading to amplifying resonance effects. In this context, a proper analysis and accurate modeling of the applied load are essential, especially when implementing specific mitigation strategies such as Tuned Mass Dampers (TMDs).

9.5.1 DEFINITION OF PEDESTRIAN-INDUCED LOAD

The function $F_p(t)$ represents the time-dependent vertical force exerted by a pedestrian while walking. It is, by nature, a periodic force whose frequency is directly related to the step cadence. Its waveform can be idealized using a harmonic series, expressed as follows:

$$F_p(t) = G * \left[1 + \sum_{n=1}^N a_n \cos(2\pi * f_s * t + \phi_n) \right]$$

Where:

- G is the static weight of the pedestrian.
- f_s is the step frequency, typically ranging between 1.8Hz and 2Hz.
- a_n is the dynamic coefficient of the n -th harmonic.
- ϕ_n is the phase angle of the n -th harmonic, which can be either assumed as zero or randomized for advanced simulations.
- N is the number of harmonics considered.

SETRA provides recommended values for the harmonics and their corresponding dynamic coefficients, resulting in a final function that reproduces the cyclic behavior of the dynamic load

induced by human walking. This function can subsequently be scaled according to the number of pedestrians, whether synchronized or not.

9.5.2 CLASSIFICATION OF LOAD MODELS

Based on the SETRA guidelines⁶⁸, it is indeed possible to identify three main categories of load that can be used for an accurate simulation of pedestrian-induced actions.

Moving Dynamic Load

It is a model that allows for a realistic representation of the action of a walking pedestrian, considering both the time variation of the force (strictly related to the walking cadence) and the longitudinal displacement along the footbridge. The model follows the mathematical formulation below:

$$F(x, t) = F_p(t) * \delta(x - v_p * t)$$

Where:

- $F_p(t)$ corresponds to the previously described vertical dynamic force.
- v_p is the walking speed of the pedestrian, typically ranging between 1.4 m/s and 1.8 m/s.
- δ is the Dirac delta function, which instantaneously localizes the load at a specific position $x = v_p * t$.

Stationary Dynamic Load

It represents a simplified variant, in which the time-varying force is assumed to be applied at a fixed point of the structure, generally at midspan (as it is typically the most stressed node):

$$F(x, t) = F_p(t) * \delta(x - x_0) \text{ con } x_0 = \frac{L}{2}$$

Moving Static Load

In this case, the dynamic component of the walking action is neglected, and the force is assumed to be constant over time, moving along the footbridge at a constant speed.

$$F(x, t) = P_p * \delta(x - v_p * t)$$

Where P_p corresponds to the static weight of the pedestrian, assumed to be 700 N.

⁶⁸ (SETRA, 2006)

9.5.3 PEDESTRIAN CONFIGURATIONS

For an accurate representation of the structural actions, based on the models described, three different pedestrian configurations are defined. These are summarized in the following *Table 41*:

PEDESTRIAN LOAD CONFIGURATIONS		
CONFIGURATION	DESCRIPTION	FORMULATION
SINGLE PEDESTRIAN	BASIC MODEL	$F(x, t) = F_p(t) * \delta(x - v_p * t)$
GROUP ⁶⁹	MULTIPLE SYNCRONIZED PEDESTRIANS	$\sum_{i=1}^9 F_p(t) * \delta(x - v_p * t - d_i)$
CROWD	LOAD DISTRIBUTED ALONG THE ENTIRE WALKWAY	$\sum_{i=1}^N F_{p,i}(t) * \delta(x - x_i(t))$

Table 41: Pedestrian Load Configurations

A subsequent step for a more comprehensive project analysis would involve the implementation of these models in the time domain, directly applied to the structure. However, such an analysis extends beyond the scope and parameters of the current study and may therefore be considered as a foundation for future research developments.

The study of dynamic comfort is a broad and complex topic, which could constitute an independent subject of in-depth analysis. Furthermore, the implementation of such models in conjunction with a simplified structural representation, especially in terms of dimensional assumptions, may lead to significant simplifications in the resulting outputs, potentially introducing errors in their interpretation.

Therefore, within the contextual framework of this document, the study of this topic is limited to a theoretical level, laying the groundwork for future implementations and computational developments.

9.5.4 THEORETICAL CONSIDERATIONS ON THE USE OF A TUNED MASS DAMPER (TMD)

One of the possible solutions to improve structural performance under dynamic actions is the use of passive damping devices, among which the Tuned Mass Damper (TMD) is particularly effective. The TMD consists of a mass-spring-damper system which, when properly positioned and dimensioned, can reduce structural vibrations by selectively targeting specific natural modes.

The TMD is composed of a secondary mass that is elastically connected to the main structure through a spring element and a viscous damper. When the structure is excited at a frequency close to the TMD's natural frequency, the device resonates in anti-phase with respect to the structure, absorbing part of the vibrational energy.

The combined system of the TMD and the main structure can be modeled as a coupled two-degree-of-freedom system, which is governed by the following differential equations:

⁶⁹ Reference is made to a group of 9 individuals (with i ranging from 1 to 9).

$$\begin{cases} m * u'' + c * u' + k * u + c_d(u' - u'_d) + k_d(u - u_d) = F(t) \\ m_d * u''_d + c_d(u'_d - u') + k_d(u_d - u) = 0 \end{cases}$$

Where:

- $u(t)$ is the displacement of the main structure.
- $u_d(t)$ is the displacement of the TMD.
- m, c, k are the mass, damping, and stiffness of the main structure, respectively.
- m_d, c_d, k_d are the corresponding parameters of the TMD.
- $F(t)$ is the dynamic forcing function acting on the structure ($F_p(t)$).

The behavior of a Tuned Mass Damper (TMD) is primarily governed by a set of parameters, which can be summarized into three main categories. First, the mass ratio, which typically ranges between 1% and 5% of the modal mass associated with the target mode to be damped. Higher values increase the effectiveness of the device but also result in greater size and cost. Second, the natural frequency, which must be tuned to match the natural frequency of the mode to be mitigated. It is crucial to note that a frequency mismatch can not only reduce effectiveness but may even lead to amplification phenomena. Lastly, the damping ratio, usually in the range 0.05 to 0.15, represents a compromise between response speed and maximum displacement amplitude.

From a theoretical standpoint, the adoption of a TMD can produce significantly different effects, mainly depending on the excited mode-shape, its frequency, the nature of the forcing function, and the tuning accuracy.

If the TMD is perfectly tuned to the dominant mode being excited, a considerable reduction in vibration amplitude can be observed, both in terms of peak acceleration and RMS values.

Conversely, if the TMD is tuned to a frequency different from that effectively excited, its effectiveness is evidently diminished and, in extreme cases, it may lead to amplification effects, behaving similarly to a resonant system, which is entirely undesirable.

In the presence of multiple significant modes, the effectiveness of a single TMD depends on the spectral proximity between its natural frequency and the modal frequencies of the structure. In this regard, the TMD is particularly effective only for a limited number of modes, namely those closest to its tuning frequency.

It can thus be concluded that the implementation of a TMD system on a pedestrian footbridge such as the one under analysis must be preceded by an accurate modal assessment. The primary objective should be the identification of the most critical modes in terms of perceived acceleration, the estimation of the corresponding modal mass for proper TMD sizing, and the evaluation of the structural and architectural compatibility of the device integration. In the case of relatively lightweight structures, such as those made of timber, it is important to consider their high sensitivity to dynamic loads, which makes the adoption of a TMD not only technically effective but also a potentially economical solution, provided that proper design is ensured.

10 TECHNICAL AND ECONOMIC FEASIBILITY – STRUCTURAL SOLUTION COMPARISON

The design analysis continues with a technical-economic feasibility study of the structure. The design, having been completed regarding the details relevant to this study, allows for a preliminary sizing of the volumes employed in the construction of the structure. These volumes can be categorized according to the structural element and the construction material used (GL24h, GL26h, and steel).

To determine a metric-quantitative cost estimate of the structure, and to establish a reliable basis for the overall construction cost, the values listed in official construction price lists are used. Specifically, reference is made to the construction material prices provided in the official price lists of Emilia-Romagna (PR EM 2025) and Campania (2025)⁷⁰.

A summary of the prices used for the economic evaluation of the structure is provided in the following *Table 42*. It is important to note that some values are expressed in euros per cubic meter (€/m³), while others are expressed in euros per 100 kilograms (€/100 kg); this depends on the type of material under analysis and the standard method of classification - steel (whether reinforcement or structural) is typically priced per 100 kg.

Furthermore, structural GL timber is formally classified based on the length of the structural elements to be manufactured and the curvature required. For this reason, two categories are created: One for the structural arches, referred to as “boomerang beams,” with lengths of up to 45 m (the longest arch-beam in the analyzed project has an axial length of 43 m); the other for beam-type structural elements (horizontal members), with lengths of up to 25 m, which includes all beam elements of the structure.

TABLE OF SUPPOSED PRICES [€/x]	
GL CURVED BEAM - BOOMERANG 45m [€/m ³]	1883.78
GL BEAMS - UP TO 25m [€/m ³]	1535.43
S275 [€/100kg]	483

Table 42: Table of Supposed Prices - €/m³ - (Prezzario Regione Campania - Prezzario Lavori, 2025)

Based on these values, and on the overall volumetric calculation of the structural elements (derived from the FEM model developed in MasterSap 4U), the following summary table is produced (*Table 43*). The structural elements are listed along with their corresponding geometric reference values (cross-sections and lengths), their respective volumetric footprints, and their associated costs - taken from *Table 42*. The exact total costs are calculated and then summed up and rounded up, to provide a high-level estimate of the overall construction cost.

⁷⁰ (Prezzario Regione Campania - Prezzario Lavori, 2025) - An adaptation of the Italian construction cost index is carried out in accordance with the topic under analysis, aligning it with standard or approximate material values commonly adopted at the European level, and following a series of considerations regarding the values themselves. Specific adjustments are also made based on the boundary conditions considered in the analysis.

VOLUMETRIC & PRICE EVALUATION OF THE STRUCTURAL ELEMENTS – TIMBER FOOT BRIDGE							
GROUP NUMBER	ELEMENT	MATERIAL	SECTION [mxm]	TOTAL LENGTH [m]	VOLUME [m³]	PRICE [€/x]	TOTAL PRICE [€]
1	SECONDARY BEAMS	WOOD - GL24h	0.2x0.4	128	10.24	1535.43	15723
2	PRIMARY BEAMS	WOOD - GL26h	0.2x1.0	219.1	43.82	1535.43	67283
3	ARCH BEAMS	WOOD - GL26h	0.3x1.5 (comp.-CS)	300.2	270.18	1883.78	508960
4	VERTICAL HANGERS	7 Wire Strand S275	φ=15mm x2	208.2	0.17	483	6446
5	TRANSVERSAL BEAMS	WOOD - GL26h	0.4x0.7	6.4	1.792	1535.43	2751
6	CENTRAL PRIMARY BEAMS	WOOD - GL26h	0.25x0.9	106.6	23.98	1535.43	36820
7	LATERAL PRIMARY BEAMS	WOOD - GL26h	0.2x0.1.0	42.62	8.525	1535.43	13090
8	ARCH CONNECTION BEAMS	WOOD - GL26h	0.4x0.8	99.2	31.74	1535.43	48735
9	DECK BRACINGS DIAGONALS	STEEL S275	φ=0.076x0.004	347.4	0.2849	483	10802
10	ARCH BRACINGS DIAGONALS	STEEL S275	φ=0.076x0.004	291.9	0.2394	483	9077
11	DECK CENTRL BRACINGS	STEEL S275	φ=0.076x0.004	16	0.01312	483	497
FINAL PRICE EVALUATION OF THE STRUCTURAL MATERIALS - EXACT							720182
FINAL PRICE EVALUATION OF THE STRUCTURAL MATERIALS - ROUNDUP							730000

Table 43: Volumetric & Price Evaluation of the Structural Elements - Timber Foot Bridge

10.1 COST ESTIMATION – CONCRETE AND STEEL ALTERNATIVES

With the aim of providing a comparative analysis between structural solutions also from an economic perspective - specifically regarding the cost of the structure itself - the same procedure for estimating volumetric footprints and costs was applied to the alternative structural solutions in concrete and steel.

These alternatives, described in the initial chapters of the study, are analyzed volumetrically based on preliminary dimensional assumptions derived from the pre-design CAD drawings. Therefore, these do not represent final and definitive volumetric quantities, as they have not been verified through appropriate limit state calculations.

Table 44 reports the assumed prices for the structural materials of the alternative solutions:

TABLE OF SUPPOSED PRICE [€/m³]	
CONCRETE - XC4, S4, C35/45 [€/m³]	206.33
FORMORK [€/m³]	35.61
COST ESTIMATE INCLUDING LABOR - CONCRETE [€/m³]	500
B450C [€/100kg]	253
STEELWORK S275 + GALVANIZATION [€/100kg]	637

Table 44: Supposed Prices for Alternative Structural Solutions - €/m³ - (Prezzario Regione Campania - Prezzario Lavori, 2025)

Regarding the prices reported in the *Table 44*, the following clarifications must be made:

- Concrete, assumed to be of class XC4 with slump class S4 and strength grade C35/45, is broken down into cost per cubic meter of material, formwork cost, and final cost including labor. This breakdown is necessary because concrete requires on-site processing and construction work, unlike steel or timber, for which the prices already include production costs.
- For reinforcing steel, B450C is selected, with ribbed threaded bars to ensure enhanced bond performance. Since no detailed reinforcement calculation has been carried out, an approximate estimate is made by assuming the presence of 100 kg of reinforcement steel per cubic meter of concrete.
- Steel elements not intended for reinforcement, identified as structural steelwork elements, are accounted for along with a chemical galvanization process for surface protection. This process modifies the final cost, with galvanization priced at approximately €154 per 100 kg.

At this stage, for the three alternative structural solutions - cable-stayed bridge, arch and frame bridge, and frame bridge - the following summary tables are provided (*Table 45*, *Table 46* & *Table 47*), following the same criteria used in the table developed for the timber solution.

PRE-DESIGN PROPOSAL CABLE STAYED BRIDGE - CONCRETE AND STEEL							
GROUP NUMBER	ELEMENT	MATERIAL	SECTION [m ²]	TOTAL LENGTH [m]	VOLUME [m ³]	PRICE [€/x]	TOTAL PRICE [€]
1	DECK	CONCRETE C35/45	1.488	144.05	214.3	500	107173
2	FRAME (x4)	CONCRETE C35/45	0.1225	30.912	3.8	500	1893
3	PYLON (x2)	CONCRETE C35/45	0.1225	62.36	7.6	500	3820
4	REINFORCEMENTS	STEEL S275	100 kg/m ³ of concrete =22600kg			253	57120
5	CABLES (x10)	STEEL S275	0.01767	340.45	6.01	253	119476
FINAL PRICE EVALUATION OF THE STRUCTURAL MATERIALS							289482
FINAL PRICE EVALUATION OF THE STRUCTURAL MATERIALS - ROUNDUP							290000

Table 45: Volumetric & Price Evaluation of the Structural Elements – Cable Stayed Bridge - (Prezzario Regione Campania - Prezzario Lavori, 2025)

PRE-DESIGN PROPOSAL SINGLE ARCH AND FRAME BRIDGE - CONCRETE AND STEEL							
GROUP NUMBER	ELEMENT	MATERIAL	SECTION [m ²]	TOTAL LENGTH [m]	VOLUME [m ³]	PRICE [€/x]	TOTAL PRICE [€]
1	ARCH	STEEL S275	0.108	166.78	18.0	637	900693
2	DECK	CONCRETE C35/45	1.488	144.05	214.35	500	107173
3	FRAME	STEEL S275	0.108	32	3.46	637	172816
4	REINFORCEMENTS	STEEL S275	100 kg/m ³ of concrete =22000kg			253	54230
5	CABLES	STEEL S275	0.01767	69.8	1.23	253	24495
FINAL PRICE EVALUATION OF THE STRUCTURAL MATERIALS							1259407
FINAL PRICE EVALUATION OF THE STRUCTURAL MATERIALS - ROUNDUP							1260000

Table 46: Volumetric & Price Evaluation of the Structural Elements – Single Arch & Frame Bridge - (Prezzario Regione Campania - Prezzario Lavori, 2025)

PRE-DESIGN PROPOSAL FRAME BRIDGE - CONCRETE AND STEEL							
GROUP NUMBER	ELEMENT	MATERIAL	SECTION [m²]	TOTAL LENGTH [m]	VOLUME [m³]	PRICE [€/x]	TOTAL PRICE [€]
1	DECK	CONCRETE C35/45	1.488	144.05	214.34	500	107173
2	FRAME	STEEL S275	0.108	101.4	10.95	637	547609
3	REINFORCEMEN TS	STEEL S275	100 kg/m³ of concrete =22000kg			253	54230
FINAL PRICE EVALUATION OF THE STRUCTURAL MATERIALS							709012
FINAL PRICE EVALUATION OF THE STRUCTURAL MATERIALS - ROUNDUP							710000

Table 47: Volumetric & Price Evaluation of the Structural Elements – Frame Bridge - (Prezzario Regione Campania - Prezzario Lavori, 2025)

10.2 COMPARATIVE COST EVALUATION AND RESULTS

The final comparison between the structural solutions described is carried out through the creation of a horizontal bar chart, which visually illustrates the difference in values (*Figure 139*). The results are first compared on a basis of thousands of euros (k€), and then on a normalized basis, relative to the surface area of the deck - assumed to be the same for all structural solutions (434 m²).

COMPARISON OF THE RESULTS IN PRICE EVALUATION		
STRUCTURAL SOLUTION	PRICE [k€]	PRICE/AREA [k€/m ²]
TIMBER FOOT BRIDGE	730	1.7
CABLE STAYED	290	0.7
ARCH AND FRAME	1260	2.9
FRAME	710	1.6

Table 48: Comparison of Structural Results in Price Evaluation - [k€] & [k€/m²]

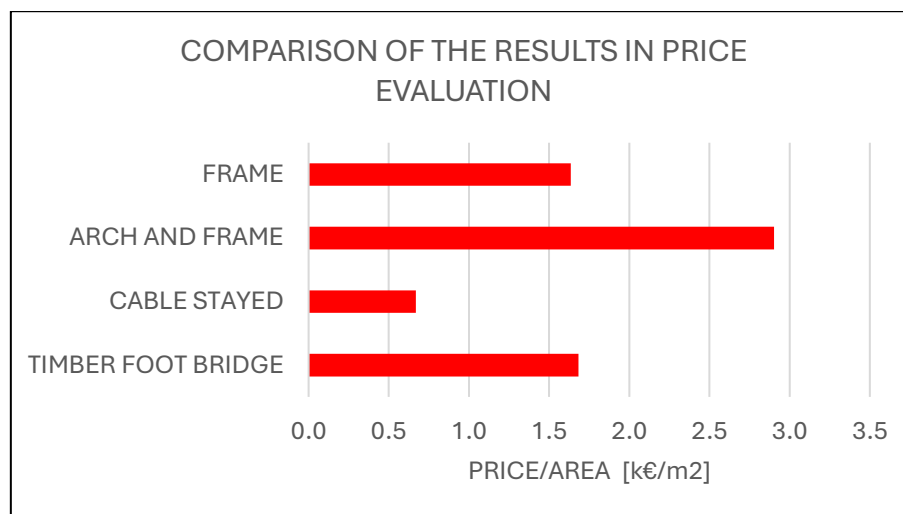


Figure 139: Comparison Bar Chart – Cost in k€ per Unit Area in m² – Different Structural Solutions

From the results reported in the *Table 48* and subsequently represented in the *Figure 139*, it is clear that the arch and frame bridge structural solution are the most economically demanding, with a unit cost of approximately 2.9 k€/m². This is followed by the frame bridge and the timber solution, both with costs stabilizing around 1.6–1.7 k€/m². The most cost-effective structural solution is the cable-stayed bridge, with a unit cost of approximately 0.7 k€/m².

However, these results do not fully reflect the actual cost differences between structural solutions made of different materials. While it is true that the cable-stayed solution shows a substantially lower cost compared to the other alternatives, it must also be considered that it involves the largest volumetric quantity of concrete - a construction material that, in terms of unit material cost, is among the least expensive. Nevertheless, this does not necessarily imply that the final overall cost will be the lowest. In fact, when considering the construction phase and the time required for concrete casting and curing, the final cost can vary significantly - not only in terms of total structural expenditure, but also with respect to the overall duration of the construction site. Furthermore, the potential use of pre-stressed concrete introduces considerable uncertainty regarding the actual final cost of the structure.

It is nevertheless important to note that the structures with a higher quantity of structural steelwork are those with a significantly higher cost - even on a per-square-meter basis. This observation clearly reflects the high mechanical and strength properties of the steel used, which are required for supporting a complex and heavy structure such as a bridge.

In conclusion, the timber structure falls within a final cost range that can be considered standard when compared to more commonly used construction materials for bridges of this type and span length. It therefore represents a feasible solution from an investment standpoint, considering its economic compatibility relative to other structural materials. It is important to note, however, that GL timber beams of these dimensions are difficult to source and, above all, very challenging to transport - an aspect that should be considered in a more detailed economic assessment.

11 DURABILITY AND ENVIRONMENTAL SUSTAINABILITY – CO₂ EMISSION ANALYSIS

To make the structural comparison and analysis even more comprehensive and competitive, the next step is the evaluation of the various structural solutions, in timber and in the alternative materials of concrete and steel, from the perspective of environmental sustainability. This involves a procedure aimed at assessing the environmental footprints of the structures under consideration, examining not only the impact of construction but also the emissions generated during the life cycle and end-of-life phases, with particular attention to transportation methods.

These considerations are framed within the contemporary context of the climate emergency and global environmental challenges, in which the construction sector plays a crucial role in achieving carbon neutrality goals. According to data provided by the International Energy Agency (IEA), the building and construction sector is responsible for approximately 40% of global CO₂ emissions⁷¹.

For the development of a quantitative comparison of the environmental impact of the different structural solutions, a MATLAB code has been developed. The main output consists of an estimate of the equivalent CO₂ emissions (CO₂e⁷²) associated with each structural solution over its entire life cycle. Appropriate comparisons of the results are made, supported by graphical representations that make the comparison not only theoretical but also visually practical.

The analysis itself is conducted based on the principles defined by the standard EN 15804:2012 + A2:2019⁷³ and the ISO standards 14040 and 14044⁷⁴, which govern Life Cycle Assessment (LCA). Based on these standards, the calculation includes all phases from raw material production (A1) to end-of-life (C4), also accounting for transportation (A4) and maintenance (B2–B5).

11.1 CODE FRAMEWORK AND INPUT PARAMETERS

The developed code was structured in a modular fashion, enabling a comprehensive and intuitive understanding of the emissions directly associated with each structural variant. As a first step, the geometric and material parameters of the structural elements were defined. For each individual hypothesis, the estimated material volumes were input based on preliminary design assumptions.

It is worth noting that for the timber-based solution, differentiated volumes were considered for the two construction materials - Timber GL24h and GL26h - along with the volumetric percentage of steel required for vertical hangers and for the diagonal elements used to connect and stabilize the structure. For alternative configurations, variable volumes of reinforced concrete and structural steel were adopted accordingly.

⁷¹ (Global Status Report for Buildings and Construction, 2022)

⁷² CO₂e stands for "Carbon Dioxide Equivalent" and is a standard unit for measuring carbon footprints. It expresses the impact of different greenhouse gases in terms of the amount of CO₂ that would create the same amount of warming. This allows for a unified assessment of emissions regardless of the specific gas.

⁷³ (CEN - European Committee for Standardization, 2019)

⁷⁴ (International Organization for Standardization, 2006)

11.1.1 EMISSION FACTOR DEFINITION – STRUCTURAL MATERIALS

To calculate the CO₂-equivalent footprint of the individual materials, emission factors - expressed in kg CO₂e/kg - are employed. These factors represent the amount of greenhouse gases (converted into CO₂-equivalent) released into the atmosphere for each unit mass of material used. As such, they constitute a fundamental parameter for estimating the emissions associated with the quantitative use of construction materials during the production phase.

The emission factors adopted in the present analysis were sourced from the Inventory of Carbon and Energy (ICE) database⁷⁵, originally developed by the University of Bath and currently maintained by Circular Ecology. The ICE database provides detailed data on embodied energy and carbon emissions for more than 200 construction materials, classified into over 30 primary categories including bricks, cement, concrete, glass, timber, plastics, metals, and natural stones.

The data contained in the ICE database are derived through a rigorous review of scientific and technical literature, ensuring a high degree of reliability and transparency. The database follows a "cradle-to-gate" approach, accounting for emissions from raw material extraction up to the point at which the product exits the manufacturing facility.

The emission factor values for the construction materials analyzed in this study were obtained from the database and are summarized in the following *Table 49*:

EMISSION FACTORS [kg CO ₂ e/kg]	
MATERIAL	EMISSION
GLT - Glue Laminated Timber	0.28
CONCRETE	0.15
STEEL	1.85

Table 49: Emissions Factors [kgCO₂e/kg] - (Embodied Carbon - The ICE Database - Version 4.0, 2024)

It is important to highlight that the CO₂-equivalent emission values per kilogram of material are slightly higher for timber than for concrete. However, this figure must be interpreted from a dual perspective. Firstly, for the same volume of timber and concrete, the corresponding mass of timber is significantly lower due to its density, which is approximately five times lower than that of concrete.

On the other hand, the emission factors considered in this analysis refer exclusively to the CO₂e emitted during production and do not account for CO₂e potentially absorbed by the material. In the case of timber, this would lead to a net negative emission balance, as the amount of CO₂e absorbed by the material is estimated to be nearly seven times greater than the amount emitted.

Nonetheless, such absorption data cannot be incorporated into a comparative assessment of structural materials, as it would severely distort the overall results. The disparity in carbon sequestration capacity among different materials is so substantial that it constitutes an outlier from an analytical standpoint.

⁷⁵ (Embodied Carbon - The ICE Database - Version 4.0, 2024)

Therefore, to ensure the coherence and objectivity of the comparison, the analysis relies solely on emission values associated with the production phase, deliberately excluding potential carbon absorption contributions.

11.1.2 EMISSION FACTOR DEFINITION – TRANSPORT MODES

The comparative analysis also considers the different transport options for delivering materials to the construction site. The choice of transportation method significantly influences the overall emission results, as this factor constitutes a crucial component within the broader life cycle assessment.

Accordingly, a hypothetical transport distance of 1000 km⁷⁶ is assumed, and two distinct transport scenarios are introduced:

- Scenario 1: Land transportation – This scenario assumes the use of road transport for material delivery. The associated emission factor is set at 0.12 kg CO₂e per 1000 kg of material per kilometer (i.e., 0.00012 kg CO₂e/kg·km).
- Scenario 2: Maritime transportation – This scenario assumes the use of sea freight for material delivery. The corresponding emission factor is assumed to be 0.015 kg CO₂e per 1000 kg of material per kilometer (i.e., 0.000015 kg CO₂e/kg·km).

The difference between the two scenarios is illustrated in the following *Figure 140*, which displays two highly divergent lines.

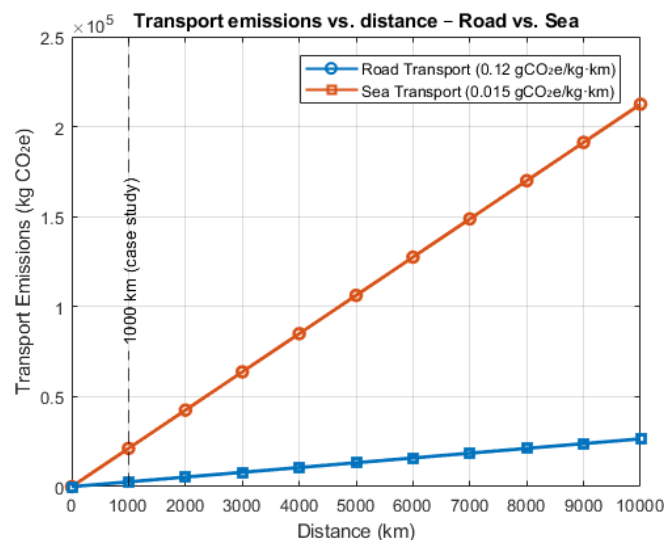


Figure 140: Transportation Emissions VS Distance - Road VS Sea

The emissions associated with each transportation method are plotted as a function of both the mass of the materials to be transported and the travel distance, ranging from 0 to 10,000 km. As the distance

⁷⁶The transport distance is hypothetically set at 1000 km to better highlight the differences in emissions between the selected transportation methods. While actual distances may vary and are often shorter, this assumption is made to clearly illustrate the impact of transport on the overall carbon footprint.

increases, the gap between the emission values becomes progressively wider, eventually reaching levels that are nearly incomparable. A vertical reference line is included in the graph to indicate the distance selected for this study.

Subsequent references to this difference are made throughout the analysis, particularly in the context of calculating the relative percentage contributions of each component to the total emissions associated with the individual structural solutions.

11.1.3 LIFE CYCLE ASSESSMENT PARAMETERS

The analysis also included the introduction of data related to the life cycle parameters of the structures under examination. A uniform service life of 50 years was assumed for all structural solutions, with a consistent maintenance frequency of once every 10 years.

However, the parameter that effectively differentiates the various solutions is the maintenance percentage, which represents the proportion of the structure required to be replaced during each maintenance cycle. Based on the characteristics of the construction materials, this percentage was set at 10% for the timber structure and 2% for the concrete and steel structures. This parameter reflects the greater vulnerability of timber in terms of resistance to external environmental conditions, while still considering the properties of the highly treated material.

Parameters related to the end-of-life phase of the structures are also included, assuming that all structural solutions reach the end of their 50-year service life with 100% of their structural components intact.

Within this framework, CO_{2e} emission values are defined for dismantling and landfill activities: Structural dismantling, considering the potential reuse of some elements from the original structure and construction materials, is assigned a CO_{2e} emission value of 0.02 kgCO_{2e}. For landfill disposal, a value of 0.05 kgCO_{2e} is considered, accounting for the treatment and disposal of materials deemed non-reusable.

11.2 EMISSION CALCULATIONS – RESULTS INTERPRETATION

For all structural solutions, the emissions were calculated for each individual phase: Each phase described was related to the material mass and the corresponding emission factor, applied as a multiplicative coefficient, resulting in a final emission value.

Emissions are therefore calculated for the production phase, for transportation (with appropriate differentiation between maritime and land transport), for maintenance activities, and for end-of-life treatment (including both disposal and recycling). The individual emission values for each phase are then summed up to obtain the total emissions for each of the structural solutions.

The overall results are illustrated in the following bar chart (*Figure 141*), where the values are expressed in kg CO_{2e} × 10⁵. In the same graph, the delta values - representing the differences from

the highest-emission solution - are also included and rounded up to the nearest thousand, to highlight the relative emission savings of each structural option.

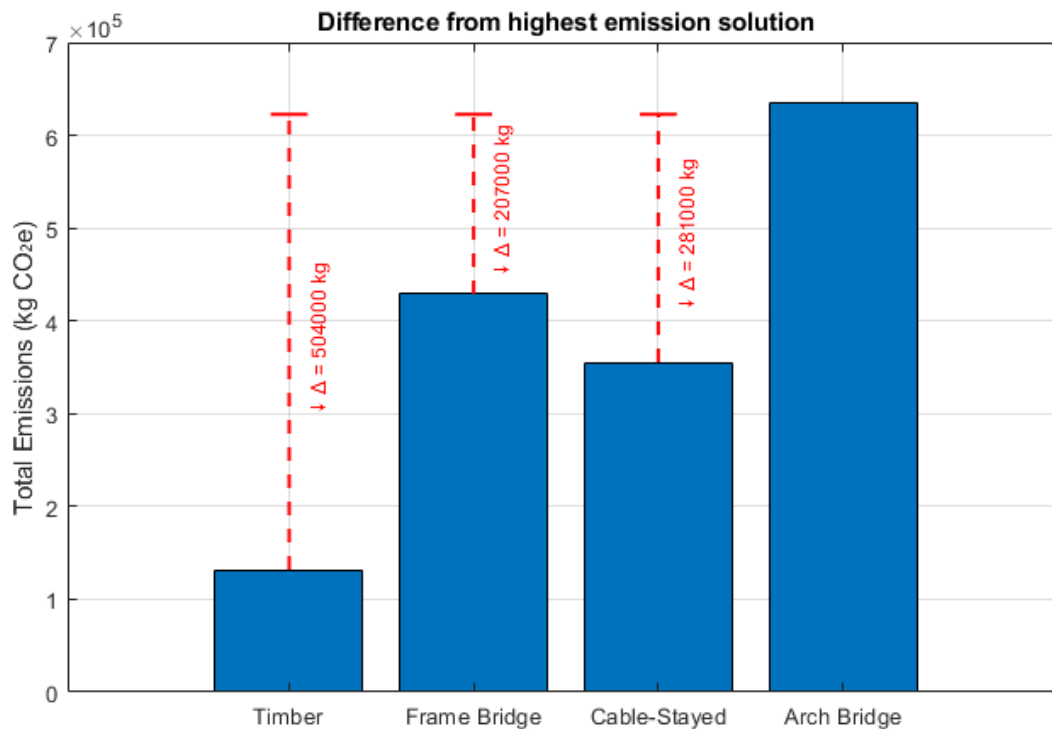


Figure 141: Total Emissions kgCO₂e x10⁵ - Comparison between Structural Solution & Difference from Highest Emission Solution

It is readily observable from the plot that the timber structure exhibits emission values nearly five times lower than those of the structural solution with the highest emissions (the arch structure). For ease of interpretation, the values of the individual contributions are also reported in the accompanying Table 50, where they are rounded up to the nearest whole number to enhance clarity.

TOTAL EMISSIONS [kg CO ₂ e x10 ⁵]		
STRUCTURAL SOLUTION	TOT. EMISSIONS	TOT. EMISSIONS - ROUNDUP
TIMBER	131776.3	132000
FRAME BRIDGE	429026.4	430000
CABLE STAYED BRIDGE	354970.6	355000
ARCH&FRAME BRIDGE	635361.7	636000

Table 50: Total Emissions kgCO₂e x10⁵ – Round Up

These results reflect all previously discussed considerations regarding the structural properties: They are consistent with the significantly lower mass of the timber bridge compared to those made with other construction materials and align with the material distribution percentages adopted in each structural solution.

The arch bridge, at least in the preliminary design phase, shows a substantially higher volumetric quantity of steel compared to the other solutions, resulting in a considerable increase in total emissions.

11.2.1 EMISSIONS DISTRIBUTION BY PHASE

Of particular interest in structural comparison is the analysis of total emissions broken down by each life cycle phase: Production, transport, maintenance, and end-of-life.

Accordingly, four pie charts are presented (*Figure 142, Figure 143, Figure 144 & Figure 145*), each corresponding to one of the four structural solutions. For each chart, the percentage contribution of each phase to the total emissions is reported.

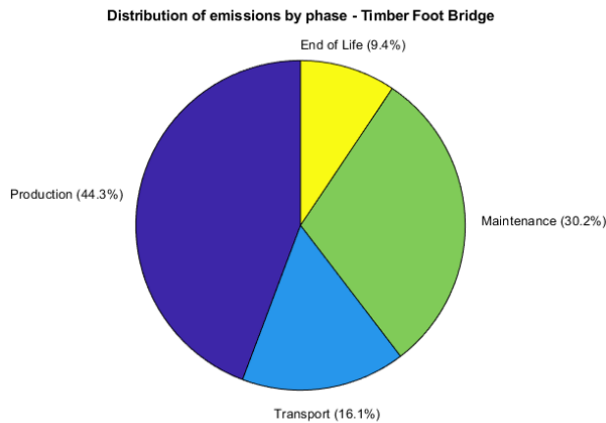


Figure 142: Distribution of Emissions by Phase - Timber Foot Bridge

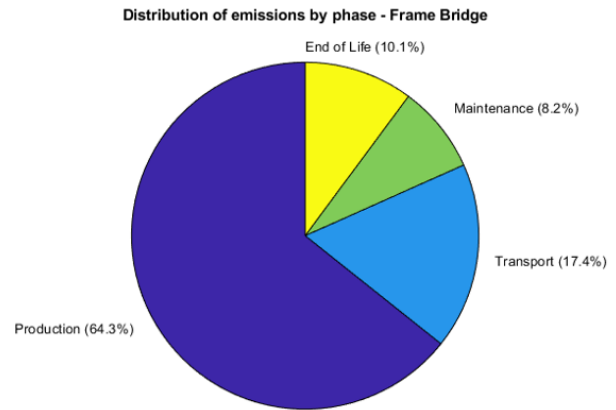


Figure 143: Distribution of Emissions by Phase – Frame Bridge

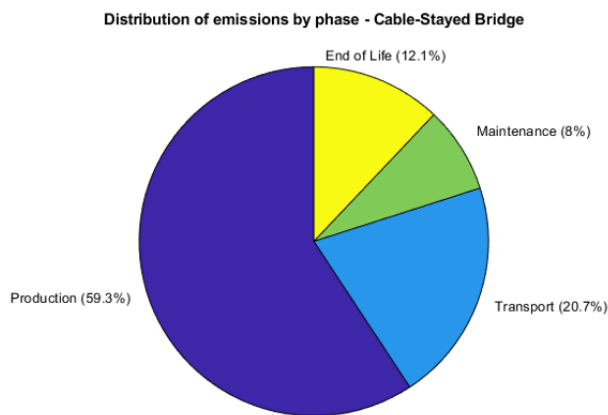


Figure 144: Distribution of Emissions by Phase – Cable-Stayed Bridge

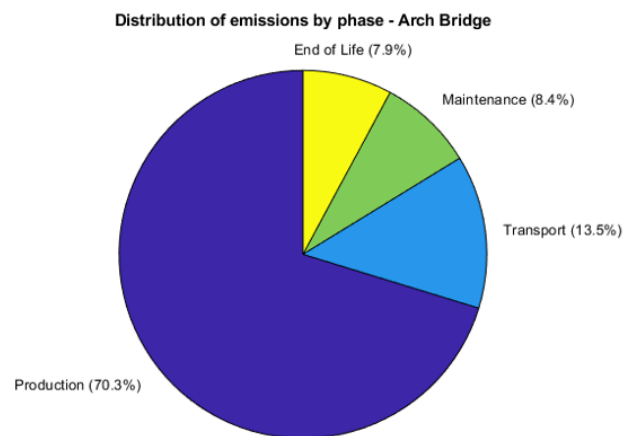


Figure 145: Distribution of Emissions by Phase – Arch Bridge

From these diagrams, it is important to observe how the percentage distribution of phase-specific emissions changes significantly when moving from a timber-based structural solution to a non-timber one. In fact, for each individual phase, we observe the following:

- **Production:** While for the concrete and steel solutions the production phase accounts for approximately 60–70% of the total emissions, the timber solution shows a significantly lower percentage, with production contributing less than 45% of the overall emissions.

- **Transport:** The transport percentage, in the context of a general comparison, is of limited significance as it depends solely on the mass to be transported rather than on the structural typology. Nevertheless, it generally ranges between 15% and 20% across all solutions.
- **Maintenance:** For the concrete and steel structural solutions, the percentage of emissions related to maintenance is approximately 8-9%, whereas in the timber solution the final value reaches around 30%. This outcome reflects the higher maintenance demands of timber as a structural material over its service life, and particularly the input assumption of a 10% maintenance rate for timber compared to 2% for the other materials.
- **End-of-life:** Like transport, this phase does not represent a direct element of comparison based solely on the percentage values. The figures for all structural solutions stabilize around 8-10%. However, it is important to note that neither the differences in material recyclability nor the potential CO_{2e} absorption during the life cycle (as previously discussed) are considered. These factors could, in fact, significantly alter the emission percentages associated with the end-of-life phase.

Based on the observations made, it can be concluded that, in percentage terms, the emission pattern changes substantially with respect to total emissions. Production shifts its role significantly, being the predominant source of emissions for concrete and steel structures, while accounting for less than half of the total in the case of the timber structure. A notable difference also emerges in the percentage contribution of the maintenance phase, as previously discussed and analyzed.

11.2.2 TEMPORAL EMISSION TRENDS

Based on the assigned service life of the structure (50 years), an evaluation is carried out regarding the cumulative progression of emissions over the structural lifespan, i.e., as a function of time.

To compare this temporal trend, a graph is plotted (*Figure 146*), in which a broken-line curve is shown for each of the structural solutions under examination, representing the cumulative emission values over time.

This is followed by an analysis of the trend of each curve, depending on the structural typology, with a detailed explanation of the reasoning behind the shape of each curve.

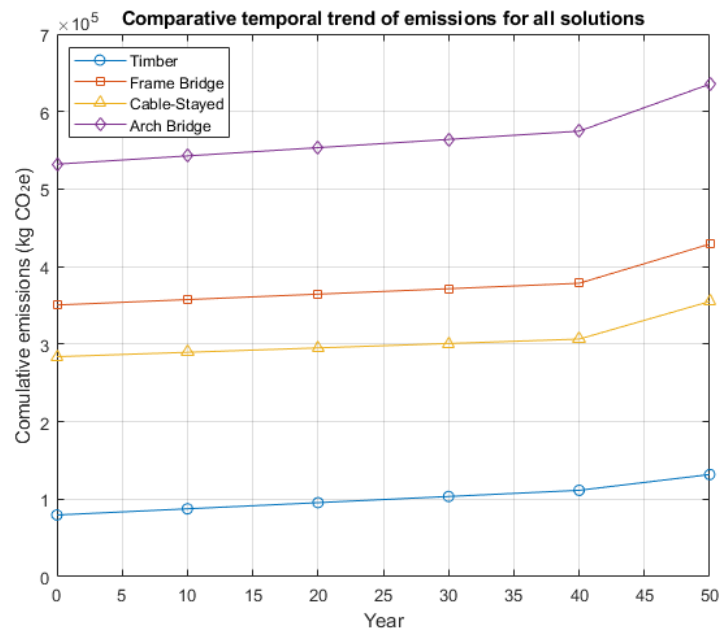


Figure 146: Comparative Trend of Emissions for all Solutions

- **Timber Footbridge Structural Solution** - This solution exhibits significantly lower initial emission values compared to the alternative configurations. It shows a moderate and linear temporal trend, with a relatively low gradient. At the end of the 50-year service life, cumulative emissions reach approximately 1.1×10^5 kg CO_{2e}. These values reflect the high efficiency of timber materials in terms of embodied carbon. Furthermore, although the maintenance cycle involves replacing 10% of the structure every 10 years, the emissions generated by this process are offset by the low emission factor associated with timber. Naturally, the reduced weight also leads to a lower absolute transport-related emission impact.
- **Cable-Stayed Bridge Structural Solution** - This configuration shows intermediate cumulative emissions overall, with a modest increase up to the 40th year, followed by a final acceleration. By year 50, it reaches approximately 3.6×10^5 kg CO_{2e}. Among the alternative solutions, it is the one with the lowest volume of concrete. Its temporal behavior suggests a low initial impact, but with increasing contributions from maintenance and component transport over time.
- **Frame Bridge Structural Solution** - The emission trend is similar to the one of the cable-stayed solution, with nearly parallel overall growth and slightly higher values due to the larger volumes of concrete and steel employed in the structure. At year 50, cumulative emissions reach approximately 4.4×10^5 kg CO_{2e}. The impact of periodic maintenance is significant, due to the higher emission factors of the materials being replaced (compared to timber).
- **Arch Bridge Structural Solution** - This is the solution with the highest cumulative emissions throughout the entire analysis period, exceeding 6.5×10^5 kg CO_{2e} at year 50. The reasons behind this trend lie in the substantial structural mass (with large volumes of concrete and steel compared to the other solutions), the high embodied energy of the materials, and the significant contributions from transport, maintenance, and disposal phases.

In conclusion, it is evident that the timber solution proves to be significantly more sustainable in terms of long-term environmental impact. All differences among the “traditional” alternatives can, in fact, be explained by the mass of the construction materials used and their corresponding emission factors. The arch bridge emerges as the least sustainable structural choice from an environmental perspective, while the cable-stayed bridge offers a better compromise compared to the frame and arch solutions - though still inferior to the overall sustainability of timber.

In this context, *Figure 146* highlights the general principle that adopting low-impact materials, such as timber in this case, yields clear benefits across the entire service life of the structure, not just during the initial phases of its lifecycle.

11.2.3 EMISSIONS PER SQUARE METER

To represent the structural comparison on a unified basis and ensure consistency across the different solutions - while accounting for the varying nature of the materials - a normalized comparison of emissions per unit area is carried out.

The total emissions are divided by a reference area expressed in useful square meters, corresponding to the surface area of the bridge deck. As already done in the previous chapter concerning the cost estimation of the various solutions per square meter, the values obtained here serve as an effective and normalized basis for comparison, grounded on a common reference parameter. Indeed, the useful deck area is assumed to be the same across all structural solutions, thereby providing a valid foundation for a consistent comparative analysis.

The differences are illustrated in the graph shown in the following *Figure 147*, where the deltas in kilograms are highlighted with respect to the highest emission solution (arch bridge).

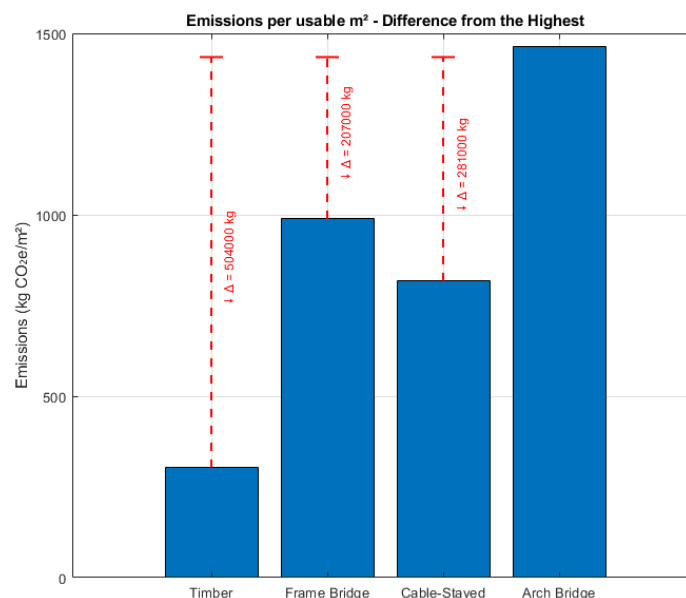


Figure 147: Emissions per Usable m² - Comparison between Structural Solutions - Delta of Difference from the Highest

The results related to the emission values per square meter are summarized in the following *Table 51*:

TOTAL EMISSIONS PER USABLE m ² [kg CO ₂ e/m ²]		
STRUCTURAL SOLUTION	TOT. EMISSIONS	Δ FROM HIGHEST
TIMBER	303.6	1160.3
FRAME BRIDGE	988.5	475.4
CABLE STAYED BRIDGE	817.9	646
ARCH & FRAME BRIDGE	1463.9	0

Table 51: Total Emissions per Usable m² - Delta from the Highest

By highlighting these differences, it becomes possible to understand the potential margin for environmental improvement achievable through specific sustainable design choices. It can indeed be concluded with absolute certainty that the timber solution - with its significantly reduced emissions and a delta difference of nearly 1200 kg CO₂e/m² compared to the worst-performing solution - represents a highly virtuous benchmark, particularly considering general structural considerations.

The representation per square meter has enabled a fair comparison between structures with differing total mass and materials, placing particular emphasis on the environmental efficiency of the functional unit.

11.2.4 EMISSIONS BY TRANSPORT MODE

Returning to the observations regarding the substantial differences in emissions depending on the selected transportation method, a comparison is carried out to analyze the effect of switching the transport mode on the total emissions of all the structural solutions under consideration.

Accordingly, the following graph is plotted (*Figure 148*), in which the total emissions for each structural solution are shown for both land transport and maritime transport scenarios. The graph also highlights the delta differences between the two options.

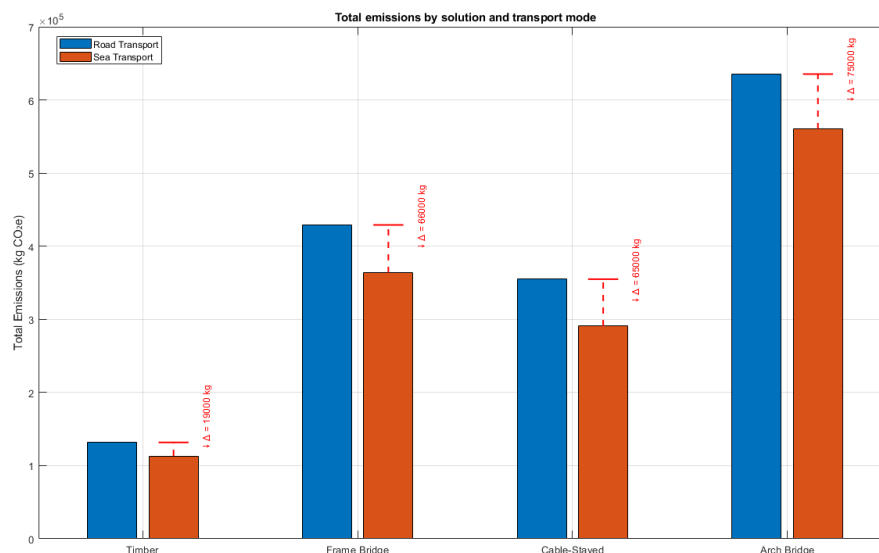


Figure 148: Total Emissions by Solution and Transport Mode

It is evident that the change in transport modality significantly affects the total emission values, leading to a substantial overall reduction in environmental impact. It is particularly noteworthy that the reduction is more pronounced for structures with higher total emissions, such as the arch bridge solution. This outcome is directly linked to the structural mass, which influences transport-related emissions that are dependent on weight rather than volume.

Furthermore, these results are based on a transport distance fixed at 1000 km, as previously explained. Since emissions increase linearly with respect to transport distance, a longer distance would further amplify the difference in total emissions between the two transport scenarios. Conversely, a shorter transport distance would reduce this gap, making the difference almost negligible below 250 km.

To enhance the understanding of the actual differences, it is of particular interest to analyze how the percentage of emissions by phase - relative to total emissions - varies depending on the chosen transport method. These considerations are carried out exclusively for the timber solution, as the effect is considered generally similar across all structural configurations, and it is therefore not necessary to introduce additional sections for the other cases.

Accordingly, pie charts are once again presented (*Figure 149*) to illustrate the distribution of total emissions, now offering a direct comparison between land transport and maritime transport scenarios.

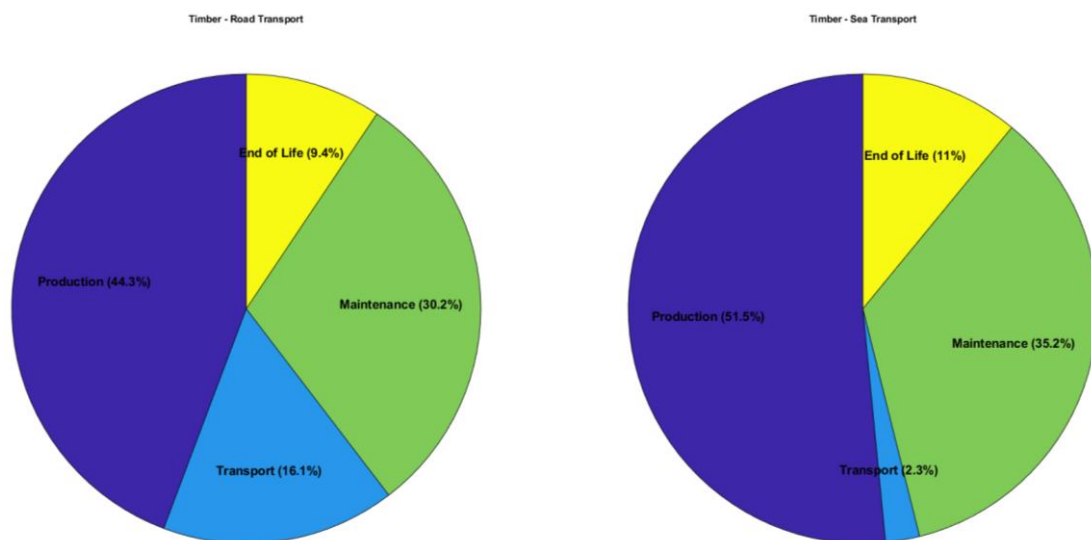


Figure 149: Pie Charts - Timber Solutions - Difference of Emissions by Phase - Road VS Sea Transport

The change is substantial: The percentage related to transport drops from approximately 16% to about 2.3%, while the share of emissions from production increases from around 45% to over 50%. This clearly illustrates how the choice of transport mode can significantly alter the distribution of emissions across different life cycle phases for a given structural solution.

Moreover, this serves as a starting point for a potential study on strategies for implementation and improvement of the overall environmental impact of the structure, offering valuable insights into which phases should be prioritized to make the structure as environmentally efficient as possible.

11.2.5 ENERGY CLASS ESTIMATION

To finalize the comparison and emission estimates for each of the different structural solutions, an evaluation and classification are carried out, ranking the solutions from Class A to Class G based on the CO₂ equivalent emissions per square meter. The classification is represented using color-coded classes shown in the legend in *Figure 150*, and is inspired by the energy rating labels commonly used for buildings and systems.

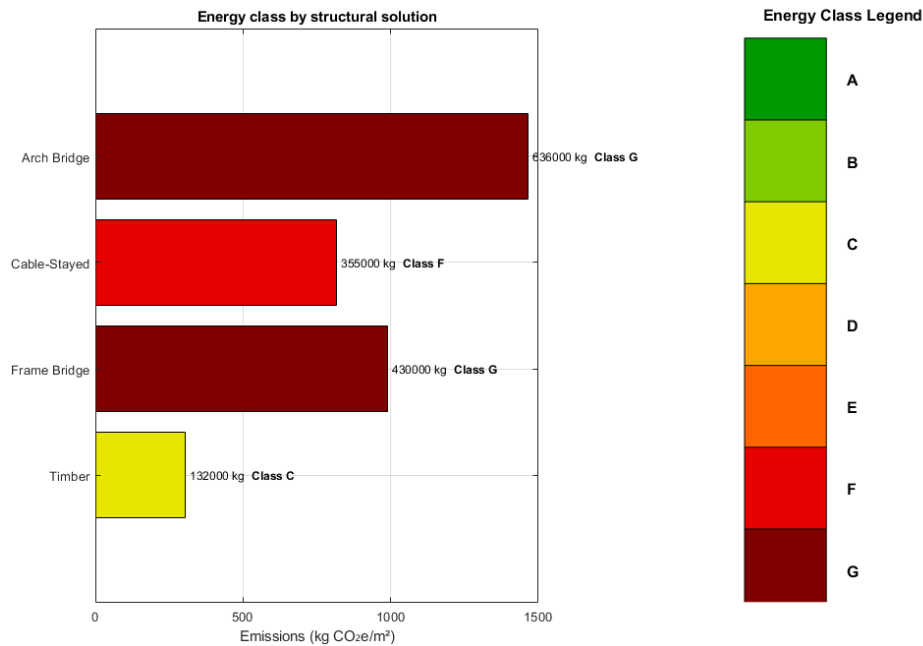


Figure 150: (a) Energy Class by Structural Solution – (b) Legend - Classes from A to G

A reference table is provided showing the benchmark values corresponding to the selected energy classes (*Table 52*):

ENERGY CLASSES - DEFINITION OF THE CLASSES [kgCO ₂ e/m ²]							
CLASS	A	B	C	D	E	F	G
RANGE	$x \leq 150$	$150 < x \leq 300$	$300 < x \leq 450$	$450 < x \leq 600$	$600 < x \leq 750$	$750 < x \leq 900$	$x > 900$
COLOR	Green	Light Green	Yellow	Orange	Dark Orange	Red	Dark Red

Table 52: Energy Classes - Definition of the Classes Range of Values [kgCO₂e/m²]

A direct reference is made to the data illustrated in *Figure 150*, where the horizontal bars represent, for each structural solution, the emission value per square meter and the corresponding energy class assigned based on the defined conventional threshold. It follows that the timber bridge is classified as a Class C solution, confirming it as the most environmentally sustainable option. The other structural alternatives, on the other hand, fall within Class F and Class G, showing a significantly higher environmental impact and a much lower energy class compared to the timber solution.

The use of an energy class, such as the one previously defined in conventional terms, proves to be very useful for comparative purposes. However, it is essential to note that, at present, there is no

official regulation that clearly and definitively defines energy classes based on the embodied CO₂ emissions of construction materials for infrastructure such as bridges.

In the building sector, in fact, the energy classification of buildings is governed by European and national regulations, including Directive 2010/31/EU (recast in Directive 2018/844/EU) on the energy performance of buildings, Delegated Regulation (EU) 244/2012 on the methodology of calculation, and standards EN 15603 / EN ISO 52000-1 concerning the energy analysis of buildings.

However, these regulatory references apply to the operational energy of buildings and not to the embodied energy in structural materials, nor do they concern complex infrastructures such as bridges and viaducts.

It can therefore be stated that the energy classification carried out in the present detailed analysis has a purely indicative value, which proves useful for an immediate comparison of the environmental impact related to the different design solutions. This classification serves as a directly effective tool for raising environmental awareness, but it must not in any way be interpreted as a certification based on official values. It is thus appropriate to affirm that a future introduction of embodied emission thresholds within reference standards could make these types of assessments binding also for infrastructure such as bridges.

In conclusion, it can be stated that, based on the empirical classification provided, the timber structural solution, due to the low energy content of the construction materials and the good efficiency in transport and end-of-life phases, is confirmed as the most sustainable design choice. The other solutions in concrete and steel, by contrast, show significant environmental issues. More generally, the adoption of comparison tools based on energy classes, although not yet regulated for infrastructure works, can represent a fundamental step towards truly sustainable design.

12 FINAL CONSIDERATIONS AND CONCLUSIONS

The primary objective of this thesis was the analysis, design, and verification of a timber pedestrian bridge, developed within the framework of the European project Seine-Escaut Est, with reference to the Walloon section and Sector 5 of the Nimy-Blaton-Péronnes Canal. Additionally, the work aimed to establish a direct comparison between different structural proposals using alternative construction materials (such as concrete and steel), to provide a decision-making basis for the future selection of the structural solution to be implemented during construction. The entire work has been articulated in a coherent sequence of phases which, starting from the territorial and infrastructural framework, led to the definition and selection of a structural solution optimized from a static, dynamic, economic, and environmental perspective.

The initial part of the document is dedicated to a historical and typological analysis of timber bridges, with the objective of providing a solid cultural and engineering foundation for the subsequent design phase. In this context, it emerged that timber represents a remarkably contemporary structural material, capable of combining traditional construction practices, environmental sustainability, and favorable mechanical performance. The in-depth study of the main structural configurations - including beam bridges, truss bridges, arch bridges, and suspension bridges - allowed for the contextualization of the design choice within the framework of current best practices.

Subsequently, various preliminary design alternatives were developed and compared, following the general objective of identifying the solution that best meets the functional, aesthetic, and structural constraints of the project. The final choice fell on a glued laminated timber arch configuration, featuring vertical hangers and a stiffened deck composed of a system of primary, secondary, and transversal beams. This solution proved particularly suitable considering the site constraints, durability requirements, and performance demands, both in terms of structural resistance and dynamic comfort.

The technical core of the work focused on the development of a finite element model (FEM) of the entire structure. Through a detailed analysis of the loads (permanent, variable, snow, wind, and temperature) and their combinations in accordance with Eurocode 0, the internal forces and static deformations in the various structural elements were determined. Particular attention was devoted to the definition of modelling assumptions and support conditions, the accurate representation of structural connections, and the proper distribution of loads across the deck.

In compliance with the provisions of Eurocode 5 – Part 1-1, safety verifications were performed for both ultimate limit states (ULS) and serviceability limit states (SLS). A detailed analysis was carried out on the effects of lateral-torsional instability, the structural response under differential thermal loads, and the role of correction factors (such as k_{mod} , k_{def} , and k_{sys}) in the evaluation of the ultimate resistance of timber sections. The verifications covered all load-bearing components of the structure, including the arches, deck beams, linking beams, and vertical hangers.

A specific focus was dedicated to the dynamic comfort of the bridge, with particular attention to the effects of pedestrian traffic. Initial verifications were carried out based on the SETRA guidelines and Eurocode 5 – Part 2, Annex B, limited to a preliminary level of assessment. Subsequently, theoretical considerations were developed regarding the implementation of a time-domain analysis, evaluating possible load models according to different traffic conditions.

Further reflections were made on potential mitigation strategies for vibration effects, focusing on the theoretical application of Tuned Mass Dampers (TMDs). These devices were analyzed from a conceptual standpoint, laying the groundwork for more detailed future investigations and emphasizing the inherent complexity of the subject.

In addition to the structural study, an environmental sustainability and economic feasibility analysis was carried out. Using the Life Cycle Assessment (LCA) model, the equivalent CO₂ emissions associated with the various phases of the structure's life cycle - material production, transport, maintenance, and end of life - were estimated. The comparative results between the different structural solutions in alternative construction materials highlighted that the glued laminated timber option presents a significantly lower environmental impact compared to the steel and concrete alternatives. This advantage is mainly attributed to timber's capacity for carbon storage and the potential for local material sourcing.

The study also introduced an energy classification of the different structural alternatives based on the specific emissions per square meter of usable deck area. This classification was inspired by criteria typically used in the building sector but adapted with due methodological caution. With this approach, the transfer of energy performance assessment logic from the building sector to infrastructure underscores the need to develop more suitable regulatory tools for evaluating the environmental impact of infrastructures such as bridges and viaducts.

In conclusion, the results confirm the validity of the adopted structural solution, both from a structural and environmental-economic standpoint. The selection of a glued laminated timber pedestrian bridge emerges as a modern and sustainable choice, integrating technical innovation, environmental responsibility, and user comfort. The comparison with alternative solutions provides a solid basis for a well-informed final selection, grounded in the advantages and limitations highlighted throughout the thesis.

Although preliminary assumptions and theoretical considerations were introduced regarding dynamic behavior and construction methods, the study remains open to further developments. Future work should include a more detailed evaluation of feasible construction methodologies, supported by site-specific data, to verify the applicability of the proposed concept to construction techniques and local boundary conditions.

Overall, this thesis shows how structural engineering can support the ecological transition, delivering efficient, low-impact solutions aligned with the EU's zero-emission goals, and paving the way for future projects that unite sustainability and technical excellence.

13 REFERENCES

- Aluminium Parapets with Perforated Panels*. (2025). Retrieved from aluscalae.it: chrome-extension://efaidnbmnnnibpcajpcglclefindmkaj/https://www.aluscalae.it/wp-content/uploads/2019/04/Orizzonte_SCHEDA-PRODOTTO.pdf
- Amir Khorraminejad, Mahmoud R. Shiravand, Mohammad Safi. (2022, June 15). *Damage Analysis of Concrete Open-Spandrel Deck Arch Bridges under Seismic Loads*. Retrieved from ASCE LIBRARY: <https://ascelibrary.org/doi/10.1061/%28ASCE%29BE.1943-5592.0001911>
- Bell, K. (2006). *Timber Bridges*. WP 3 – Workbook 1, Nordic Timber Bridge Project.
- Brunel's Timber Viaducts*. (2007). Retrieved from www.railwaywondersoftheworld.com: https://www.railwaywondersoftheworld.com/timber_viaducts.html
- Canal Nimy-Blaton-Péronnes*. (2025). Retrieved from Wikipedia: https://fr.wikipedia.org/wiki/Canal_Nimy-Blaton-P%C3%A9ronnes
- CEN - European Committee for Standardization . (2019). *EN 15804:2012+A2:2019 – Sustainability of construction works – Environmental product declarations – Core rules for the product category of construction products*. Bruxelles: CEN.
- Crocetti, R. (2014). *Timber Bridges: General Issues, with Particular Emphasis on Swedish Typologies*. Internationales Holzbau-Forum IHF 2014.
- Design and Construction of Bridges, Frederic Gens*. (2025).
- Embodied Carbon - The ICE Database - Version 4.0*. (2024). Retrieved from Circular Ecology: <https://circular ecology.com/embodied-carbon-footprint-database.html>
- EN 1990 - Eurocode 0: Basis of Structural Design & Relevant Annexes*. (2002).
- EN 1991 - Eurocode 1: Actions on structures & Relevant Annexes*. (2003).
- EN 1993 - Eurocode 3: Design of steel structures & Relative Annexes*. (2005).
- EN 1995 - Eurocode 5: Design of timber structures & Relative Annexes*. (2004).
- Gens, F. (2024). *Design and Construction of Bridges - Chap 03b-2 - Bowstring Bridges*.
- Gens, F. (2024). *Design and Construction of Bridges - Chapter 03b-1 - Arch Bridges*.
- Gens, F. (2024). *DESIGN AND CONSTRUCTION OF BRIDGES - Verification of comfort (footbridges)*.
- Global Status Report for Buildings and Construction*. (2022). Retrieved from International Energy Agency (2022): <https://www.iea.org/>

- International Organization for Standardization. (2006). *ISO 14040:2006 – Environmental management – Life cycle assessment – Principles and framework & Requirements and guidelines*. Geneva: ISO.
- Le Projet Seine - Escaut*. (2022). Retrieved from Seine Escaut: <https://seine-scheldt.eu/lunion-europeenne-attribue-une-4eme-subvention-au-reseau-fluvial-a-grand-gabarit-seine-escaut/>
- Model of the main structural members of the timber bridge over the Rhine River in Schaffhausen, Switzerland*. (2017). Retrieved from [www.researchgate.net: https://www.researchgate.net/figure/Model-of-the-main-structural-members-of-the-timber-bridge-over-the-Rhine-river-e-in_fig2_309293735](https://www.researchgate.net/figure/Model-of-the-main-structural-members-of-the-timber-bridge-over-the-Rhine-river-e-in_fig2_309293735)
- NBN EN 10480*. (2013).
- Pont Rouge Harbour Platform in Comines-Warneton*. (2020). Retrieved from Bureau Greisch: <https://www.greisch.com/en/projet/pont-rouge-harbour-platform-in-comines-warneton>
- Ponte degli alpini*. (2019). Retrieved from [www.ostellobassanodelgrappa.it: http://ostellobassanodelgrappa.it/cosa-vedere/ponte-degli-alpini/](http://ostellobassanodelgrappa.it/cosa-vedere/ponte-degli-alpini/)
- Prezzario Regione Campania - Prezzario Lavori*. (2025). Retrieved from Prezzario Regione Campania: <https://prezzario.regione.campania.it/2025/prezzario?deviationRangeFromModel=2024>
- Programme Seine-Escaut Est*. (2021). Retrieved from Service Public de Wallonie: <https://infrastructures.wallonie.be/home/infrastructures-et-vous/projets-europeens/programme-seine-escaut.html>
- Rome versus the Germans, Part II*. (2019). Retrieved from [https://tldrhistory.com/: https://tldrhistory.com/2019/08/22/rome-versus-the-germans-part-ii/](https://tldrhistory.com/)
- SETRA. (2006). *Footbridges: Assessment of Vibrations Induced by Pedestrian*. Paris.
- Widening of the Nimy-Blaton Canal*. (2020). Retrieved from Bureau Greisch: <https://www.greisch.com/en/projet/widening-of-the-nimy-blaton-canal/>